

Physical Research Report 171

March 2019

Pile Deformation Stresses and Strains in Integral Abutment Bridges

Final Report

Prepared for:

**Illinois Department of Transportation
Bureau of Bridges and Structures
2300 South Dirksen Pkwy.
Springfield, Illinois 62701**

Prepared by:

**Illinois Department of Transportation
Bureau of Materials & Physical Research
126 East Ash St.
Springfield, Illinois 62704**

Technical Report Documentation Page

1. Report No. PRR 171	2. Government Accession No.	3. Recipient's Catalog No.	
4. Title and Subtitle Pile Deformation Stresses and Strains in Integral Abutment Bridges		5. Report Date March 2019	
		6. Performing Organization Code	
7. Author(s) Christopher Volkman and Christopher Hahin		8. Performing Organization Report No.	
9. Performing Organization Name and Address Illinois Department of Transportation Bureau of Materials & Physical Research 126 East Ash St. Springfield, Illinois 62704		10. Work Unit (TR AIS)	
		11. Contract or Grant No.	
		13. Type of Report and Period Covered Final Report, 2008-2019	
12. Sponsoring Agency Name and Address Illinois Department of Transportation Bureau of Bridges & Structures 2300 South Dirksen Pkwy. Springfield, Illinois 62704		14. Sponsoring Agency Code	
15. Supplementary Notes			
16. Abstract / Executive Summary Integral abutment bridges have definite advantages, including less deck deflection than bridges with simply-supported members, simpler construction, and lesser maintenance of the abutment and superstructure supports. This investigation examined the extent of strains induced by thermal expansion and contraction in driven piles and the reinforcing bars that connect the pile cap to the abutment diaphragm. Bridges selected for strain gage instrumentation had single and multiple spans. Three bridges used HP 12 x 53 piles oriented in the "strong" X-X axis and one bridge used shell piles. Strain gages and wires were armored with epoxy and attached to piles and reinforcing bars. Results indicated that piles had variable stresses as function of depth from the top of the pile to their points of fixity. Deflections in several piles did not conform to the deformed shape of a cantilever pile with fixed end loading as predicted by theoretical mechanics. Some piles exhibited the onset or presence of a plastic hinge. Differences in soil compressive strengths at various depths also influenced the deformation behavior of the pile. Mean stresses that were established in several piles were substantial and generated some concern as to factors of safety of piles with respect to fatigue life. HP piles were evaluated in terms of their expected fatigue life by the widely used Goodman failure equation and related fatigue data of ASTM A36 structural steel and ASTM A706 and A615 rebars. The effects of mean and alternating stresses and corrosion fatigue data of A36 steel were also included. Rebars at the pile cap were particularly vulnerable where several had clearly sustained stress levels significantly beyond the AASHTO high cycle fatigue limit for reinforcing bars. Recommendations to extend the life of piles subjected to stresses above their yield strength and corrosion in soils with low resistivity include: (a) thermally sprayed zinc or aluminum coatings; (b) hot dip galvanizing of the piles; (c) coating the piles with fusion-bonded epoxy and (d) cathodically protecting them with replaceable magnesium or zinc or aluminum sacrificial anodes, depending on the prevalent soil resistivity.			
17. Key Words Integral abutment; deformation; strain; stress; HP pile, pipe pile; thermal spray; fusion-bonded epoxy; sacrificial anodes; cathodic protection		18. Distribution Statement No restrictions. This document is available to the public through the National Technical Information Service, Springfield, VA 22161.	
19. Security Classification (of this report) Unclassified	20. Security Classification (of this page) Unclassified	21. No. of Pages 99	22. Price

ACKNOWLEDGEMENTS

The authors, Christopher Volkman, CE, PE, and Christopher Hahin, MetE, CorrE, PE, owe a significant debt of gratitude to Mr. Brian Zimmerman, an instrument technician (now deceased) in assisting them in the layout, attachment, instrumentation set-up and gathering of field data for this project. Mr. Volkman was responsible for the selection of bridges, gathering and plotting of data, coordination during bridge construction with contractors and the Resident Engineers of Districts 6, 7 and 8 where these bridges are located. Mr. Hahin was responsible for the data analysis, fatigue and corrosion resistance of steels, and research on new elastomeric composites to reduce expansion and contraction stresses on decks and approach slabs.

The authors sincerely acknowledge and appreciated the advice of Mr. Salah Khayatt, Mr. Todd Ahrens, Mr. Kevin Riechers and Mr. Mark Shaffer, and other helpful engineers of the Bureau of Bridges and Structures on this project involving integral abutments, and the various contractors and fabricators who cooperated with us regarding instrumentation of bridge components during construction. Discussions with Prof. Scott Olson of the University of Illinois and Dr. Brent Phares of the Iowa Department of Transportation regarding integral abutment bridge design are also acknowledged.

DISCLAIMERS

Throughout this report, trade names and products are mentioned. Use of these names or products do not constitute an endorsement of these products or their manufacturers by the authors or the organizations they represent. They are mentioned because they are indicative of typical practice. There may be other suitable or equal products of service available. Citations of specific trade names or products are intended for research and illustration purposes only and do not represent any intentional or explicit commercial endorsement.

The contents of this report reflect the views of the authors, who are responsible for the facts and accuracy of the data represented in this report. The contents do not necessarily reflect the official views or policies of IDOT. This report does not constitute a standard, specification, or regulation at IDOT.

TABLE OF CONTENTS

Introduction..... 1

Current Integral Abutment Design in Illinois..... 4

Purpose and Scope of the Investigation 8

Selection of Bridges 9

Instrumentation and Strain Gaging of Bridges12

Results of Strain Gage Instrumentation15

Effects of Daily Ambient Temperature Changes on Pile Strains28

Vertical Reinforcing Bar Strains in the Abutments.....44

Pile and Reinforcing Bar Stress and Strain Data and Design Life.....48

Pipe Piles.....76

Methods to Extend Life of the Piles Under Adverse Conditions79

Deck and Approach Slab Problems86

Reducing Pile Deformation Stresses in Integral Abutments90

Summary and Conclusions92

References96

LIST OF FIGURES

1a. Integral abutment design prior to July 2012 policy memo change.....	6
1b. Integral abutment design after July 2012 policy memo change.....	7
2. Weldable strain gages.....	13
3. Portable strain gage micro-spot welding unit	14
4. Armoring strain gage and wiring with epoxy	14
5. Pile strain and compressive strength of soil, Pile 6, N Abutment, Pike County.	16
6. Pile strain and compressive strength of soil, Pile 6, S Abutment, Pike County.....	17
7. Pile strain, 31 °F to 93 °F, Pile 5, N Abutment, Pike County.....	18
8. Pile strain, 31 °F to 93 °F, Pile 6, N Abutment, Pike County.....	19
9. Pile strain, 31 °F to 93 °F, Pile 5, S Abutment, Pike County.....	20
10. Pile strain, 31 °F to 93 °F, Pile 6, S Abutment, Pike County.....	21
11. Pile strain, 4 °F to 90 °F, Pile 4, E Abutment, Macon County	23
12. Pile strain, 4 °F to 90 °F, Pile 4, W Abutment, Macon County	24
13. Pile strain, 30 °F to 91 °F, Pile 4, N Abutment, Madison County	25
14. Pile strain vs. soil compressive strength, Pile 6, E Abutment, Madison County	27
15. Pile strain, 17 °F to 91 °F, Pile 4, N Abutment, Scott County	27
16. Daily pile strains, top of Pile 6, N Abutment, Scott County.....	29
17. Daily pile strains, Pile 6 at 2-ft depth, N Abutment, Scott County.....	30
18. Daily pile strains, Pile 6 at 4-ft depth, N Abutment, Scott County.....	31
19. Daily pile strains, Pile 6 at 6-ft depth, N Abutment, Scott County.....	32
20. Daily pile strains, Pile 6 at 10-ft depth, N Abutment, Scott County.....	33
21. Daily pile strains, top of Pile 6, N Abutment, Madison County.....	34
22. Daily pile strains, Pile 6 at 2-ft depth, N Abutment, Madison County.....	35
23. Daily pile strains, Pile 6 at 6-ft depth, N Abutment, Madison County.....	36
24. Daily pile strains, Pile 6 at 8-ft depth, N Abutment, Madison County.....	37
25. Daily pile strains, Pile 6 at 10-ft depth, N Abutment, Madison County.....	38
26. Daily pile strains, top of Pile 5, N Abutment, Pike County	39
27. Daily pile strains, Pile 5 at 2-ft depth, N Abutment, Pike County	40
28. Daily pile strains, Pile 5 at 4-ft depth, N Abutment, Pike County	41
29. Daily pile strains, Pile 5 at 6-ft depth, N Abutment, Pike County	42
30. Daily pile strains, Pile 5 at 8-ft depth, N Abutment, Pike County	43
31. Alternating stress vs. fatigue life, notch effects on 0.20% carbon steel	50
32a. Corrosion fatigue of 0.17% carbon steel with 50 ksi yield strength	55

32b. Cracked expansion joint web due to corrosion fatigue	56
33. Influence of cyclic frequency on the severity of corrosion fatigue.....	57
34. Corrosion rate of steel as a function of soil resistivity	59
35. Corrosion rate of carbon steel as function of temperature	60
36. Corrosion rate of carbon steel as function of sulfate concentration	61
37. Maximum pit depth rate as a function of chloride concentration.....	62
38. Failure of Pier 22 pilings due to corrosion, I-43 Bridge, Green Bay, WI	63
39. Cyclic crack growth rates vs. cyclic stress intensity	68
40. Alternating fatigue strengths of cathodically protected steel vs. cycles to failure.....	70
41. Corrosion of steel pipe vs. soil resistivity	77
42. Corrosion rate / pitting rate ratios for pipe.....	78
43. Effect of magnesium, aluminum and zinc anodes on fatigue life.....	79
44. Corrosion rates of aluminized steel in various soils	80
45. Corrosion rates of galvanized steel in various soils	81
46. Polyurethane approach slab joint and pockets	87
47. Deformation characteristics of Vytaflex 10 in compression	88
48. Deformation characteristics of Vytaflex 20 in compression	89

LIST OF TABLES

1. Characteristics of the four bridges in this study.....	10
2. Summary of annual stresses for bridges in this report	28
3. Integral abutment reinforcing bar stresses.....	44
4. Stresses and factors of safety for reinforcing bars	46
5. Required minimum mechanical properties of HP steels.....	49
6. Variability of pile strain with daily temperature changes.....	52
7. Summary of daily stress changes.....	54
8. Fatigue safety factors based on maximum annual stress changes	54
9. Deflection and surface stresses for a 12 x 84 HP pile.....	66
10. Resistivities of common water environments	69
11. Pit depth and stress intensity for A36 piles in soils with a resistivity of 100 ohm-cm ...	71
12. Pit depth and stress intensity for A572 piles in soils with a resistivity of 100 ohm-cm .	72
13. Pit depth and stress intensity for A36 piles in soils with a resistivity of 17 ohm-cm	73
14. Pit depth and stress intensity for A572 piles in soils with a resistivity of 17 ohm-cm ...	74
15. Types of sacrificial anodes	83

TERMINOLOGY USED IN THIS REPORT

Anode—A sacrificial quantity of a metal or alloy which is galvanically active that provides electrons when coupled to steel to protect structural members from corrosion in specific environments, such as conductive soils, river or ground waters, or from deicing salt runoff that percolates into permeable foundations.

Corrosion Fatigue—The effect of corrosive media on the fatigue strength of metals and alloys compared to their fatigue strength in air; the corrosion fatigue strength of steel is substantially less in moist air, soil or water environments than its fatigue strength in dry air.

Corrosion Rate—The rate at which metals lose their sectional load-carrying capacity through the process of corrosion, usually expressed in mils per year (mpy) or as weight loss per unit area. Although corrosion rates and section penetration are often expressed as uniformly distributed over surface areas, in soils and other heterogeneous media, corrosion rates of penetration may be localized.

Crack Propagation—The growth in length or depth of a crack which starts at defects or stress concentration sites in structural members and then spreads to wider areas under the action of cyclic and mean stresses that occur over a period of many years.

Fatigue Strength—The number of stress cycles, often reported from 10^4 to 10^7 cycles, that steels can sustain undergoing cyclic stress, which can vary from zero to peak stress or alternate from compression to tension, and is typically measured by testing steel bars in rotating bending or subjecting tensile specimens to variable tension loads.

Fracture Toughness—A mechanical property of steels that indicates their resistance to fracture as a function of sectional stress and critical crack length, typically represented as K_I (tension), K_{II} (shear) or K_{III} (torsion), and is expressed in units of ksi [in]^{0.5} or MPa [m]^{0.5}.

Impact Toughness—A mechanical property of steels that is typically conducted at higher strain rates but is correlated with fracture toughness measurements conducted at much slower strain rates through various tests.

Integral Abutments—Bridges that have abutments directly connected to a set of driven piles by a reinforced concrete pile cap which eliminates expansion joints and establishes end fixity to bridge decks, in contrast to bridges with simply supported beams that do not have end fixity.

Pitting—The formation of localized depressions in metals and alloys, resulting in stress concentrations and the formation of cracks which can propagate by corrosion action; pit depth formation is typically 2-5 times greater than the general corrosion rate of steel, which is measured by overall weight loss per unit surface area in soil and water environments.

Resistivity—A physical property of conductive materials which is the reciprocal of conductivity and is used to measure the ability of a material to transfer electrons. Highly conductive metals of electrical conductors like copper have very low resistivity, in contrast to soils or various water solutions that have variable resistivity. Dry sandy soils or distilled water have high resistivity whereas salt water has very low resistivity (see Table 10).

Stress Intensity—The stress state K of a structural member that describes its nominal stress state and how stress is applied (tension, bending or shear), crack size(s) and location (edge, center, or partial depth) and described by a geometry factor Q (or Y in some texts). Stress intensity is expressed in the form of $K = Q \times \sigma \times [\pi a]^{0.5}$, where Q (or Y) is the crack geometry factor, σ is the nominal stress in ksi, and a is the crack length or depth in inches.

Pile Deformation Stresses and Strains in Integral Abutment Bridges

INTRODUCTION

Integral abutment bridge designs have been gradually adopted by 41 states since their first construction in Colorado in 1920. Missouri has more 4,000 integral abutment bridges, Tennessee at least 2,000, and eight other states with more than 1,000 each (Ref. 1). According to a survey conducted by the State of Tennessee, there are approximately 13,000 integral abutment bridges in the United States apportioned among 39 states (Ref. 2). Illinois has been using integral and semi-integral abutment bridge designs for about 30 years.

Proponents claim numerous advantages of integral abutment bridges, including (a) simplicity of design; (b) no joints at the abutments that can leak onto bearings and superstructure elements; (c) supposed uniformity of abutment pressure on approach pavements; (d) rapid construction due to use of vertically driven piles; (e) wider construction tolerances; (f) simple forms and the ability to build around existing substructures; (g) uniform load distribution on pile foundations; and (h) improved ride quality (Ref. 3).

However, integral abutments are not entirely free of problems, including slab failure due to subsidence of the approach fill material. Subsidence is due to the periodic oscillation of the abutment due to thermal cycling of the deck and superstructure. A survey of 140 integral abutment bridges in South Dakota found subsidence under every slab, with depths ranging from 0.5 in to 14 in, and extending back from the abutment up to 36 in. Solutions to this problem have included mechanically stabilized earth walls using geosynthetic tie backs, tire chips, and the use of polyurethane and polystyrene foams (Ref. 4). Deck cracking has also been noted in certain designs as the deck shrinks during the colder temperatures of the year. For this reason, integral abutment bridges, notably in Alaska and Arizona due to their large temperature extremes, have limited deployment (Ref. 1).

Thermal cycling does influence the girders of integral abutment bridges. Investigators at the University of Minnesota (Ref. 5) found that concrete girders on a 3-span, 216.5 ft long bridge decreased in length over a seven-year period by 175-275 μ strain / in. The worst shrinkage was sustained at the bottoms of the girders at 275-500 μ strain / in. In addition, the curvature of HP 12 x 53 piles increased about 260 μ strain / in, which indicated that the piles had yielded,

assuming that they were within commercial tolerances of straightness before and during installation.

Integral abutment bridges do not have any expansion joints, whereby the girders are directly connected to the abutments and support piles by reinforced concrete, and the approach slab extends away from the abutment, as shown in *Figures 1a* and *1b*. The joint between the approach slab and highway theoretically absorbs the expansion stresses, and the earth, gravel or non-compacted aggregate fill absorbs the deformation of the piles. Ideally the driven piles supporting the bridge will bend either as a cantilever or sigmoid at the points of contact and below when the pile ends are fixed by driving them to a specific depth. The driven depth to obtain fixity depends on soil and foundation characteristics.

Compared to simply-supported or semi-integral bridges, an integral abutment bridge provides end fixity for the span which increases its resistance to deformation by truck loadings and decreases mid-span stresses. For a uniformly loaded simply supported span, the maximum moment developed at mid-span is $M = 0.125 w L^2$, where w = unit loading per ft. In contrast, when both ends of the span are subject to uniform loading and fixed by integral abutments, the maximum moment developed at mid-span is $M = 0.042 w L^2$. Maximum mid-span stress is reduced significantly for integral abutments compared to simply supported or semi-integral bridges. Deflections under mid-point loading in simply supported spans are 4 times greater at mid-span than equivalently loaded integral abutments with rigidly fixed ends (Ref. 6).

The States of Tennessee, Iowa, Colorado and Utah have well-developed design guidelines for integral abutment construction. These states have the greatest permissible lengths and skews and have performed extensive research on integral abutments. Other states have restrictions on length and skew; others are liberal and leave length at the discretion of design engineers and relevant site conditions.

New Jersey DOT designs (Ref. 7) are relatively conservative. No provisions are required for the expansion of the bridge superstructure if it less than 50 ft in length, unless the approach slab is rigid concrete. Sleeper slabs for approaches are used for bridges of total length in the range of 50-140 ft. Integral abutments are not approved for designs greater than 140 ft in length. H piles are used, driven to a minimum depth of 20 ft, with the web of the pile perpendicular to the center line of the bridge, permitting weak axis bending and greater deflections. Pre-stressed and box

beams of reinforced concrete and steel WF girders are permitted for the superstructure. Prestressed members are connected to the pile cap with dowels, and steel girders have slotted holes to permit their adjustment. Piers are divided into various categories, depending on their ability to absorb deflections due to thermal expansion and contraction, the extent of their rigidity, and their height. Wing walls are cantilevered off the abutment not to exceed 13 ft in length, and skew is limited to 30°. Semi-integral abutments are allowed, but they require more than a single row of piles or require a foundation on bedrock. Curved structures are not permitted with semi-integral or integral abutments unless the beams are straight.

Iowa and Colorado, on the other hand, have virtually no appreciable limits on bridge length, although end spans are generally limited to 105 ft for steel and 120 ft for concrete. Iowa permits up to 575 ft in length for concrete piles; Colorado limits length to 790 ft. For steel piles, Iowa allows lengths up to 400 ft; Colorado allows up to 640 ft. Skews up to 45° are permissible in Iowa, limited at 425 ft for concrete piles and 300 ft for steel. Skew angles in between are linearly interpolated between 0° and 45° skew limits. Pile loadings are limited to a maximum of 6 ksi. If the piles are adjacent to mechanically stabilized earth (MSE) walls, corrugated pipe surrounds each pile. The temperature expansion of these structures results in about 2 in of expansion, causing yielding of steel piles (Ref. 8).

Tennessee has been a tireless advocate for the adoption of integral abutment designs, although they have found in their nationwide surveys a wide spectrum of length and design features that vary widely from state-to-state. Lengths of integral abutment bridges using concrete piles vary from 150 ft up to 1,175 ft; for those using steel piles, lengths vary from 120 ft to 550 ft. Skew angles are also highly variable, ranging from as low as 15° up to 70°, and curvatures from 0° to no upper limit (Ref. 2).

Tennessee recommends several design requirements to accommodate large thermal expansion and contraction. These include: (a) vertically driven piles and only in a single row; (b) weak axis orientation of the pile parallel to the long axis of the bridge; (c) compaction of porous, granular backfill under the approach slab; (d) provisions for drainage of the backfill; (e) an expansion joint at the approach slab-deck interface that contains no metal. Expansion joints in Tennessee designs use multiple layers of asphalt-saturated felt paper (Ref. 2).

A recent and very thorough investigation of the thermal behavior of integral abutments in Illinois was conducted by Olson and his colleagues at the University of Illinois (Ref. 9). It was found that skews above 40° induced additional pile stresses, but the increases were deemed to be not excessive. Strong axis pile bending was found to be favorable because it reduced bending, particularly in skewed bridges. Since piles with a lesser section modulus permit the most deflection, they were recommended. Compacted granular backfills were recommended because the pressure from their compaction helped to attenuate stresses in piles caused by the thermal expansion of the bridge. Live loading from HL-93 trucks induced abutment rotation, which could cause problems when there is significant thermal expansion. The study also confirmed the findings of other investigators, including shrinkage of the concrete decking and cyclic increases in backfill pressure. They felt yielding was an appropriate response of the structure to redistribute loads from expansion, contraction, or the effects of live truck loads on piles. They recommended further work to find mechanisms to reduce pile moments due to any increases in the length of integral abutment bridges.

CURRENT INTEGRAL ABUTMENT DESIGN IN ILLINOIS

Revised Design Guidelines

In 2005 and 2012, Illinois revised its design guidelines for integral abutment bridges (Ref. 10).

- A. *Maximum skew.* The degree of skew was increased from 30° to 45°.
- B. *Bridge length.* The total length of the bridge was increased from 310 ft to 550 ft.
- C. *Corbels.* The corbel which previously supported the approach slab on earlier designs was abandoned. The support step for the approach slab is now incorporated into the abutment.
- D. *Pile encasement.* Pile encasement of HP piles was previously added to provide corrosion protection; however, it increased rigidity, so it was removed. In the newest pile selection chart, extra pile thickness accommodates section loss due to corrosion. For HP 12 x 75 or larger piles, spiral reinforcement is required.
- E. *Integral slab bridges.* Slab bridges were also limited to a total length of 130 ft and a maximum individual span length of 40 ft.
- F. *Backfill and drainage.* Abutment backfills must be well drained and may be either compacted or non-compacted; either method can work. Typically compacted backfill is used when steel railings are used on the bridge, permitting railing posts to extend and anchor into solid backfill.
- G. *Abutment reinforcement.* The superstructure diaphragms shall be connected to the

abutment cap with an equivalent area of #8 steel bars on 12 in centers in the front and back for the full length of the cap. The diaphragms shall a minimum shear stirrup reinforcement of #5 bars on 12 in centers.

Because of cracking problems that were experienced as nightly temperatures dropped after pouring concrete in the afternoon, precast approach slabs were used on longer structures to mitigate this problem. A predictive equation was developed, based on the natural log of the number of pile blow counts that determines whether an integral abutment is suitable for specific locations. The user of this report is referred to Ref. 10 for a more thorough discussion of the determination of suitability based on soil conditions.

Design Features That Remained the Same

However, there were other conditions of integral abutment construction that remained the same:

A. Parallelism of key elements. Abutments, piers and wing walls must be perpendicular to the central longitudinal axis of the roadway. If the bridge is skewed, the abutments, piers and wings must also be skewed to the same angle.

B. Wing walls. The maximum length of the wing wall connected to the structure remained at 10 ft. Independent wing wall extensions can be used to extend embankments when necessary.

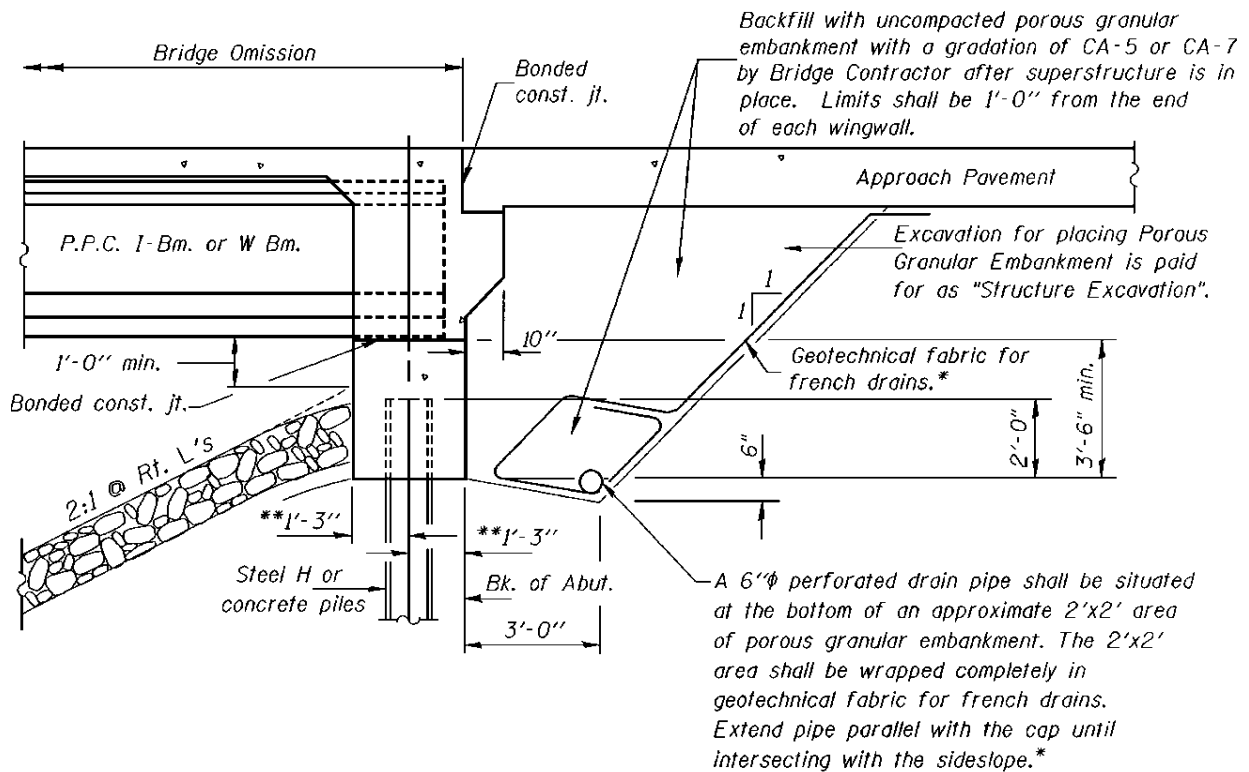
C. Pile reinforcement. Reinforcing bars shall be provided in all metal shell piles at abutments.

D. Bearing surfaces. Steel beams are still required to be set on 2 in thick rocker plates and 0.125 in reinforced elastomeric neoprene mats the size of the entire beam bearing area bolted to the abutment cap. Precast prestressed concrete (PPC) I-beams are to be set on a 1.0 in thick fabric bearing pad.

E. Construction stability. Cross frames shall be provided near the abutments for all plate girders to ensure stability during construction.

Based on annual inspections, integral abutment bridges in Illinois have shown no major signs of distress and have so far been proven to decrease the maintenance costs previously incurred using traditional expansion joints at approach slabs. Traditional expansion joints collect road debris, leak deicing fluids onto supports and girders, damaging both upper and lower expansion joints and structural members. The Illinois DOT intends to increase the number of integral

abutment bridges, based on the effective expansion length and soil conditions at the critical pile depth (Ref. 10).

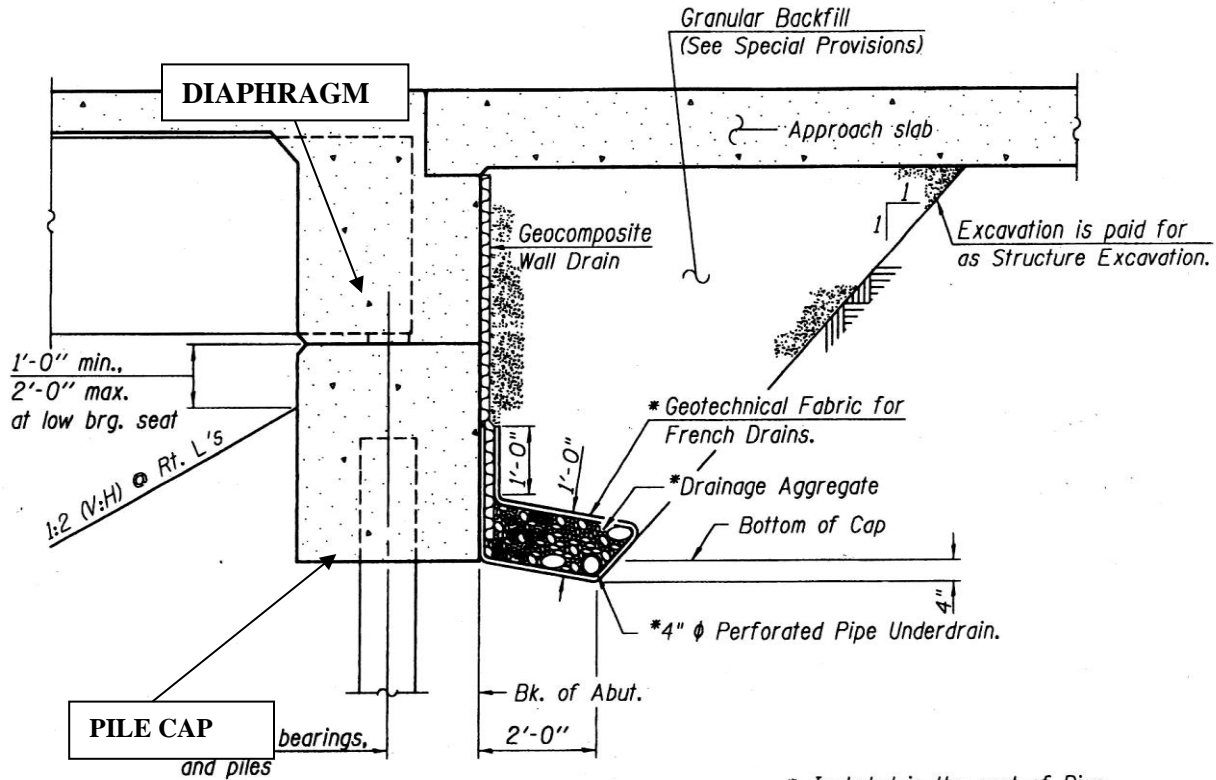


*Included in the cost of "Porous Granular Embankment".
 **1'-6" for Bulb-T.

SECTION THRU INTEGRAL ABUTMENT

(Porous Granular Embankment, drain pipe & geotechnical fabric omitted for structures less than 100 feet.)

Figure 1a. Cross section of a typical integral abutment in Illinois used in this report; this design was used in the construction of the bridges in this report. The revised current design geometry is shown in Figure 1b.



* Included in the cost of Pipe Underdrains for Structures. (See Special Provisions).

All drainage system components shall extend to 2'-0" from the end of each wingwall except an outlet pipe shall extend until intersecting with the side slopes. The pipes shall drain into concrete headwalls. (See Article 601.05 of the Standard Specifications and Highway Standard 601101)

Figure 1b. When the pile cap and the diaphragm are connected with reinforcing bars, they become an abutment. The modifications of 2005 and 2012 changed the corbel geometry and widened the pile cap and abutment. A wall drain was added. This side view is for a redundant steel WF bridge; prestressed concrete beam design is virtually the same. Pay item references and any site conditions that warrant adjustment are addressed by Special Provisions directly stated in the contract. The drainage system note refers to Illinois *Standard Specifications for Road and Bridge Construction* and specific Highway Standards that are located on the Illinois DOT web site.

PURPOSE AND SCOPE OF THE INVESTIGATION

The purpose of this experimental study was to determine the strains and stresses that are sustained by integral abutments, including piles, connections, their expansion and contraction movements, and propose design remedies to minimize these effects but still preserve the advantages of integral abutment bridges.

To better understand the behavior of integral abutment bridges, an evaluation of pile stresses and reinforcement bars was needed. By attaching strain gages and their instrumentation to the piles, girders and deck, it was determined whether the piles were yielding and what was the nature and shape of pile deformation when subjected to bending. Most investigators treat each pile as a single cantilever with a fixed end length at a specified pile depth, diagrammatically showing the bending of the pile conforming to the following deformation equation:

$$\Theta = (0.5 W L^2) / (E \times I)$$

Where

Θ = deflection angle at the end of the pile

W = expansion or contraction force

L = length of the pile

E = modulus of elasticity of steel

I = moment of inertia

The force applied in expansion is limited by (a) the backfill adjacent to the abutment, (b) compressive strength of the concrete deck, and (c) coefficient of thermal expansion of the decking materials. The contractive force is largely related to the coefficient of expansion of steel and concrete, which are relatively similar in magnitude, depending on the aggregate used for the concrete, although design details can affect expansion and contraction. For concrete, the typical range of the coefficient of expansion is 4.1 to 7.3 x 10⁻⁶ in / in / °F. Illinois principally relies on dolomite and limestone for its aggregate, where the coefficient of expansion would range from 4.1 to 5.0 x 10⁻⁶ in / in / °F (Ref. 11). The typical coefficient of expansion for ASTM A706 Grade 60 rebar whose carbon content ranges from 0.20% to 0.29% from 68 °F to 212 °F is 6.67 x 10⁻⁶ in / in / °F (Ref. 12). Since concrete has a tensile strength of 8-10% of compressive strength, deck cracking can occur if constraint on the deck from the abutment is too rigid.

In this investigation, deformations and incipient strains at various pile depths were measured, whereby the susceptibility of the pile to yielding and bearing capacity was considered.

The first objective of this study was to measure the bending strains in piles due to thermal expansion and contraction of the bridge. Four bridges were included in this study. Structural behavior resulting from thermal changes was observed over seasonal extremes. Strain gages were attached to the piles at various depths, armored by epoxy, and then were monitored on a daily and annual basis.

The second objective of the study was to consider and design an integral abutment that permitted expansion and contraction without inducing large strains in the piles or abutment reinforcement or the girders, yet still preserve sufficient end fixity for the girders so that the bridge would be virtually equivalent to an integral abutment. Since several design concepts were never constructed and their characteristics never measured, only the composite elastomeric materials for end expansion joints have been included in this report. These composite materials of polyurethanes and tire chips were tested in severe compression and the composite remained intact after unloading.

The third objective was to determine how soil environments and their resistivity affect the life of integral abutments. This was accomplished by considering the effects of corrosion on both uncoated and coated pilings during highly stressed states, and proposed methods to extend the life of integral abutment piles with coatings and sacrificial anodes.

The integral abutment bridges in this study were constructed with HP or metal shell piles. Shell piles were filled with concrete, and the HP piles had a 2 ft diameter encasement extending about 3 ft below the abutment. The piles in the bridges of this study had the “strong” X-X axis of HP piles parallel to bridge expansion & contraction. In 2005, the Illinois DOT altered its policy and placed the “weak” Y-Y axis of HP piles parallel to expansion & contraction which decreased restrictions on pile deformations in bending.

SELECTION OF BRIDGES

The bridges selected for the study were chosen by girder and pile type, along with length. The objective was to instrument combinations of pre-cast pre-stressed concrete and steel beams connected to metal shell and HP piles. A total of eight bridges that were initially selected for the study. During the first few attempts at instrumenting these bridges, there were several gage failures on piles, so those bridges were omitted from the study.

A new gage installation procedure was designed and implemented with much greater success, using full encapsulation with epoxy to armor both the gages and the wiring during driving conditions. Several more bridges were omitted due to conflicting construction schedules, which did not allow ample time for gage installation. Four bridges were completely instrumented, of which three had H-piles and one had metal shell piles. The structures were of varying lengths and spans. Their various dimensions and parameters of construction are described in *Table 1*.

Table 1. CHARACTERISTICS OF THE FOUR BRIDGES IN THIS STUDY

<i>Parameter</i>	<i>Pike</i>	<i>Macon</i>	<i>Madison</i>	<i>Scott</i>
Total Bridge Length, ft	115	171	145	295
Width, ft	36	36	58	35
Number of Lanes	Two	Two	Four	Two
Number of Spans	Single	Two	Three	Four
Type of Girder	PPC I-beam, 6 each	PPC I-beam, 6 each	WF 27 x 94, 8 each	W 33 x118, 6 each
Depth of Girder, inches	63	48	26.9	32.9
Girder Length, ft	113	85	Center span 60 Outer spans 41	Center spans 77 Outer spans 70
Type of Pile	HP 12 x 53	HP 12 x 53	14 in Ø metal shell, ¼ in wall	HP 12 x 53
Number of Piles per Abutment	9	6	11	6

In the following paragraphs, bridges that were fully instrumented and provided meaningful data are listed, including type of girder, total bridge length, type of pile, location of gages, and what gages survived during construction.

A. *Macon County*. This bridge has two spans using PPC girders, 171 ft total length and has H-piles for its integral abutment. Two piles were instrumented, with eight strain gages per pile, for a total of 16 gages. On the east abutment of the bridge, strain Gage 1 was located 2 ft below the encasement; on the west abutment, Gage 1 was located 1 ft below the encasement.

Two gages were applied to each girder, for a total of four. Girder gages were located at mid-span and placed on bottom of top flange and top of the bottom flange and were attached to an

interior beam and a southern-most fascia beam. Each deck had two gages per span, for a total of four gages, and were placed at mid-span.

B. Madison County. This bridge has three spans span using steel girders, 145 ft total length, and has metal shell piles for its integral abutment. Only the north abutment pile was instrumented, because the contractor inadvertently cut off the gages on the pile on the south abutment. The north abutment had 8 gages attached. Gage 1 was located very near the top of the pile encased in the pile cap. Two steel girders were instrumented with two gages each, for a total of four. Gages were located at mid-span and placed on bottom of top flange and top of bottom flange and attached to an interior beam as well as the southern-most fascia girder. Each deck had two gages per span for total of six gages, each placed at mid-span. Four gages are placed on vertical rebar at the interface of each abutment and diaphragm, for a total of 8 gages.

C. Pike County. This is a single span bridge with PPC girders, 115 ft total length, using H-piles in its integral abutment. Four piles were instrumented with eight gages per pile, for a total of 32 gages. At the north abutment, the interior pile Gage 1 was located 2 ft below the encasement, and an exterior pile Gage 1 was located 2 ft below the encasement. At the south abutment, both interior and exterior pile gages (Gage 1) were located 1 ft below encasement. Two girders were instrumented with two gages each, for a total of four. Gages were located at mid-span and placed on the bottom of the top flange and the top of the bottom flange and attached to an interior beam as well as the southern-most fascia girder. The deck had two gages, one placed at mid-span and the other at the center-lane of span. Four gages are placed on vertical rebars at the interface of each abutment and diaphragm, for a total of 8 gages

D. Scott County. This is a 4-span bridge with steel girders, 295 ft total length, using H-piles for the integral abutment. Two piles were instrumented with eight gages per pile, for a total of 16 gages. On the north abutment, interior and exterior pile gages (Gage 1) were located at the bottom of the encasement. Two girders were instrumented with two gages per girder, for a total of four. Gages were located at mid-span and placed on the bottom of the top flange and the top of the bottom flange and attached to an interior beam as well as the southern-most fascia girder. Since there were four spans, each deck had two gages per span placed at mid-span of each span, for a total of 8 gages. Four gages are placed on vertical rebars at the interface of each abutment and diaphragm, for a total of 8 gages.

INSTRUMENTATION AND STRAIN GAGING OF BRIDGES

The bridges were instrumented with strain gages and recordings were taken on the warmest and coldest days of the year. The gages were placed on the piles, girders, deck, and reinforcing bars in the abutments during construction of the bridges.

It was originally intended that the gages be applied to the piles at 2 ft intervals of pile depth, starting just below the abutment. It was anticipated the final depth of the piles was to be approximately known before they were driven into the ground. Prediction of pile depth was made based on the soil borings, test pile depths and depths of piles from the first stage of construction. However, the accuracy of the predictions was limited, resulting in final depth variances, whereby final gage locations did not always correspond to their originally intended locations. A total of eight piles between the four bridges were not damaged during the construction of the bridges with gages intact and functioning properly. Most of the girder gages were lost due to the paint contractors stripping them off. There were a few deck gages that were broken during pouring of the concrete deck.

Each bridge was intended to have 4 piles instrumented with strain gages. The configuration was two piles per abutment, with one an exterior pile and the other an interior pile. On each pile, the gages were attached at 2 ft intervals along the depth of the piles starting just below the abutment or encasement, whichever was applicable, and continuing down to a depth of 14 ft. Details of how the gages were fastened to piles are described in *Figures 2, 3 and 4*.



Figure 2. Pile gages were weldable quarter-bridge Micro Measurements strain gages supplied by Vishay Instruments. Gages are $7/16$ in long and attached by micro-spot welding a $5/8$ in long thin steel backing to a ground and cleaned steel surface. These micro-spot-welded gages are more reliable in translating strain from the steel substrate than with gages using bonding adhesives, which frequently debond during loading, or have limited fatigue life after sustaining frequent large strains during service.



Figure 3. Strain gages were attached by micro-spot welding the thin steel sheet backing of the resistance wire using a Micro Measurements Model 700 portable strain gage welding and soldering unit. Weld input energy in joules is varied to control the depth of spot weld penetration, similar to methods used in conventional resistance spot welding of metals.

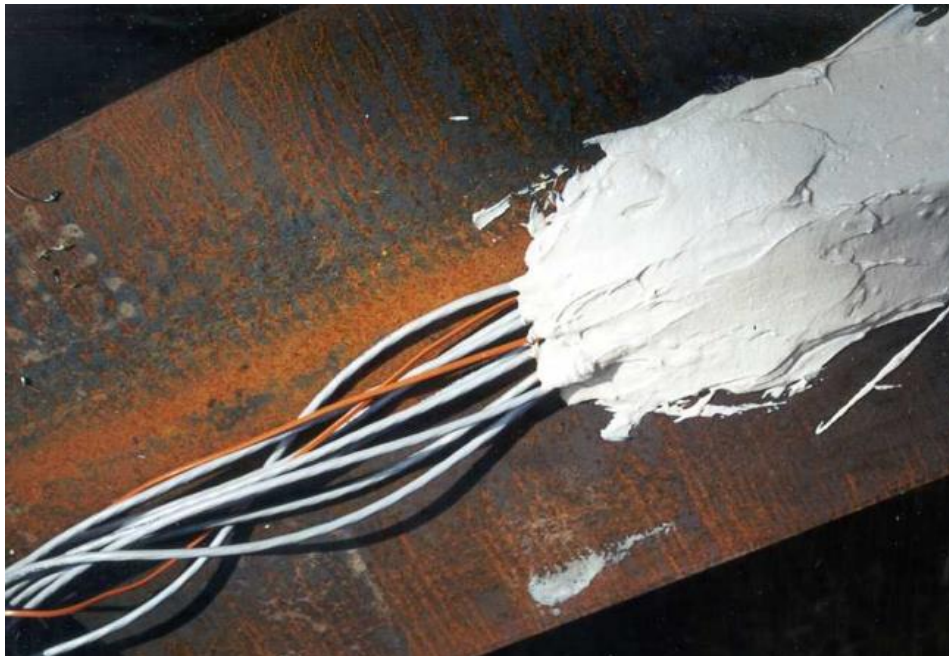


Figure 4. After the strain gages were micro-spot welded to the piles, they received a thick coating of epoxy. The wires were secured to the pile by bolting metal straps across the wires. The wires were subsequently coated with a thick layer of epoxy (not shown here) to protect them prior to driving the piles into the ground.

Because of variances in the estimates of what should be the final installed depth of the piles, some piles had to be cut off where the gages were attached. In other cases, the piles and the attached gages were driven deeper into the ground than intended.

Strain gages were also placed on the vertical reinforcing bars that tied the abutment to the diaphragm. The vertical bars in the abutments were instrumented at the intersection of the abutment and the end diaphragm, just above the abutment for determination of strain due to diaphragm movement across the top plane of the abutment. Strain gages were welded on the bars after the abutment was poured and before the diaphragm was poured. Four reinforcing bars were instrumented per abutment. At each abutment, two reinforcing bars located adjacent to the girders and two bars located between the girders were instrumented with gages. Strain readings were translated into stresses assuming linear elasticity over the strain range noted.

The girders were instrumented at the points of counter-flexure so that a coefficient for thermal expansion could be determined. Two girders per bridge were instrumented, the southern-most fascia beam and an interior beam to determine the difference in expansion between beams in full sun and those in the shade. Gages were placed on the bottom of the top flange and the top of the bottom flange of the two wide flange steel girders and the other two PPC girders.

The deck was instrumented with embedment strain gages placed at points of counter-flexure to determine an empirical composite coefficient of thermal expansion for the bridge. Two gages were placed in each span. Strain gages were read by a Micro Measurements P-3500 portable strain gage quarter bridge.

RESULTS OF STRAIN GAGE INSTRUMENTATION

Strain gage readings were recorded after construction of each bridge as an initial baseline. Subsequent readings were then recorded during warmest and cold temperatures of one single year. In addition, data loggers were installed to monitor daily strain changes associated with warmer daylight hours compared to cooler night temperatures.

A. Pile Strain as a Function of Driven Depth. The Pike County single span bridge is 115 ft long using PPC I-beam girders attached to nine HP 12 x 53 piles at the abutments. The piles extend 2 ft into the abutment and have a 2-ft diameter encasement extending to 3 ft below the abutment.

A comparison of pile strain and soil compressive strength was compiled for this bridge to determine the point of fixity and correlation of deflection with soil strength. Two piles indicated the expected inverse correlation that when the compressive strength of the soil is high, the corresponding pile strain is low, as shown in *Figure 5*.

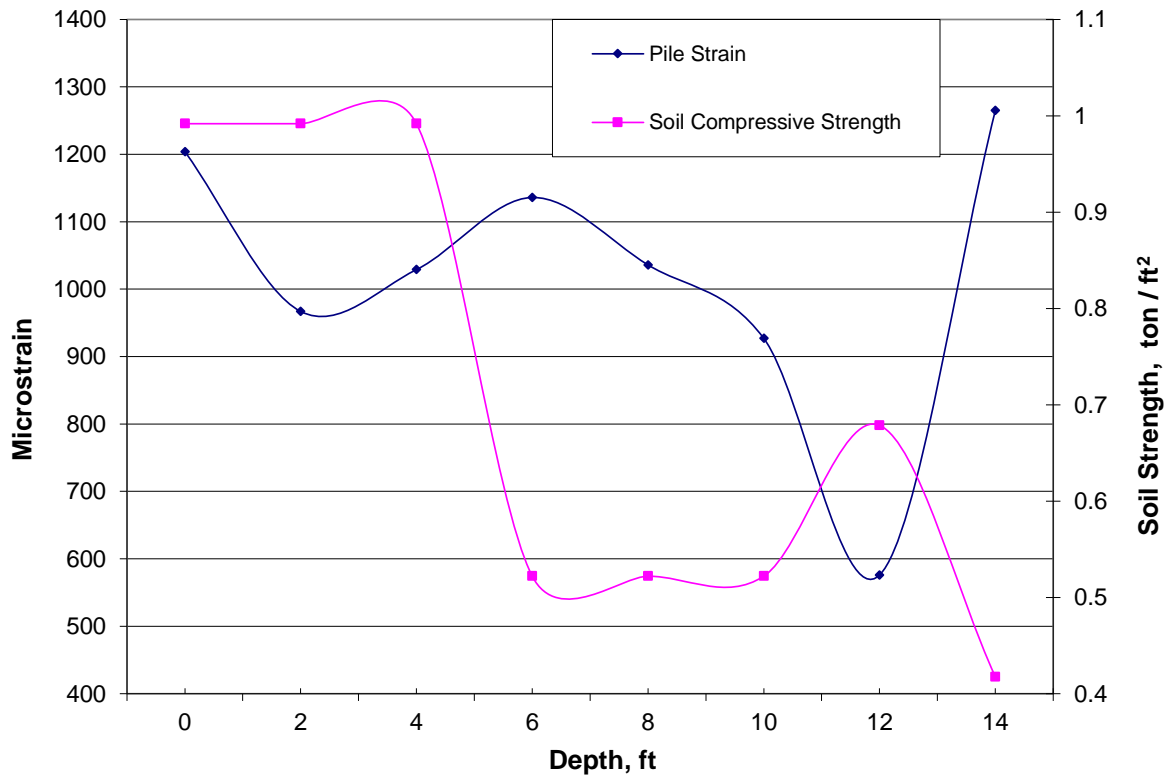


Figure 5. Pile strain and soil compressive strength at different pile depths for Pile 6 on the north abutment, Pike County Bridge. Compressive strengths of the soil horizons were obtained from project soil boring data. Micro strains are in inches/inch.

The soil compressive strength and pile strains were compared at 2 ft increments of pile depth to determine if the soil compressive strength had an impact on pile bending. *Figure 5* shows that at a shallow depth of 4 ft, there is little influence of soil strength on pile strain. However, at depths from 4 ft to 6 ft, data demonstrates a substantial increase in pile strain as soil compressive strength decreases. At 12 ft depth, soil strength increases 0.17 ton / ft², resulting in a 350 micro-strain ($\mu\epsilon$) decrease in pile strain. Continuing to the 14 ft depth, the soil strength dropped by about 0.25 ton / ft², increasing pile strain by 700 $\mu\epsilon$.

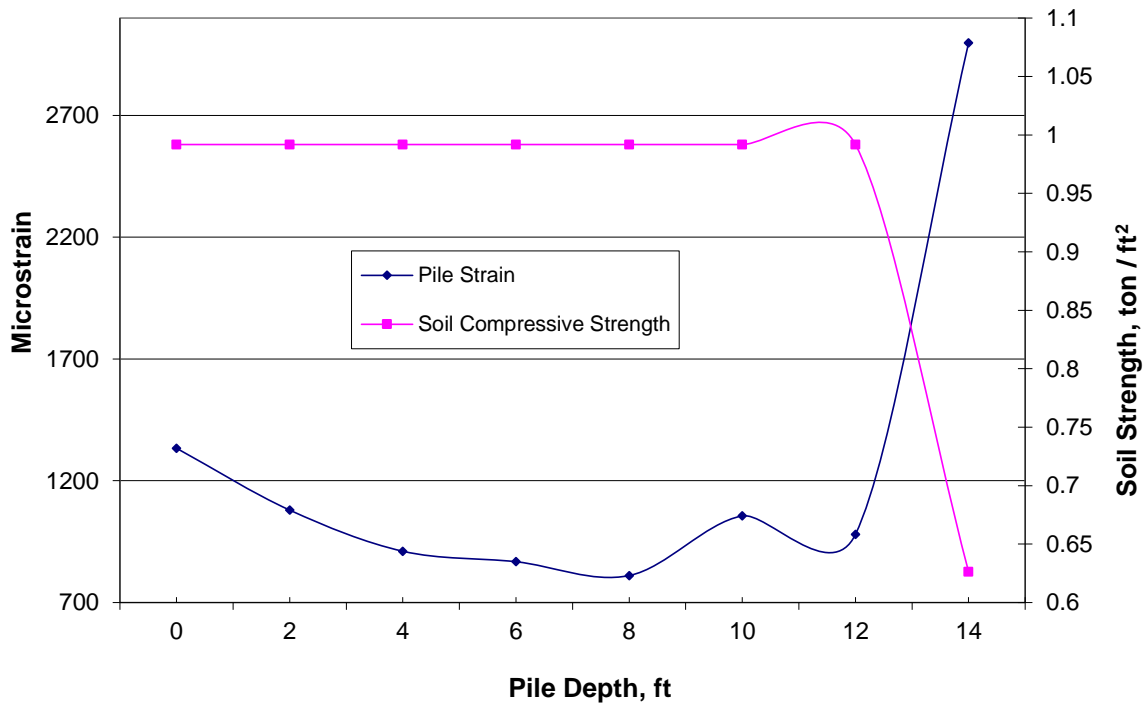


Figure 6. Comparison of pile strain and soil compressive strength at different pile depths for Pile 6 on the South Abutment, Pike County Bridge. Compressive strengths of the soil horizons were obtained from project soil borings data.

Figure 6 shows that when the soil strength is constant, the pile strains display the normal behavior of a cantilever beam showing an exponentially decreasing strain as predicted by theoretical mechanics that gradually decreased with depth. At a depth of 14 ft, soil compressive strength dropped by 0.4 ton / ft², resulting in a 2000 μ strain increase in the pile.

B. Pike County Pile Data Recorded during Seasonal Extremes. Gages were placed at 2 ft increments along the first 14 ft of pile depth. After the construction of the bridges, an initial strain reading was taken to determine a reference base line strain. Once this baseline was established, the pile strains resulting from bridge expansion and contraction were determined by taking the difference in values between the reference baseline strain and subsequent readings. The strains in Pile 5 of the north abutment of the Pike county bridge are plotted for the warmest days of the year compared to the coldest in Figure 7 as a function of pile depth and ambient air temperature. This plot appears to place the point of pile fixity at about 10 ft. The strain values

were plotted against pile depth to determine the point of fixity and if strain values indicate that the piles are yielding.

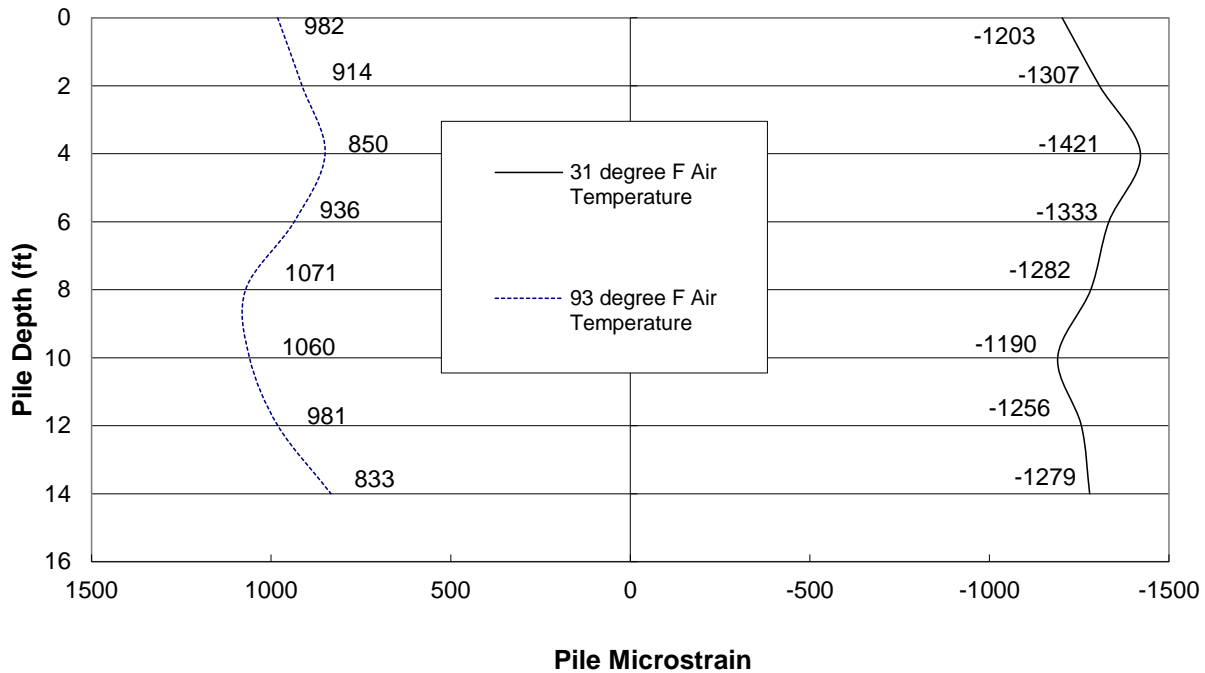


Figure 7. Pile strain vs. pile depth on Pile 5 of the north abutment, Pike County Bridge.

The graph was plotted with positive strain on the left side (tension) and negative strains on the right side of the axis (compression). *Figure 7* is a graphical representation of the strain profile of the pile during deformation due to expansion or contraction and indicated high levels of pile strain. When gages are mounted on the flanges facing the front face of the abutment (feature side) of the bridge, piles are in compression when the bridge is contracted and in tension when the bridge thermally expanded. The maximum pile strain in compression is -1421μ strain when translated into stress, assuming that the strain is linearly elastic and that the gage strain range is also linearly elastic:

$$\sigma = \epsilon \times E$$

Where:

σ = stress, psi

ϵ = strain, in/in

E = modulus of elasticity, psi

Using a modulus of elasticity of 29,000,000 psi for the ASTM A36 steel H-piles, this conversion yields a maximum compressive stress of 41,200 psi. This stress exceeds the minimum required

ASTM A 36 yield strength of 36,000 psi of the pile by 5,200 psi. At 4 ft depth, the maximum compressive stress during cold weather contraction provided the second lowest tensile stress of 24,700 psi during hot weather expansion. If the yield strength of the pile was 36 ksi, a minor amount of strain hardening occurred after yielding. All but two of the pile compressive stresses were beyond yielding, but none of the stresses in tension exceeded 31,060 psi.

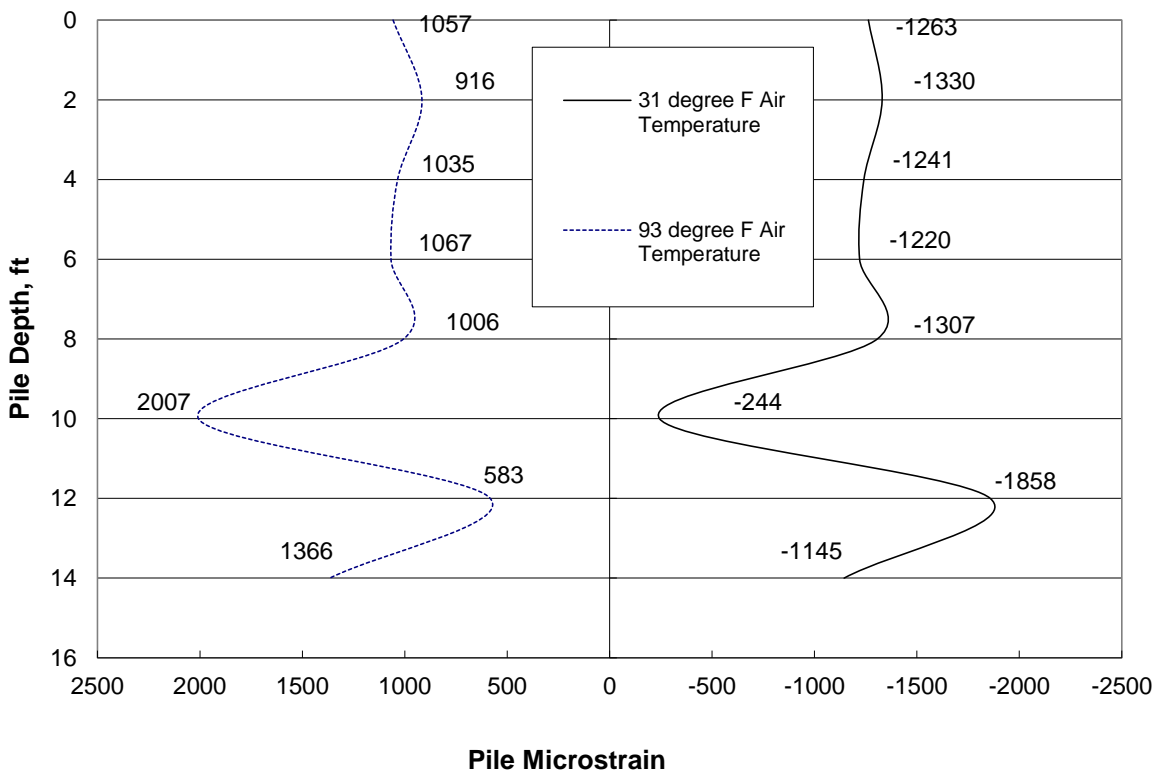


Figure 8. Pile strain vs. pile depth for two different temperature extremes on Pile 6 of the north abutment, Pike County Bridge.

The plot of *Figure 8* illustrates the high levels of strain induced in the piles due to thermal contraction and expansion at warmer and colder temperature extremes. Gages mounted on the flange facing the roadway away from the bridge would experience compression during contraction of the bridge during cold temperatures and tension during warm temperatures. The compressive stresses, except for the gages located at 6 ft, 10 ft and 14 ft, all exceed the minimum required 36,000 psi for ASTM A36 H piles. At 10 ft, the apparent point of fixity of the pile, the bridge expansion resulted in a stress of 58,200 psi, significantly beyond 36 ksi yield strength of A36. This yielding apparently induced some strain hardening, limiting the compressive strains during colder temperatures.

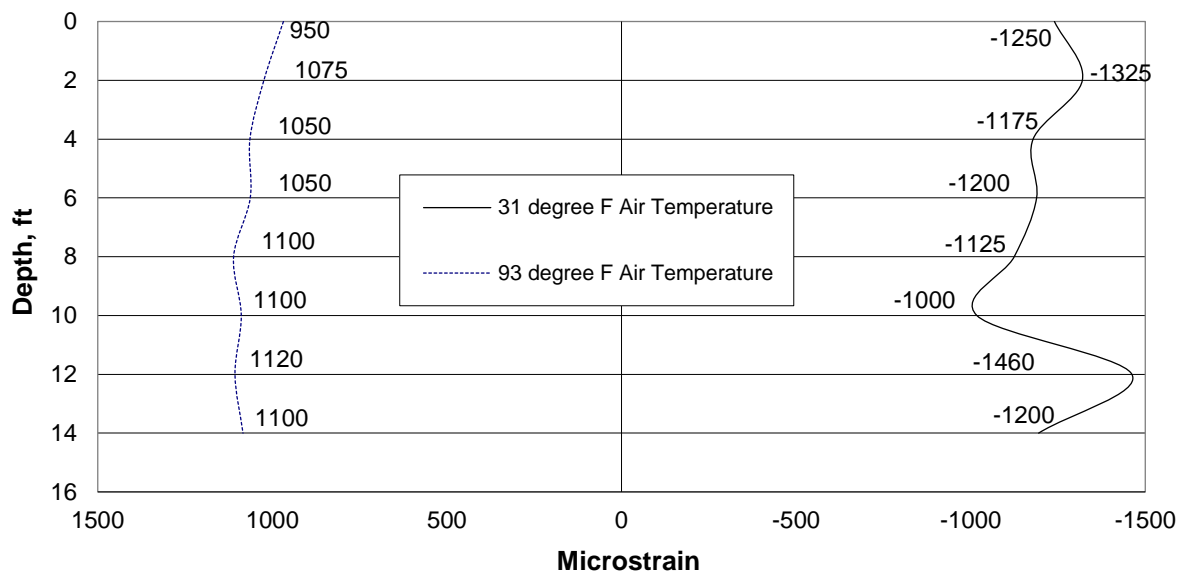


Figure 9. Pile strain vs. pile depth for two different temperatures on Pile 5 of the South Abutment for the Pike County Bridge.

The maximum pile strain shown in *Figure 9* in compression is -1460μ strain, which converts to a compressive stress of $-42,400$ psi, which exceeds the yield strength of A36 by $6,400$ psi. Assuming the point fixity at 12-ft depth, where yielding occurred, a slight reversal of strain occurs at 14 ft. The tensile stresses induced during bridge expansion were all below the minimum yield strength of the A36 HP pile, and exhibit a relatively stable behavior.

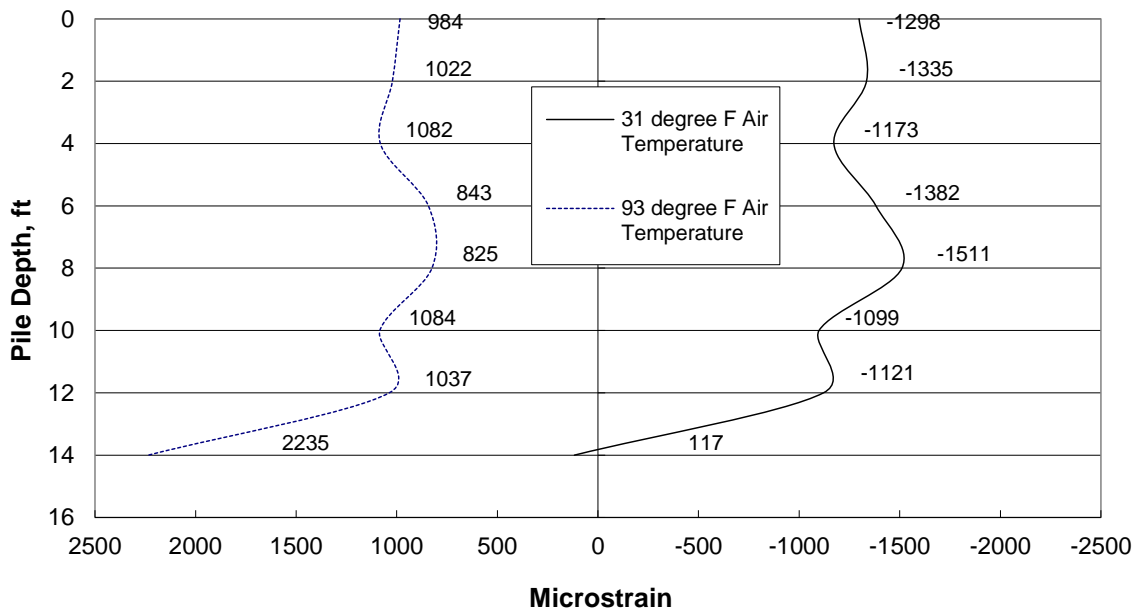


Figure 10. Pile strain vs. pile depth for two different temperatures for Pile 6 on the south abutment, Pike County Bridge.

In Figure 10, the maximum pile strain in compression is -1511μ strain, which converts to a compressive stress of 43,800 psi, exceeding the required yield strength of A36 by 7,800 psi. The plot indicates that the point of fixity appears to be at about 13 ft, which had the highest tensile stress of 64,800 psi. At this level of strain, the pile probably sustained some permanent deformation. At cold weather contraction, the pile at 14 ft depth had a stress of +3,400 psi, indicating the permanent strain induced by cold work prevented the pile going back into compression.

C. *Average Thermal Expansion.* The Pike County Bridge is 115 ft long, and induces a change in strain in the piles from 31°F in the winter to 93°F in the summer, a total temperature differential of 62°F. Out of 32 differentials of strain at various points along the piles, the mean pile strain difference for a 62°F temperature difference was $2280 \pm 103 \mu$ strain. The greatest strain differentials appeared at or near the point of fixity, which varied from 10-14 ft for various piles on the Pike County Bridge.

To induce this μ strain on the pile, an end force from the deck must generate a sufficient moment. The force to generate that moment is derived from the following deflection equation for a cantilever:

$$y = (W L^3) / (3E x I)$$

Where

y = deflection, inches

W = force, lbs

L = length of the pile, inches

E = modulus of elasticity, 29×10^6 psi

I = moment of inertia of H pile

The length of the pile was taken as 10 ft, the estimated point of fixity. The moment of inertia of an HP 12 x 53 pile in the X-X axis is 393 in^4 . The average strain of 2280×10^{-6} inches was taken to determine the value of y. The moment M that is generated at the point of fixity is $W \times L$. The value of M was determined from the basic stress equation $\sigma = M c / I$, assuming linearity of stress and strain. If the maximum stress is estimated at $(2280 \times 10^{-6}) \times (29 \times 10^6) = 66,120$ psi and $c = 5.89$ in, then the moment $W \times L = 4,411,742$ in-lbs. The deflection y is assumed to be 50% of the total thermal movement of the bridge. Since $L = 120$ in, then $W = 36,765$ lbs. Deflection of the pile is therefore $y = 1.858$ in. The entire expansion of the bridge is approx. double that of 1.858 in, so $\Delta L = 3.716$ in.

The total length of the bridge is $115 \text{ ft} = 13,800$ in. The coefficient of thermal expansion over a temperature range of 62°F is therefore $3.716 \text{ in} \div 13800 \text{ in} \div 63^\circ = 4.274 \times 10^{-6} \text{ in} / \text{in} / ^\circ \text{F}$, a result which is very similar to the coefficient of thermal expansion of dolomite, one of the predominant aggregates used in Illinois concrete bridge decks.

D. Macon County pile data recorded during seasonal extremes. The Macon county bridge is a two-span bridge with a total length of 171 ft constructed with six PPC I-beams per span, resting on a cast-in-place center pier with eight HP 12 x 53 friction piles. The abutments are cast-in-place with six HP 12 x 53 piles that extend 2 ft into the abutment with 2 ft diameter encasement extending to 3 ft below the abutment.

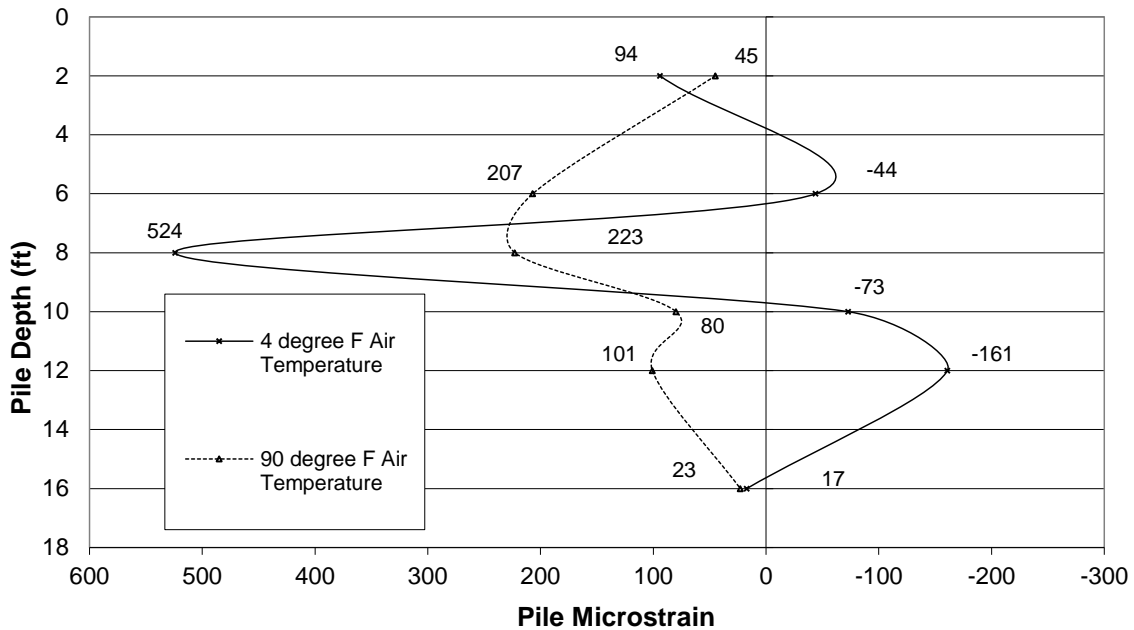


Figure 11. Pile strain vs. driven depth for Pile 4 on the east abutment, Macon County Bridge.

Figure 11 shows strains in the piles that are in compression when the bridge spans contract, and in tension when they expand. The maximum pile strain during cold weather contraction was an anomalous +524 μ strain in tension. This tensile strain is equivalent to a tensile stress of 15,200 psi. The point of fixity appears to be within 9-10 ft, which had a sharp reversal of strain that appears to indicate a precursor of buckling in the pile. All the pile stresses were positive due to thermal expansion at 90°F with a maximum tensile stress of 6,500 psi.

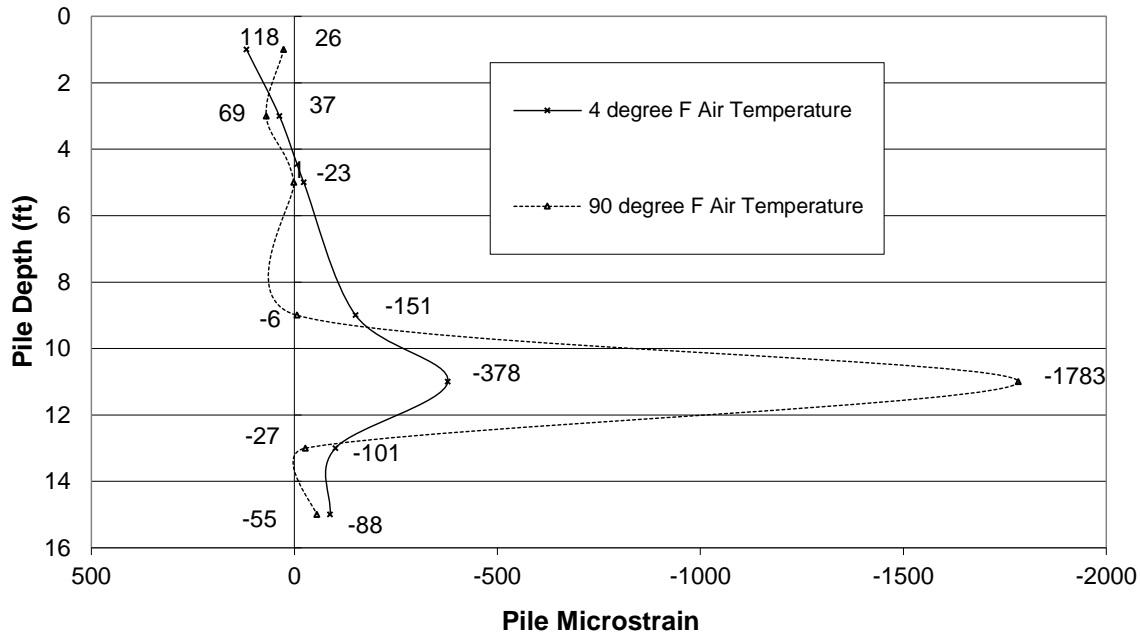


Figure 12. Pile strain vs. driven depth for Pile 4 on the west abutment, Macon County Bridge.

In Figure 12, the maximum pile strain during cold weather contraction was a compressive strain of -378μ strain, which is equivalent tensile stress of 11,000 psi on the HP 12 x 53 pile. Just as in Pile 4 on the opposite side of the bridge, the point of fixity appears to be between 10-12 ft, estimated at 11 ft, thermal expansion produced a substantial compressive stress of 51,700 psi, which exceeds the nominal minimum yield strength of ASTM A36 by 15,700 psi. The remaining pile strains produced thermal expansion stresses were all below 2,000 psi. The anomalous behavior of the sharp change in stress at the point of fixity seems to indicate the formation of a localized kink in the pile as it changes loading directions from warm to cold weather. The minimal changes from compression to tension in the piles for this bridge do lend themselves to a reasonable calculation of the coefficient of expansion for this bridge.

E. Madison County Pile Data Recorded during Seasonal Extremes. The Madison county bridge is a three-span bridge with a total length of 145 ft, constructed with eight WF 27 x 94 steel wide flange beams per span. The beams rest on two cast-in-place piers supported by fourteen 14-inch diameter $\frac{1}{4}$ in wall metal shell piles. The abutments were cast-in-place with 11 metal shell piles of the same dimensions that extended 2 ft into the abutment.

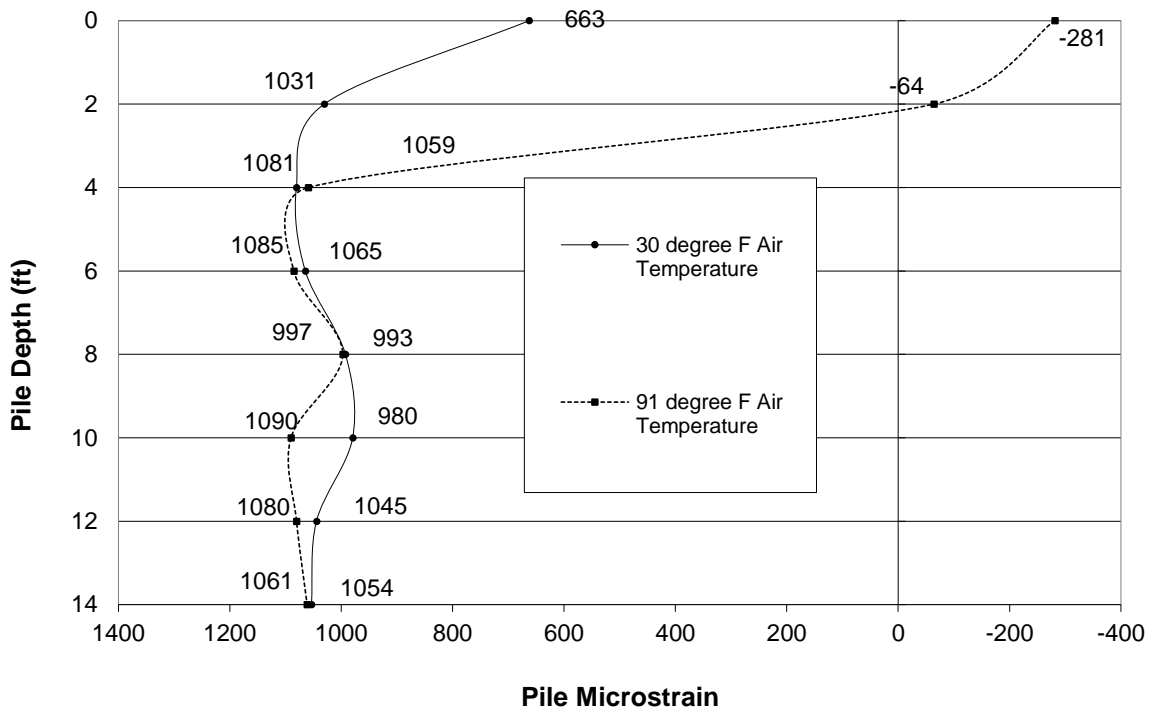


Figure 13. Pile strain vs. driven depth for Pile 11 of the north abutment, Madison County Bridge.

Figure 13 shows that the strains in the piles were in tension when the bridge was exposed to both warm and colder temperatures, except for the actual interface where the pile is encased in concrete. The maximum pile strain during cold weather contraction is a positive 1081 μ strain, which is equivalent to a tensile stress of 31,400 psi. During warm weather expansion, the pile showed compressive strains just below the 2 ft depth level. All the other strains were positive with a maximum of 1090 μ strain, which is equivalent to a stress of 31,600 psi.

The only drastic changes in strain between expansion and contraction were between the depths of 0 and 4 ft. This is a total strain change from -281 to +1081 = 1362 μ strain. It is uncertain whether the strains between 2 to 4 ft are a localized effect due to shell pile loading, because the remainder of the pile appears to have a point of fixity that lies between 10 to 12 ft.

F. Coefficient of Thermal Expansion for the Madison County Bridge. Unlike the single-span Pike County Bridge, which is constrained between the abutments, the three spans of the

Madison County Bridge are subject to constraint from the 14 in metal shell piles. These shell piles have a moment of inertia of 255.3 in⁴. Converting the 1362 μ strain in terms of stress is 39,498 psi. The moment exerted on this pile is $M = [255 \times 39,498] \div 7 = 1,438,856$ in-lbs. The load on the pile $W = 1,438,856 / 48 = 29,976$ lbs. The total deflection of the pile using the point of fixity as 10 ft, then $y = [29,976 (120)^3] / 3 (29 \times 10^6) 255 = 2.335$ in. Assuming this is only 50% of the expansion, the total expansion is estimated at 4.67 in.

The coefficient of thermal expansion for this bridge over a 61° temperature variation is estimated to be $(4.67 \text{ in}) \div (145 \times 12) \div 61 \text{ }^\circ\text{F} = 4.40 \times 10^{-6} \text{ in} / \text{in} / \text{ }^\circ\text{F}$, a value very similar to the thermal coefficient of expansion for dolomite.

G. Scott County Pile Data Recorded during Seasonal Extremes. The Scott county bridge is a four span bridge with a total length of 295 ft constructed with six WF 33 X 118 steel wide flange beams per span. The beams rest on three cast-in-place piers supported by six HP 12 x 84 piles. The abutments are cast-in-place with six HP 12 x 53 piles that extend 2 ft into the abutment with a 2-ft diameter encasement extending to 3 ft below the abutment.

Figure 14 shows the rough correlation between pile strain and soil strength, where the least pile strains generally appear at depths where soil strength is the highest. At 10 ft, the soil compressive strength sharply rises, establishing pile fixity.

The pile strain in Pile 4 of the north abutment for the Scott County Bridge is shown in *Figure 15*. Strains in the piles were entirely tensile during bridge expansion and contraction, although there was a substantial reduction in strain at 6-ft depth. This anomaly appears to be caused by a substantial increase in compressive strength of the soil, as shown in *Figure 14*. The maximum pile strain during cold weather was +1242 μ strain. Converted to stress, +1242 μ strain is equivalent to a tensile stress of 36,000 psi. During warm weather expansion, Pile 4 sustained tensile strains of +1152 μ strain, which is equivalent to 33,400 psi. The limited change in strain from 17 °F to 91 °F for the entire does not permit a realistic determination of thermal expansion for this bridge. These changes in strain also indicate lesser restraint by the abutments on this four-span bridge; however, the higher levels of strain indicate that Pile 4 had already yielded.

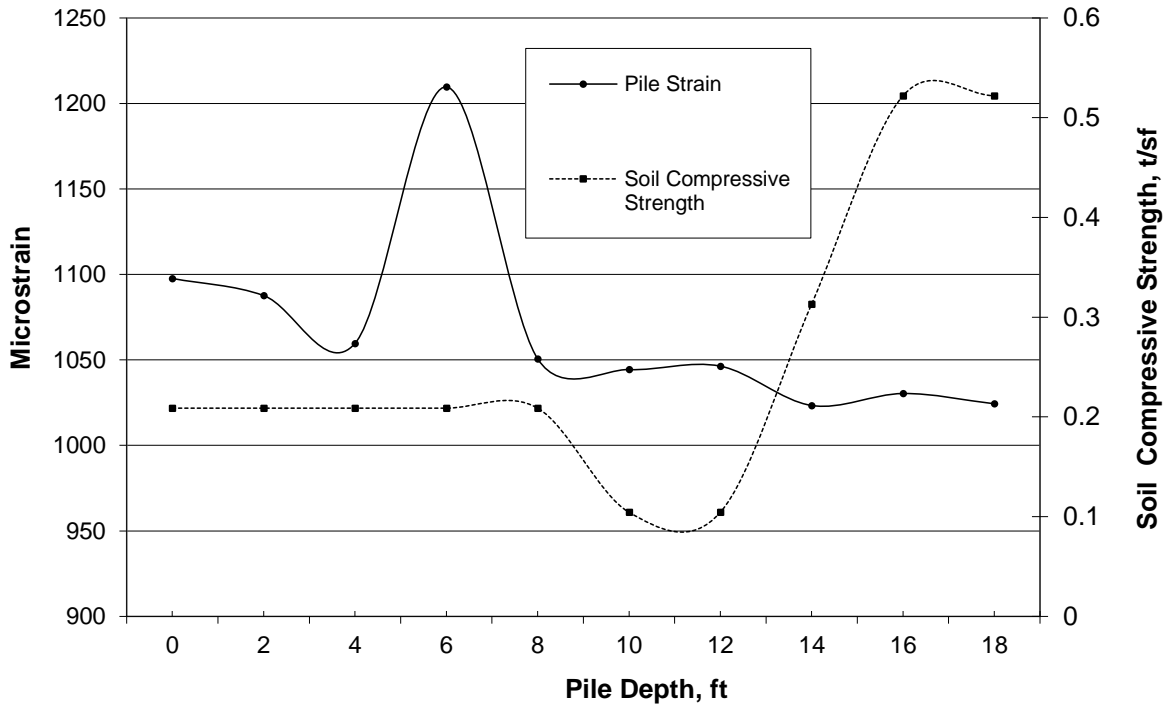


Figure 14. Pile strain vs. soil compressive strength for Pile 6 of the north abutment, Scott County Bridge.

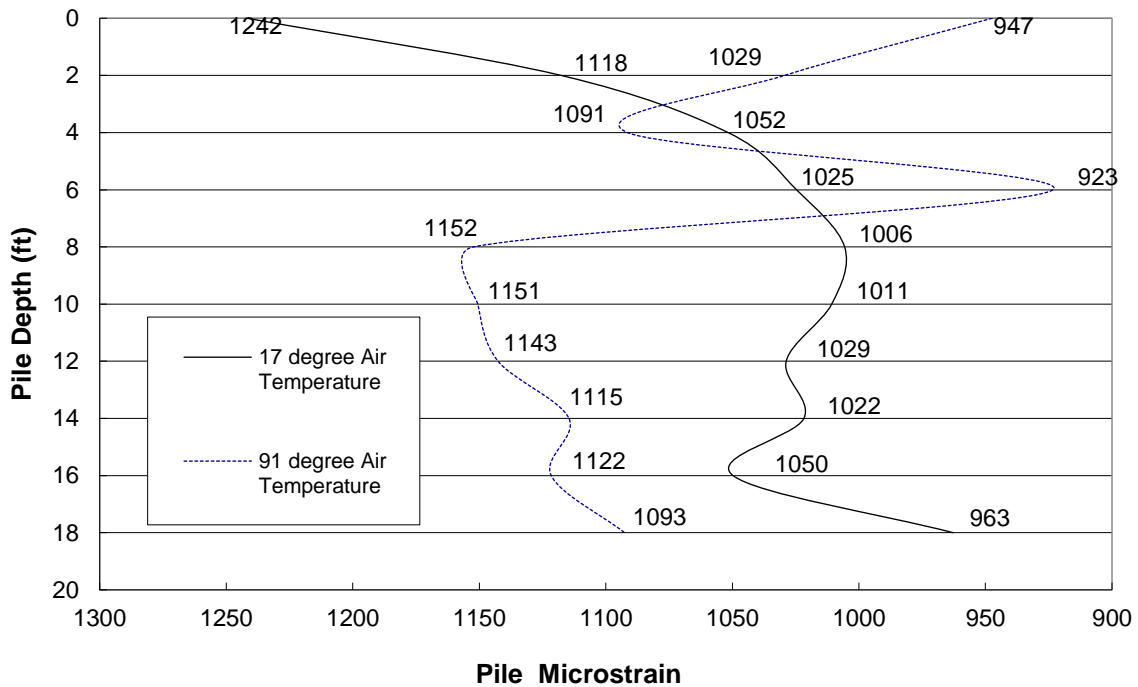


Figure 15. Pile strain vs. driven depth on Pile 4 of the north abutment, Scott County Bridge.

H. *Summary of Annual Stresses.* Table 2 summarizes the maximum annual stresses incurred during winter and summer months of a year for all four integral abutment bridges described in this report.

Table 2 SUMMARY OF ANNUAL STRESSES FOR BRIDGES IN THIS REPORT

<i>Bridge</i>	<i>Pile Number</i>	<i>Direction of Abutment</i>	<i>Alternating Stress, psi</i>	<i>Mean Stress, psi</i>
Pike	5	North	34,119	12,180
Pike	6	South	36,410	11,400
Macon	4	East	10,832	10,827
Macon	4	West	31,335	0
Madison	11	North	15,878	30,943
Scott	4	North	3,321	31,175

In this table, it is noted that in each bridge, alternating and mean stresses were identified by strain gages that were at, or very close to, the minimum required yield strength of ASTM A36 steel. In many cases, the actual strains indicated that yielding had occurred because values had exceeded the elastic strain range for A36 steel. The elastic range for A36 steel, based on a range of the modulus of elasticity of 29×10^6 to 30×10^6 psi, is 1200 to 1241 microstrain.

EFFECTS OF DAILY AMBIENT TEMPERATURE CHANGES ON PILE STRAINS

On each of the four bridges, strain gages were connected to Easy Logger® data recorders to monitor strains throughout the day at 20-minute intervals. This data was used to determine the nature of stresses induced by typical changes in daily temperatures. To avoid the confusion of the many different shapes of the plots and numerous data points, separate plots were created for each gage of the piles.

A. Daily Changes for Scott County Bridge Abutment Piles.

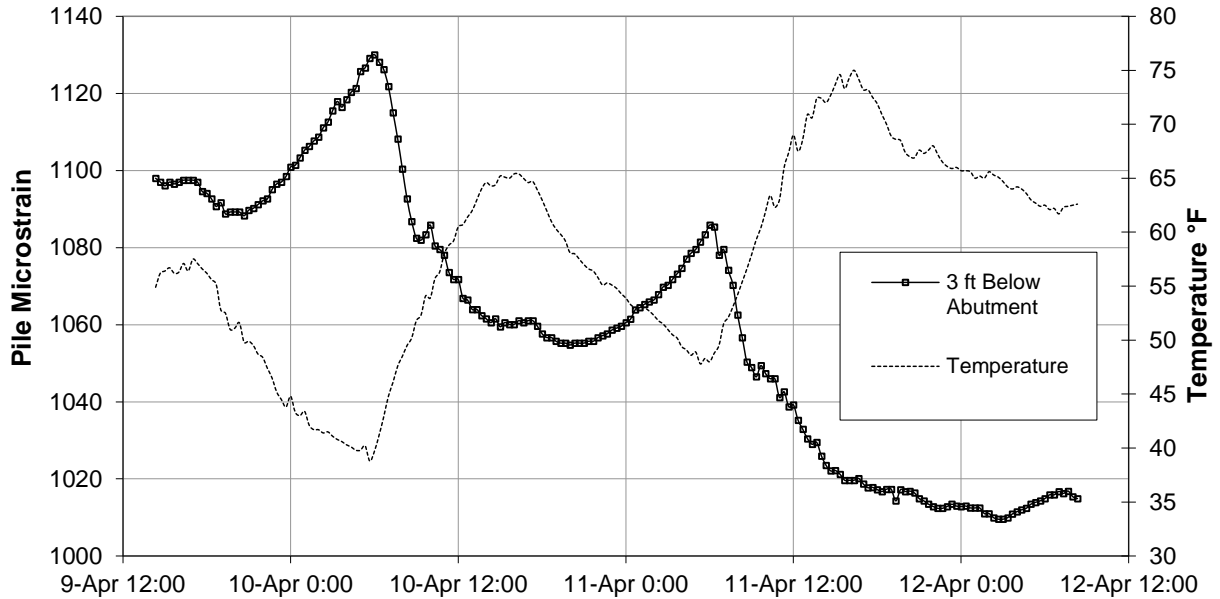


Figure 16. Pile strains induced by daily ambient temperature changes at 3 ft below the abutment of Pile 6 on the north abutment, Scott County Bridge.

Figure 16 shows the daily induced strains recorded in Pile 6 strains at a point just below the pile encasement. The encasement was a 2-ft diameter cast-in-place concrete enclosure covering the pile and extending 3 ft below the abutment. Based on a peak strain of 1135 μ strain on 9 April, the stress was 32,915 psi at the top of the pile. Figure 16 clearly shows an inverse relationship between increasing temperature and the decreasing pile strain. There are several rises and falls in temperature present to draw a relationship between strain and temperature. The first cycle consists of a rise is from 1090 to 1135 μ strain; decreasing down to 1055 μ strain based on a temperature increase of 26°F. The second cycle is a rise from 1055 to 1085 μ strain, and then decreases from 1085 to 1010 μ strain over a temperature change of 28°F. The average change of each rise and fall of strain $-2.708 \pm 0.290 \mu$ strain / °F, where ΔF is either positive or negative.

This reverse behavior at the top of the pile is attributed to the strain gage indicating compression from the point of load application from the abutment, whereas at greater depths, the strain vs. temperature relationship is direct in nature.

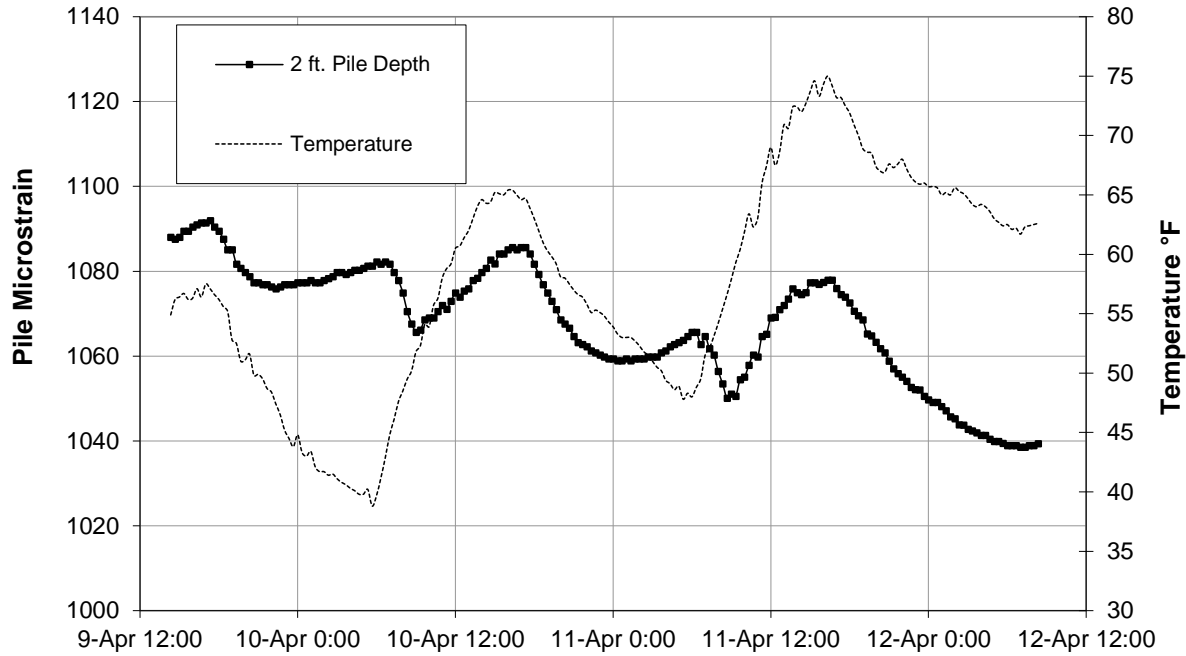


Figure 17. Daily induced pile strains in Pile 6 on the north abutment, Scott County Bridge at 2 ft depth.

In Figure 17, the daily induced pile strains were recorded from gages 2 ft below the pile encasement. At the 2 ft depth, the strain decreased as temperatures started to warm up. The peak pile stress was 31,610 psi on 9 April. In contrast to Figure 16, there is a direct relationship between temperature and pile strain, although there is slight lag between ambient temperature and strain. Based on two cycles where strain rises and falls directly with temperature, the average change in strain based on four distinct events, the average μ strain as a function is $1.799 \mu \text{ strain} / ^\circ\text{F}$.

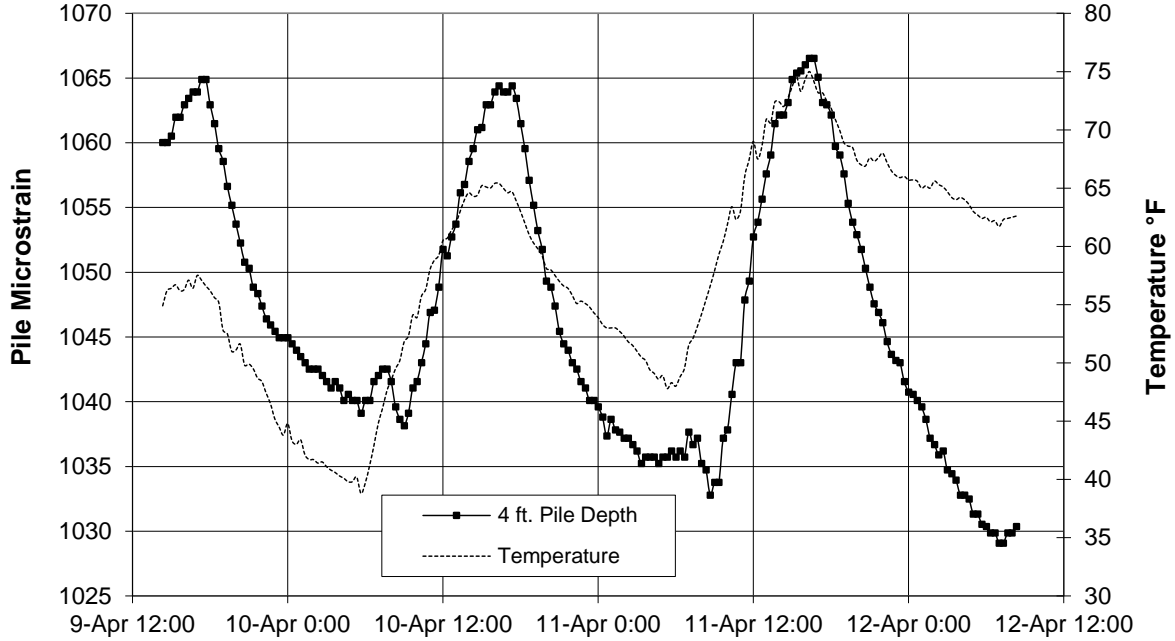


Figure 18. Daily Induced strains for Pile 6 at 4 ft on the north abutment, Scott County Bridge.

The daily induced strains for Pile 6 at 4 ft below the pile encasement are shown in *Figure 18*. In contrast to previous plots at 2 ft, the pile strain at 4 ft depth was a direct function of temperature. At a μ strain of +1067, the peak stress on the pile reached 30,943 psi. Two and one-half thermal cycles are present in the plot of *Figure 18*, with stresses decreasing in slightly larger increments as temperature rises. Each temperature rise and decrease was measured, resulting in a direct relationship of strain as function of temperature. The average increase and decrease (four total) in stress vs. temperature was $1.317 \pm 0.282 \mu \text{ strain} / ^\circ\text{F}$.

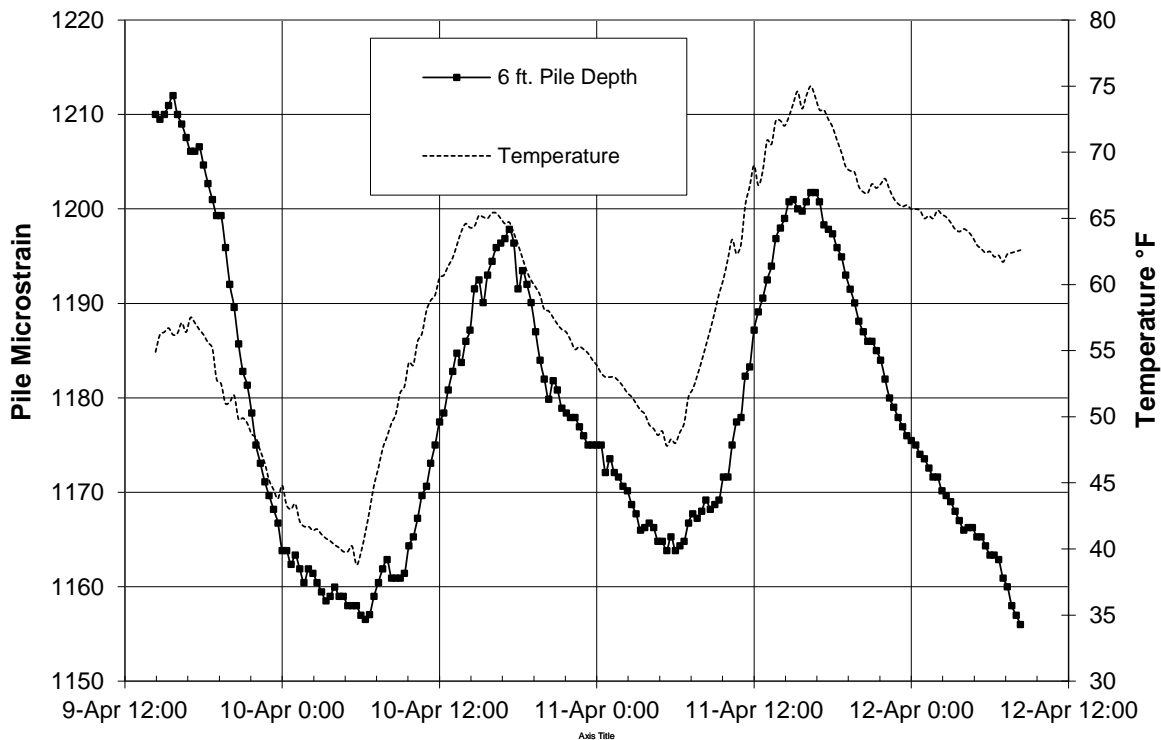


Figure 19. Daily induced strains for Pile 6 at 6 ft on the north abutment, Scott County Bridge.

Figure 19 shows the daily induced strains recorded on Pile 6 at 6 ft below the pile encasement. At the 6-ft depth, the pile strain was a direct function of temperature. During the highest temperature of 76°F shown, the pile stress was 35,150 psi. As the overnight low of 39 °F was reached, the pile stress decreased to 33,550 psi. The direct relationship between strain vs. temperature was determined by four different changes in strain starting on 9 Apr to 11 Apr. The average rate of strain for an increase or decrease in temperatures, based on four up and down changes, was $1.975 \pm 0.664 \mu \text{ strain} / ^\circ\text{F}$. A very slight hysteresis was noted since the pile is at 6 ft depth. At the 8 ft pile depth, the data logger channel failed; data at that depth was determined to be not usable.

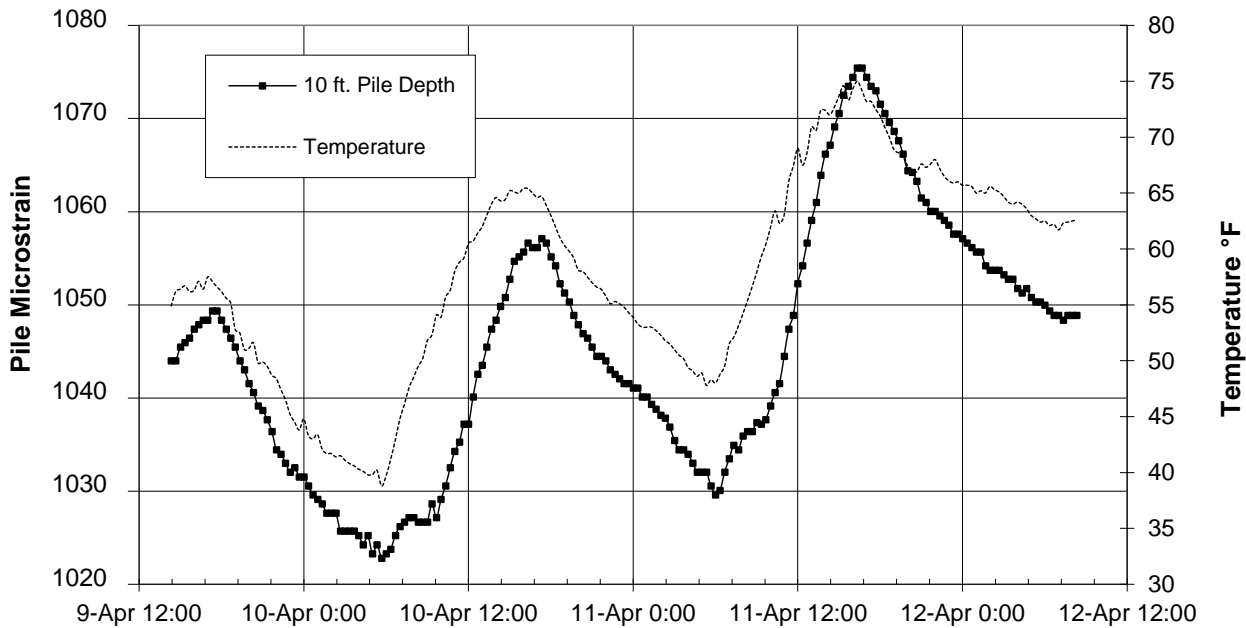


Figure 20. Daily induced strains in Pile 6 at 10 ft of the north abutment, Scott County Bridge.

In *Figure 20*, the daily induced strains recorded on Pile 6 were at 10 ft below the pile encasement. Similar to *Figure 19*, the relationship between strain and temperature is directly related. The strain at the lowest temperature of 39 °F encountered was 1022 μ strain; at the highest temperature of 75 °F, the peak strain was 1076 μ strain. The overall relationship between strain and temperature, based on two increases and two decreases in strain, was $1.573 \pm 0.146 \mu \text{ strain} / ^\circ\text{F}$.

B. Daily Changes for the North Abutment of the Madison County Bridge. The Madison County Bridge was constructed with metal shell piles where there was no encasement below the abutment. The top gage was placed on the pile just below the abutment. The temperature plot for this bridge displayed sharp changes of several degrees of temperature over short periods of time due to wind currents passing under the bridge where the thermocouples were placed.

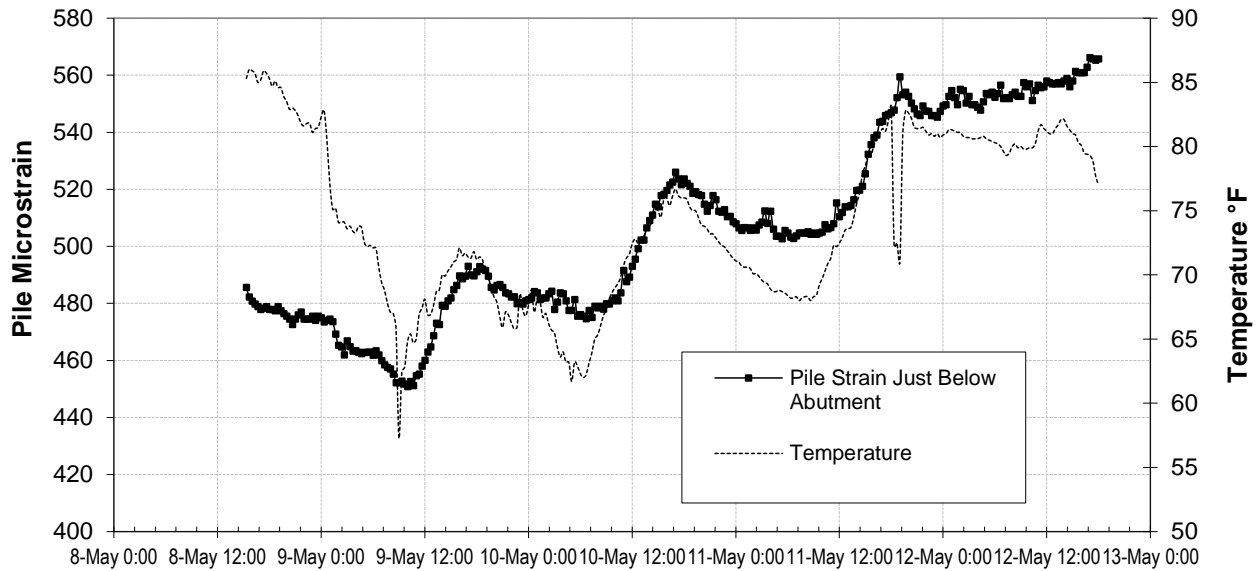


Figure 21. Daily induced pile strains at Pile 6 of the north abutment, Madison County Bridge.

The daily induced strains recorded in Figure 21 show strains just below the abutment near the top of the pile. Pile strain increased or decreased directly with the temperature. During a high temperature of 85°F, the peak pile was 555 μ strain (16,095 psi). At the lowest temperature of 57 °F, the peak strain was 452 μ strain (13,108 psi). Based on three rises and strain and two decreases in strain in direct response to ambient temperature, the overall change in strain vs. temperature was $3.004 \pm 0.585 \mu \text{ strain} / ^\circ\text{F}$.

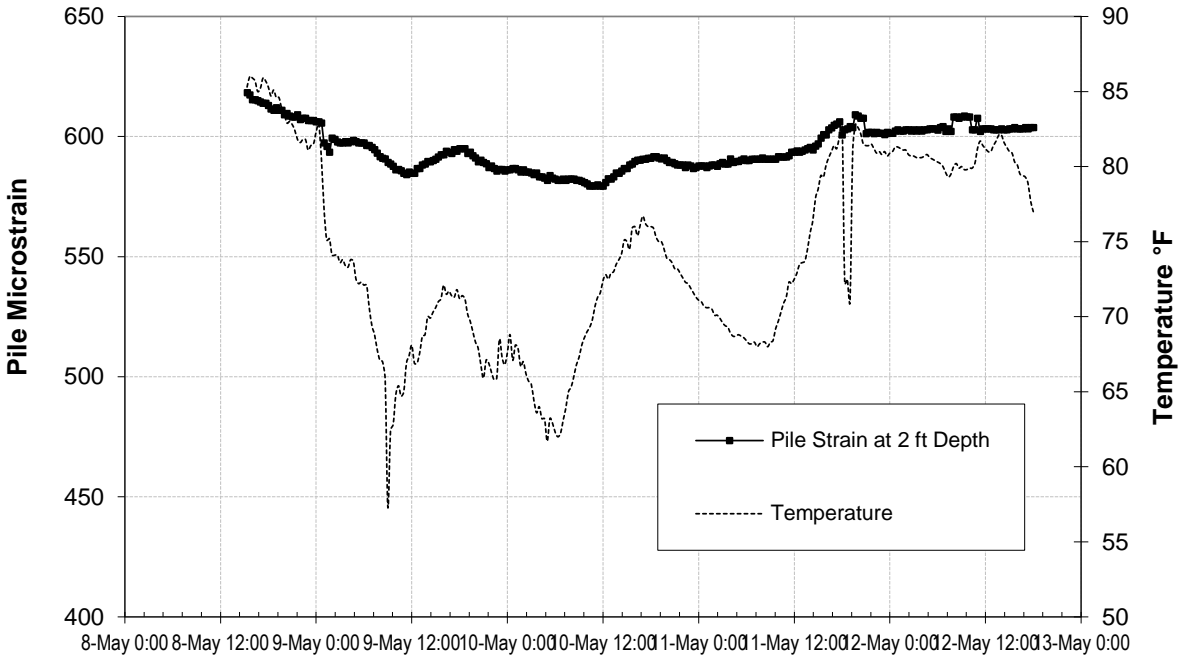


Figure 22. Daily temperature fluctuations of the north abutment, Madison County Bridge. Strain gage embedded at 2-ft depth appears to have debonded on 9 May.

Figure 22 shows the daily induced strains recorded at 2 ft below the abutment. This strain gage data is included to show an unresponsive strain gage, particularly since it is only 2 ft below the abutment. It should be registering greater strain, but instead the pile strain supposedly remained within 40 μ strain (1200 psi) during the test period. In contrast, gages at 6-ft depth show a direct strain response to temperature. It was therefore concluded that this gage was partially debonded. Strain gages at 4 ft also sustained damage upon activation, providing wide fluctuations, and then became inactive afterwards. Although ambient temperature changes were normal and substantial, no meaningful determination of strain became available after the second day of measurement.

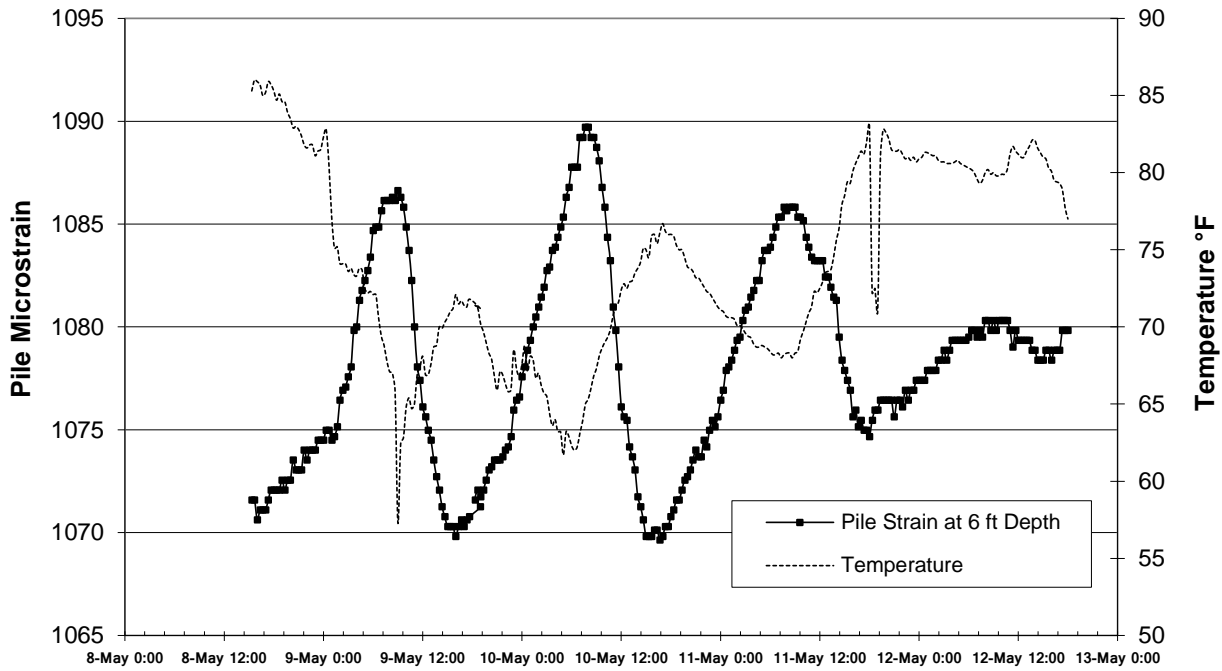


Figure 23. Daily induced pile strains at 6 ft of the north abutment, Madison County Bridge.

Figure 23 shows the daily induced strains recorded on Pile 6 strains at 6 ft below the abutment. The pile strain increased and decreased inversely with temperature. The saw-tooth stress pattern was almost 180° out of phase with respect to temperature. At the low temperature of 62 °F, the highest pile tensile stress was at 31,610 psi. There were three temperature cycles to measure the average change in strain vs. temperature. Based on three increases and three decreases of strain, the average change is strain vs. temperature was $-1.277 \pm 0.589 \mu \text{ strain} / ^\circ\text{F}$.

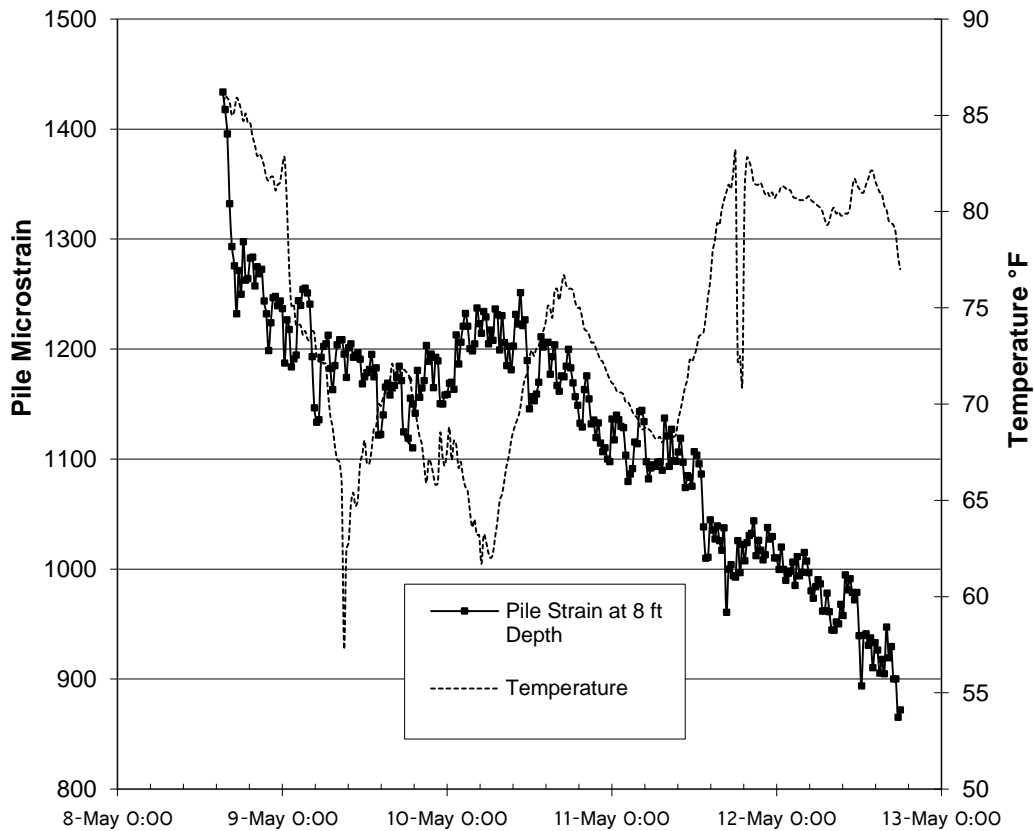


Figure 24. Daily Induced Pile Strains at 8 ft of the north abutment, Madison County Bridge.

Figure 24 shows the daily induced strains recorded on Pile 6 at 8 ft below the abutment. The pile strain decreased inversely with temperature, as it did at 6 ft, except that changes in strain had a limited response to ambient temperature, as would be expected at this depth. The overall strains, in general, continuously decreased during the test period. During a high temperature of 87°F the pile stress was at 41,600 psi, dropped within an hour to 37,700 psi, then gradually slid down to 26,100 in the afternoon of 12 May. From a low temperature of 57°F on 9 May to 83°F on 12 May, there was a strain change from 1200 μ strain down to 900 μ strain. The average change in strain vs. temperature was 11.538 μ strain / °F, the largest change for all four bridges in this study.

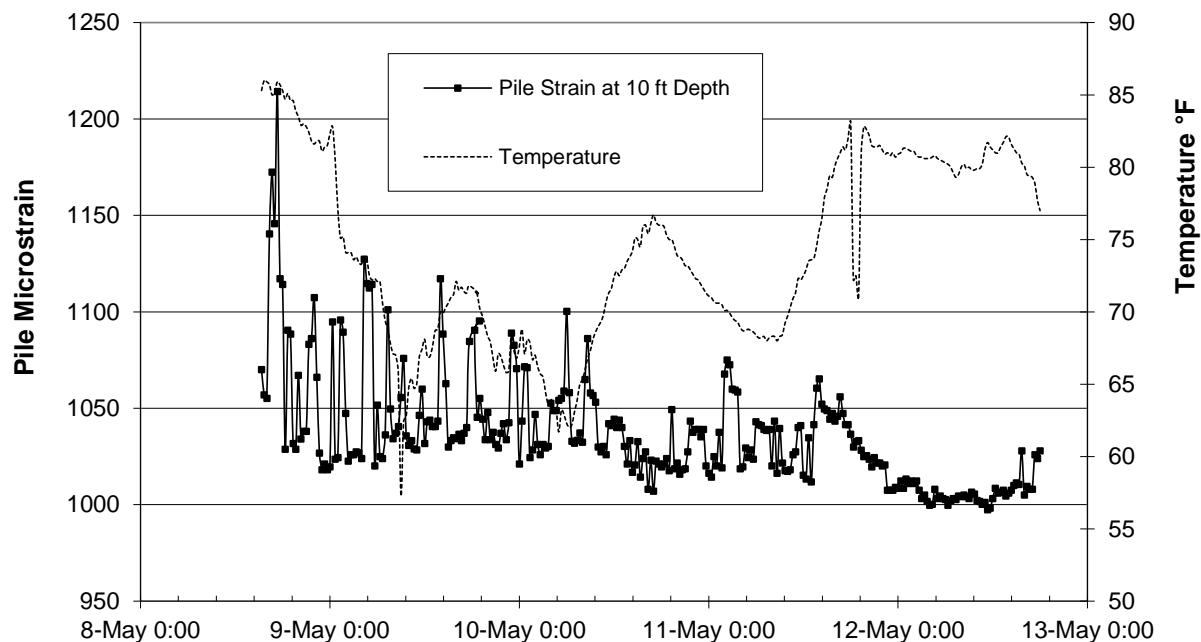


Figure 25. Daily induced strains on Pile 6 at 10 ft of the north abutment, Madison County Bridge.

Figure 25 shows the daily induced strains recorded on Pile 6 at 10 ft below the abutment. Strain gages indicated instability of readout on 8 May to 11 May, possibly caused by insufficient electrical connectivity. Overall, pile strains behaved inversely to temperature. Because of these fluctuations noted, the relationship between temperature and strain is a judgment call. Starting at 1120 μ strain on 9 May and terminating on 12 May at 1000 μ strain, the temperature changes from 72°F to 83°F resulted in an average decrease in strain of -10.9 μ strain / °F, similar to the result in Figure 24.

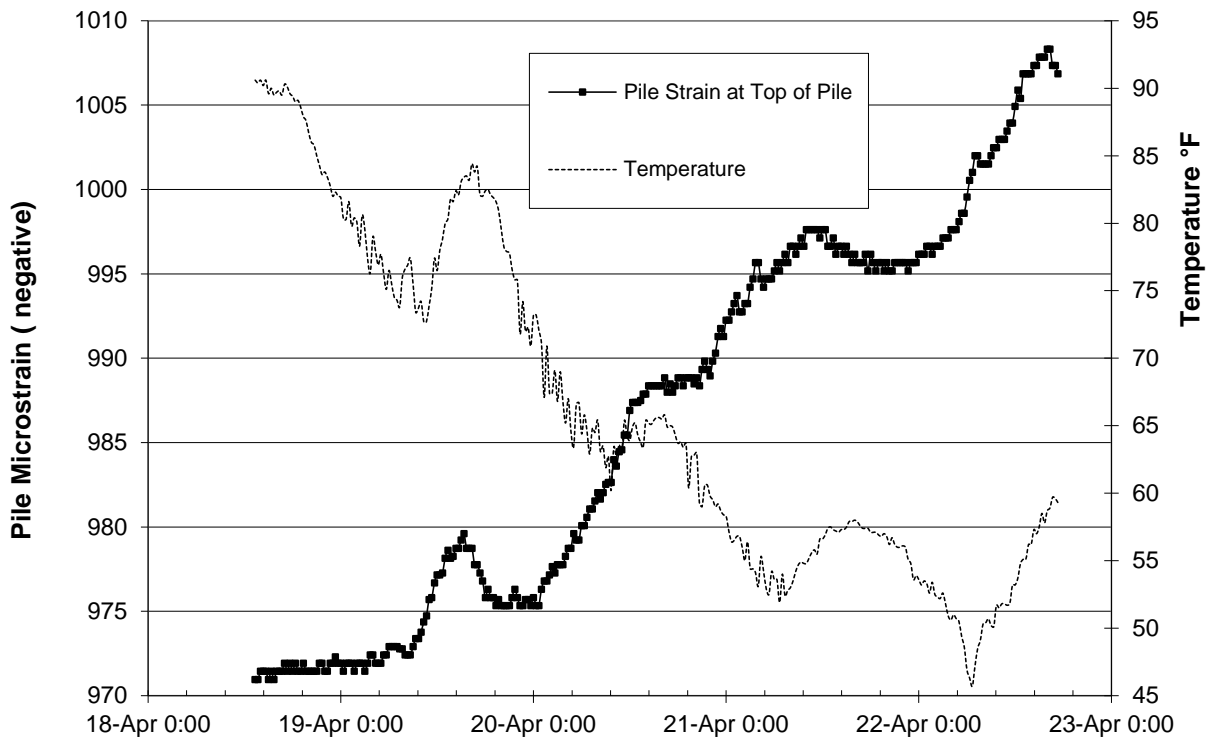


Figure 26. Daily induced strains at the top of Pile 5 of the north abutment, Pike County Bridge.

Figure 26 shows the daily induced strains recorded at the top of Pile 5 strains just below the encasement. Pile strain was an inverse relationship with temperature and has a temperature lag compared to ambient air temperature. Starting on 18 April pile stress was 29,190 psi and terminating on 22 April, and gradually reached 29,232 psi as temperature dropped from 90°F to 46°F. This change was $-0.955 \mu \text{ strain} / ^\circ\text{F}$. This inverse is due to the relaxation of stresses just below the point of load application due to abutment thermal contraction.

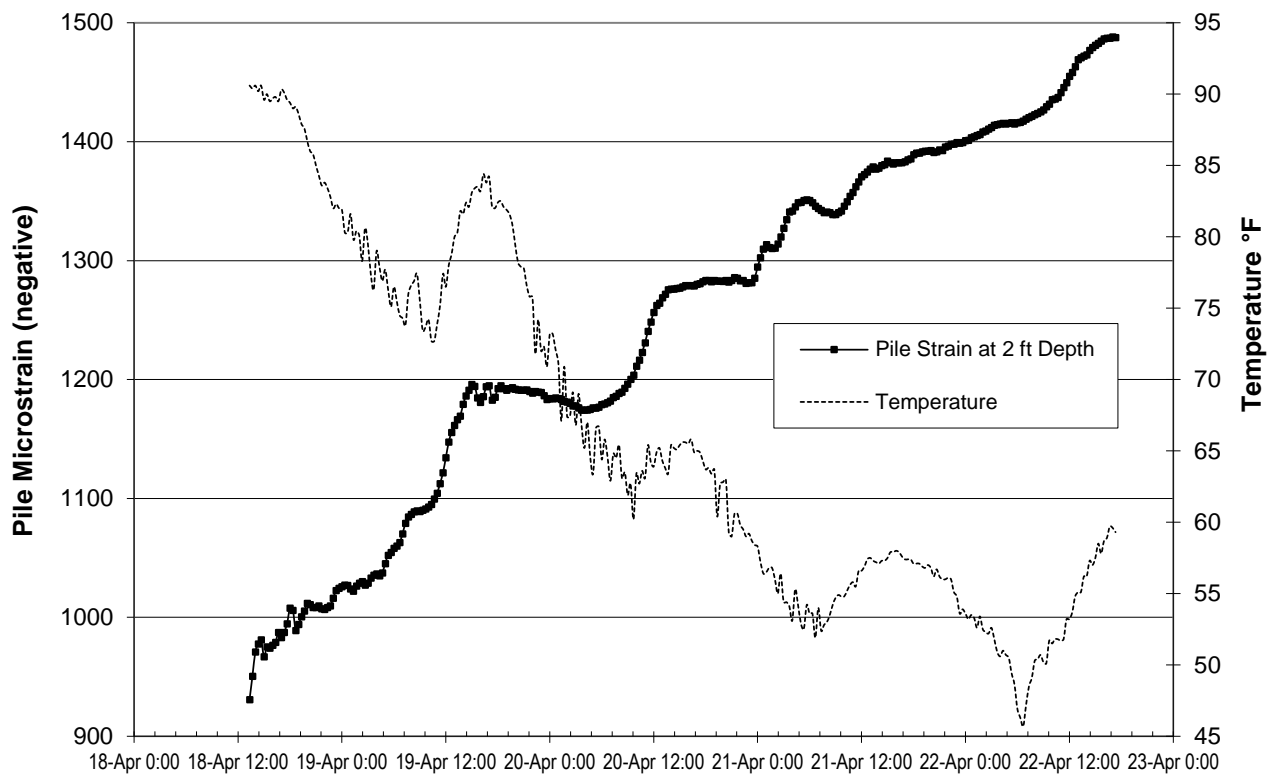


Figure 27. Daily induced strains on Pile 5 at 2 ft of the north abutment, Pike County Bridge.

Figure 27 shows the daily induced strains recorded on Pile 5 at 2 ft below the encasement. Pile strain is an inverse function of temperature. At a high temperature of 90°F on 18 April, the pile stress was at 26,680 psi. The peak stress during the test period was 43,200 psi, which occurred at 46°F. The μ strain vs. temperature was -12.954μ strain / °F.

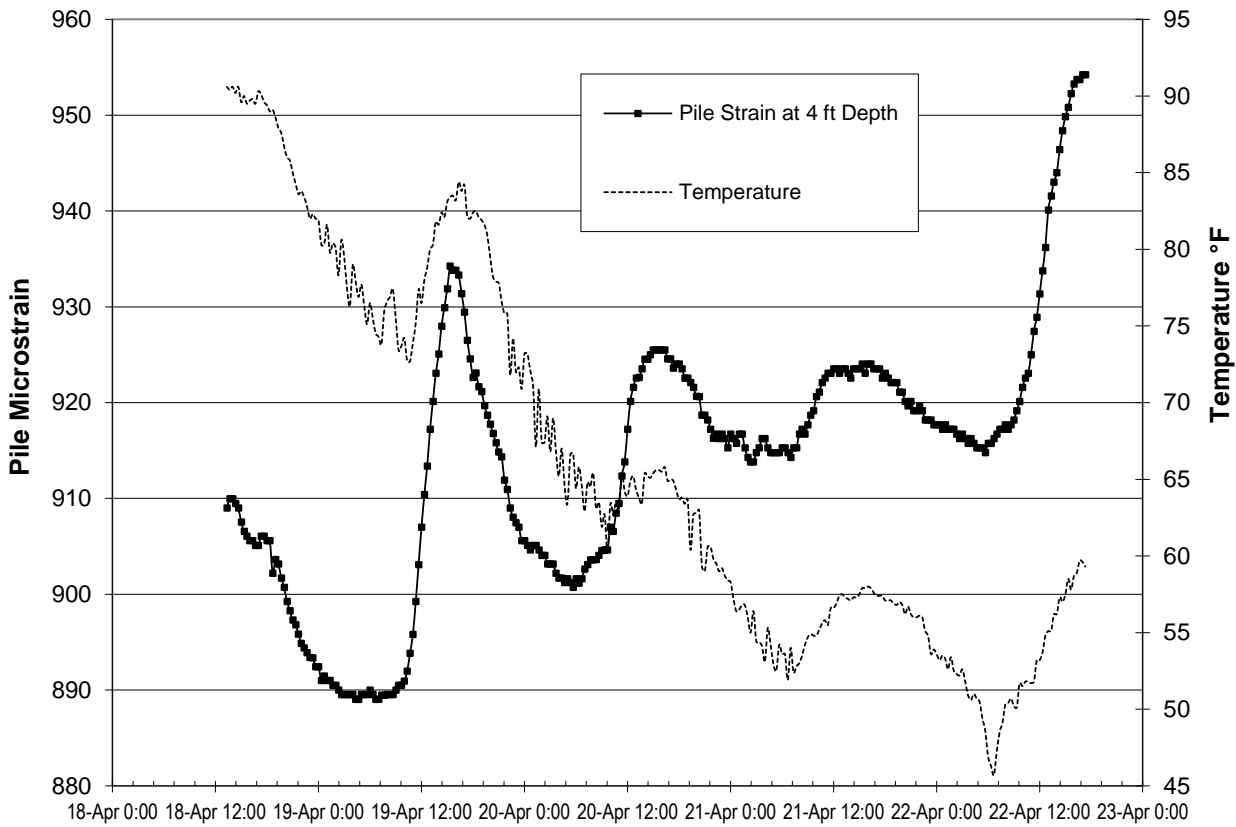


Figure 28. Daily induced strains on Pile 5 at 4 ft of the north abutment, Pike County Bridge.

Figure 28 shows the daily induced strains recorded on Pile 5 at 4 ft below the encasement. The relationship between strain and temperature is direct related. Five reversals of the three cycles were included in the calculation of average strain vs. temperate. Average μ strain vs. temperature was $1.066 \pm 0.342 \mu \text{ strain} / ^\circ\text{F}$.

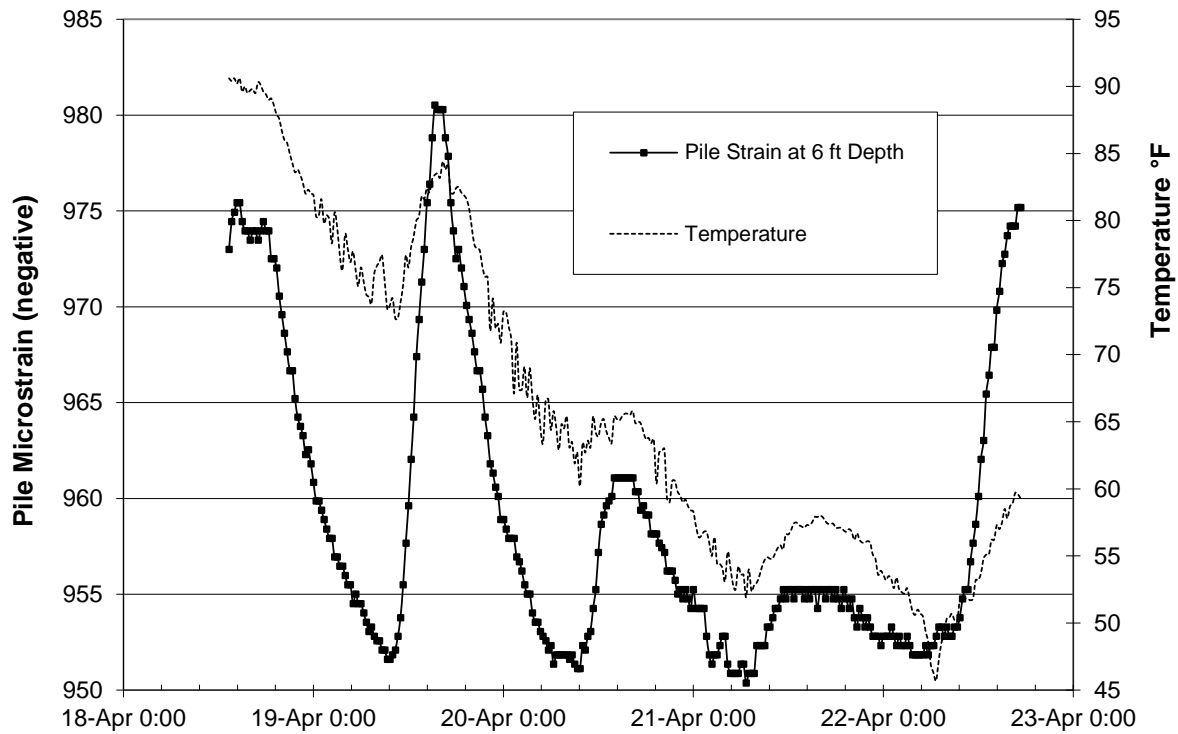


Figure 29. Daily induced pile strains on Pile 5 at 6 ft of the north abutment, Pike County Bridge.

Figure 29 shows the daily induced strains recorded on Pile 5 at 6 ft below the encasement. The pile strain was a direct function of ambient temperature with a negligible lag. At a high temperature of 90°F on 18 April, the pile stress was greatest at 28,300 psi. Six reversals of three cycles were selected to obtain an average strain vs. temperature of $1.458 \pm 0.664 \mu$ strain per °F.

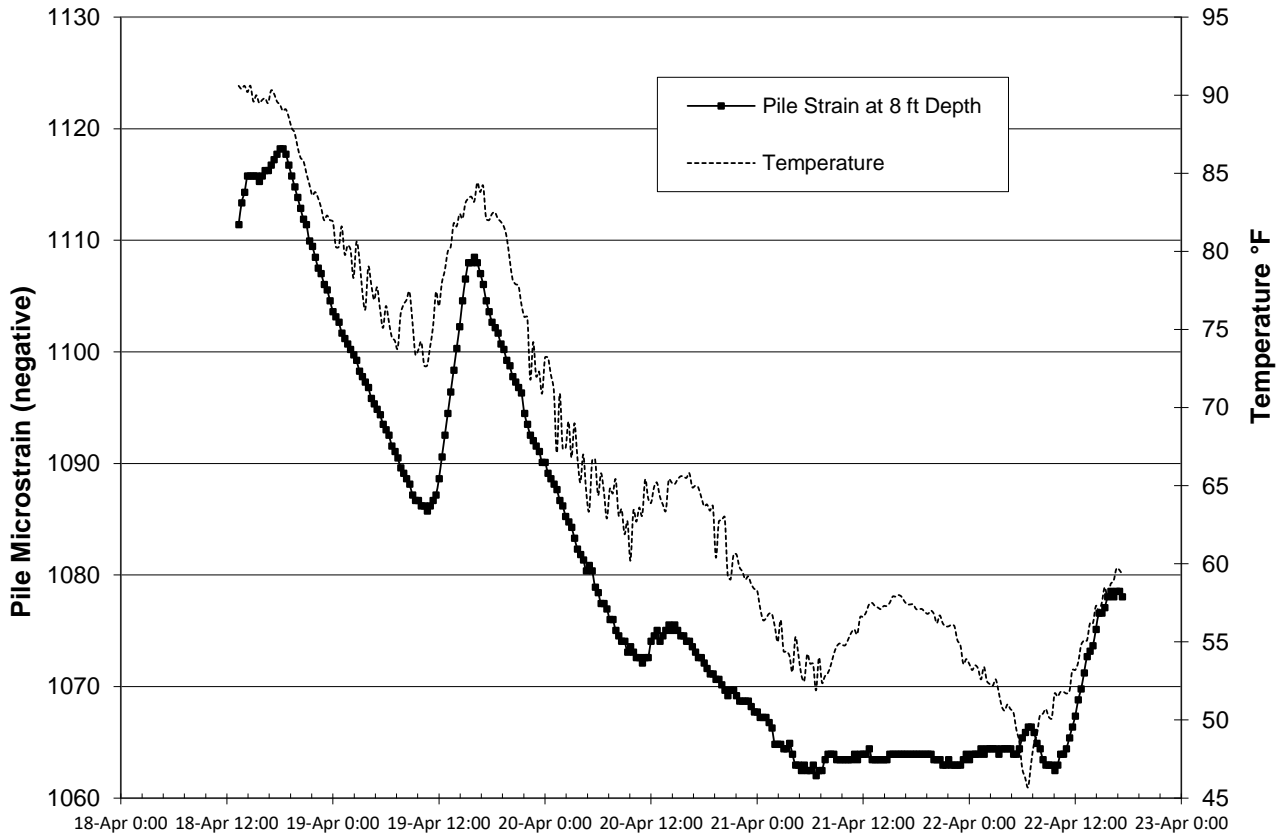


Figure 30. Daily induced strains on Pile 5 at 8 ft of the north abutment, Pike County Bridge.

Figure 30 shows the daily induced strains recorded on Pile 5 strains at 8 ft below the encasement. The pile strain was a direct function of temperature. At a high temperature of 90 °F the peak pile stress was at 32,400 psi. As the overnight lows between 46-52°F, the lowest strain reading of 1061 μ strain was recorded, decreasing pile stress down to 30,770 psi. A total of three cycles were analyzed for the relation between temperature and pile strain; three decreases and two increases were compared vs. temperature change. The average change in strain vs. temperature was $1.568 \pm 0.394 \mu$ strain / °F.

VERTICAL REINFORCING BAR STRAINS IN THE ABUTMENTS

Vertical reinforcement bars connect the diaphragm end abutment with the pile cap, typically using #5 rebars spaced on 12-in centers. Strain gages were attached by welding them to the rebars and wires were connected to the readout instruments to determine the magnitude of stresses during the year. Both shear and tensile stresses are induced in these rebars due to contraction and expansion of the superstructure. Rebar connections were only instrumented on the Madison, Pike, and Scott County bridges. Initial strain readings were taken after the bridge was complete whereby these values were taken as base lines. Initial values were then subtracted from subsequent readings to determine any increase or decrease in strain. The strains were then translated into stresses by multiplying them 29×10^6 psi, the nominal AASHTO modulus of elasticity for ASTM A706 reinforcing steel. Rebar stresses are summarized for the Madison, Pike and Scott County Bridges in *Table 3*.

Table 3. INTEGRAL ABUTMENT REINFORCING BAR STRESSES

<i>County</i>	<i>Madison</i>		<i>Pike</i>		<i>Scott</i>	
Air Temperature, °F	30	91	32	87	17	91
Gage	Rebar Stress, psi		Rebar Stress, psi		Rebar Stress, psi	
1	30,800	29,300	-41,200	23,500	41,900	27,800
2	31,000	29,900	-43,000	29,700	54,400	28,700
3	31,200	29,500	-36,900	30,200	51,100	36,300
Average of all 3 rebars	31,000	29,567	-40,366	27,800	49,133	30,933

The Madison County rebar stresses were positive, and only vary by an average of 1400 psi with a 61 °F temperature change. The rebar stresses in the Pike County Bridge abutment, which were mounted on the approach side rebars, changed from compressive stresses (negative) at freezing temperatures, and then reversed to tensile stresses (positive) as temperatures shifted upward during the warmer months. An average change of 2352 μ strain was observed for the 55°F temperature change. In the Scott County Bridge abutment, the rebar stress difference for a 74°F temperature change was 18,200 psi. The rebar stresses in Scott County Bridge abutment were all tensile. The Madison County bridges also showed tensile stresses during cold and warmer weather. The cold weather contraction of the decking induced stresses on these end cap rebars were significantly greater than stresses during the warmer temperatures. The side rebars undergo substantial reversal of stress due to their position.

A. *Fatigue Life of Reinforcing Bars.* Reinforcing bars keep the pile cap integral with the abutment. The failure of several bars would create displacement in portions of the integral abutment, leading to the failure of even more reinforcing bars. In this study, several rebars sustained very large strains and high mean stresses. Because of the deformations and rough hot rolled surfaces inherent to reinforcing bars, they have a lower high cycle fatigue strength of about 23 ksi compared to a fatigue strength of 40 ksi for smooth bars at 80 ksi ultimate tensile strength. There must be more than an adequate number of rebars to restrain the shear and bending stresses incurred when the pile cap and the integral abutments sustain significant expansion and contraction.

To avoid long-term fatigue initiation, alternating stresses applied to reinforcing bars in concrete were limited by the equation of Section 5.5.3.2 of AASHTO *LRFD Bridge Design Specifications* (Ref. 13):

$$\Delta\sigma \leq 21 - 0.33 f_{\min} + 8 \times (r / h)$$

Where

f_{\min} = min stress level (compression is negative)

r/h = ratio of the deformation base radius to its height

Since the values of r / h for rebars furnished for the bridges were not known, the value of 0.3 was used. The ratio of 0.3 provides a minor addition to fatigue strength of $8 \times 0.3 = 2.4$ ksi, making the allowable stress range $\Delta\sigma \leq 23.4 - 0.33 f_{\min}$. According to this formula, if there are compressive stresses associated with gravity or other loadings, this will improve the fatigue strength of the rebars. However, if there are additional positive mean stresses, such as from prestress loading of bars or from thermal effects, fatigue strength will decrease. In the integral abutments, the stresses incurred in the rebars are from bending and shear. Since the strain gages were mounted in the longitudinal direction, reinforcing bar shear stresses were not measured.

B. *Factors of Safety for Reinforcing Bars.* Daily strain data was not collected for rebars. However, annual changes in strain were recorded. *Table 8* summarizes the alternating and mean stresses for the reinforcing bars based on the averages of strains recorded in reinforcing bars for the integral abutment bridges of Madison, Pike and Scott Counties in *Table 3*. For comparison purposes, factors of safety for A706 and A615 rebars were computed. For ASTM A615 Grade 60 rebars, the required ultimate tensile strength σ_u is 90,000 psi minimum; for A706 Grade 60 rebars, the required ultimate tensile strength σ_u is 80,000 psi minimum.

For calculation of safety factor of reinforcing bars, the value of 23.4 ksi was used for fatigue strength σ_f in the Goodman fatigue relationship. The AASHTO fatigue strength of 23.4 ksi for rebars is slightly less than the AASHTO fatigue strength of 24 ksi in air value for Category C members in high cycle ($> 2 \times 10^6$) fatigue. The factors of safety for A706 and A615 rebars are summarized for comparison in *Table 4*, based on averages of the stresses determined in three rebars that had strain gages attached to them per each bridge.

The data of *Table 3* was placed into the Goodman fatigue failure equation (Ref.14) to evaluate the factors of safety for the abutment reinforcing bars of three bridges:

$$F = 1 \div [(\sigma_a / \sigma_f) + \sigma_m / \sigma_u]$$

Where

F = factor of safety

σ_a = alternating stress

σ_f = fatigue strength (23.4 ksi for rebar per AASHTO formula)

σ_m = mean stress

σ_u = ultimate tensile strength (80 ksi for A706; 90 ksi for A615)

Table 4. STRESSES AND FACTORS OF SAFETY FOR REINFORCING BARS

<i>County</i>	<i>Alternating Stress, psi</i>	<i>Mean Stress, psi</i>	<i>Factor of Safety, A706 Rebars</i>	<i>Factor of Safety, A615 Rebars</i>
Madison	717	30,283	2.44	2.72
Pike	34,083	-6,283	0.72	0.72
Scott	9,100	40,033	1.12	1.20

The factor of safety for A615 rebars is slightly improved compared to A706 rebars due to their higher tensile strength, except for Pike County where they were equivalent because the mean stress was compressive. However, these resulting factors of safety are somewhat deceiving considering that impact toughness is generally not required for rebars. Rebars, unlike structural steels, have low impact toughness values that seldom exceed 15 ft-lbs due to their higher carbon, sulfur, phosphorus and nitrogen contents. Typical impact toughness for ASTM A615 Grade 60 rebars is about 4-7 ft-lbs and 10-14 ft-lbs for ASTM A706 bars. These values are typical but are not certified by the manufacturers.

Due to lack of controls on basic chemical composition of steels used for A615 rebars, fracture toughness is reduced in A615 rebars due to their typically higher carbon and sulfur contents compared to A706 bars. Previous impact tests on A615 with carbon levels $> 0.30\%$ and without benefit of vanadium to bind with nitrogen had reduced their impact toughness. For A706 bars,

an impact toughness range of 10 to 14 ft-lbs is approximately equivalent to a fracture toughness range of 40 to 49 ksi [in]^{0.5} as determined by the Roberts - Newton CVN-fracture toughness correlation equation of $K_{Ic} = 9.35 [CVN]^{0.63}$, where CVN is in ft-lbs and K_{Ic} is in ksi [in]^{0.5} (Ref. 15). The tensile stresses that were sustained by rebars in this study were substantial.

Based on the low factors of safety for the Pike and Scott integral abutment bridges, it is evident that the rebars are at risk. They were subject to tensile stresses 51 to 67% of nominal yield strength and experienced wide strain ranges. Madison County was the exception, with a mean stress at about 50% of yield, but had a lesser stress range.

Fortunately, the rebars were epoxy coated, which delays the formation of pitting corrosion. However, due to rebar deformations, stress concentrations are 2 to 3 times the nominal stress. Stress concentrations in rebars arise from the deformation pattern and its notch acuity, which depends on whether a sharp base radius is used by the manufacturer. If the epoxy coating is damaged or if substantial defects in coating are present, these sites can form corrosion pits.

For bent reinforcing bars with sharp deformation acuties and low impact toughness, notches at the base of the deformations can easily form cracks and then partially or completely rupture when highly stressed due to low fracture toughness. The outside radius of a bent rebar experiences yielding where surface stresses will exceed 60 ksi. If cracks form, a rebar with minimal fracture toughness will rupture. This is the purpose of qualification bend testing for rebars prior to acceptance.

Rebar with a Charpy V-notch impact toughness of 5 ft-lbs per the Roberts – Newton correlation (Ref. 15) has a fracture toughness of $K_{Ic} = 25.8$ ksi [in]^{0.5}. The fracture mechanics relationship for a bar in bending is $K_{Ic} = 1.1 \sigma [\pi a]^{0.5}$ (Ref.16), where a = crack depth. If fracture toughness is 25.8 ksi [in]^{0.5} for a Grade 60 rebar with 5 ft-lbs impact toughness, when bent at its minimum required yield strength of $\sigma = 60$ ksi, then the critical crack depth $a = 0.049$ in. A crack depth of 0.049 in is only 8% of the diameter of a #5 rebar, which has an average minimum deformation height of 0.028 in. If one of the rebar deformations has a sharp radius crack at its base, the additional crack depth needed for bar rupture at 60 ksi is reduced to about 0.021 in.

For these reasons, ASTM A706 reinforcing bars used in the pile cap should have minimum Charpy V-notch (CVN) impact toughness values of at least 15 ft-lbs at 40°F. This is the impact toughness requirement for redundant members for Zone 2 per Table 8 of ASTM 709 for 50 ksi steels. Requiring 15 ft-lbs increases the fracture toughness to 51.5 ksi [in]^{0.5} and extends the critical crack depth to 0.194 in, which is 31% of the nominal diameter of a #5 rebar.

These considerations point to the need for design requirements that A706 rebars must have at least 15 ft-lbs of impact toughness when used in integral abutment bridges.

PILE AND REINFORCING BAR STRESS AND STRAIN DATA AND DESIGN LIFE

The data presented previously in this report shows that soil compressive strength affects pile strain and stress, but also changes the shape of the deformation of the pile. In general, a lower compressive strength of the soil surrounding the piles result in greater pile deformation and strain, increasing pile stresses.

A. Pile Strains due to Temperature Changes from Warm to Cold Weather over One Year.

Pile strains measured at temperatures at or below the freezing of water indicated that some piles were yielding. The point of fixity for the piles was found to be somewhat variable, and even varied on piles that were adjacent to each other. The Pike and Madison county bridges had piles that yielded. Even though the HP piles were placed with the strong axis parallel to the longitudinal axis of the bridge, it is doubtful that weak axis piles would have markedly different behavior under the same conditions. However, weak axis piles would probably not experience as many yielding events as strong axis piles due to their lower moments of inertia during the cantilever bending induced from bridge expansion and contraction. Daily changes in pile stress are quite small compared to that stress and strain sustained over one year. Using the data from *Figure 7* through *Figure 15*, the yearly change in strain can determine the alternating and mean stresses for piles.

For the Pike County Bridge, the largest change in stress occurred at Pile 5, where a change of 2400 μ strain occurred from contraction from 93°F down to 31°F, resulting in an alternating stress of 34,800 psi. The mean stress is -3,625 psi, which provided a small increase in fatigue life.

B. Fatigue Strengths of HP Piles. HP piles in integral abutment bridges are redundant members. HP piles are commercially available in Grade 36 and Grade 50 minimum yield strengths and are made of several commercial steels, including ASTM A36, A572, A588 and A690. Their inherent fatigue strengths are related to their tensile strengths, chemical composition and impact toughness. The mechanical properties of these four steels are summarized in *Table 5*.

Table 5. REQUIRED MINIMUM MECHANICAL PROPERTIES OF HP STEELS

<i>ASTM Standard</i>	<i>Yield Strength, ksi</i>	<i>Tensile Strength, ksi</i>	<i>% Elongation in 8 in Gauge Length</i>
A36	36	58-80	20
A572	50	65	21
A588	50	70	18
A690	50	70	18

In general, these steels have similar minimum tensile strengths, except for the variability of A36. Wide flanges have been subjected to numerous fatigue tests in air conducted on behalf of AASHTO, AWS and the Ship Structure Committees (Refs.17, 18 and 19). The former National Bureau of Standards (now NIST) and the Naval Research Laboratory, through its research partners, have extensively studied the fatigue characteristics of structural steels in both air, soils, saline and seawater environments (Refs. 20 and 21). This extensive research data base regarding the fatigue lives of A36 and A572 steels at various stress ranges and the effects of certain soil environments on fatigue and crack propagation can be very useful when integral abutment bridges will be constructed in locations where soil resistivities are less than 2,000 ohm-cm. Soil resistivity is subject to variations due to permeability of soils, their inherent heterogenous composition, intrusion of river water, and the frequent use of highway deicing salts which eventually permeate soils over the 75-year design life of piles.

HP piles are hot-rolled steel wide flange shapes that do not have any welded attachments and are considered to be a “Category A” fatigue detail by AASHTO and AWS. The AASHTO and AWS fatigue strength of 24 ksi in air beyond 2×10^6 cycles for Category A shapes made of A36 steel and other similar steels has been confirmed by many other reliable investigations. Based on a typical yield strength of 65,000 psi for A36 steel, the fatigue strength σ_f for a hot rolled steel plate at 10^7 cycles is $\sigma_f = C_1 \times C_2 \times 65,000 = 0.5 \times 0.7 \times 65,000 = 22,750$ psi, where C_1 is a conversion factor from tensile strength and C_2 is an adjustment factor for surface roughness of hot rolled steel (Refs. 22 and 23).

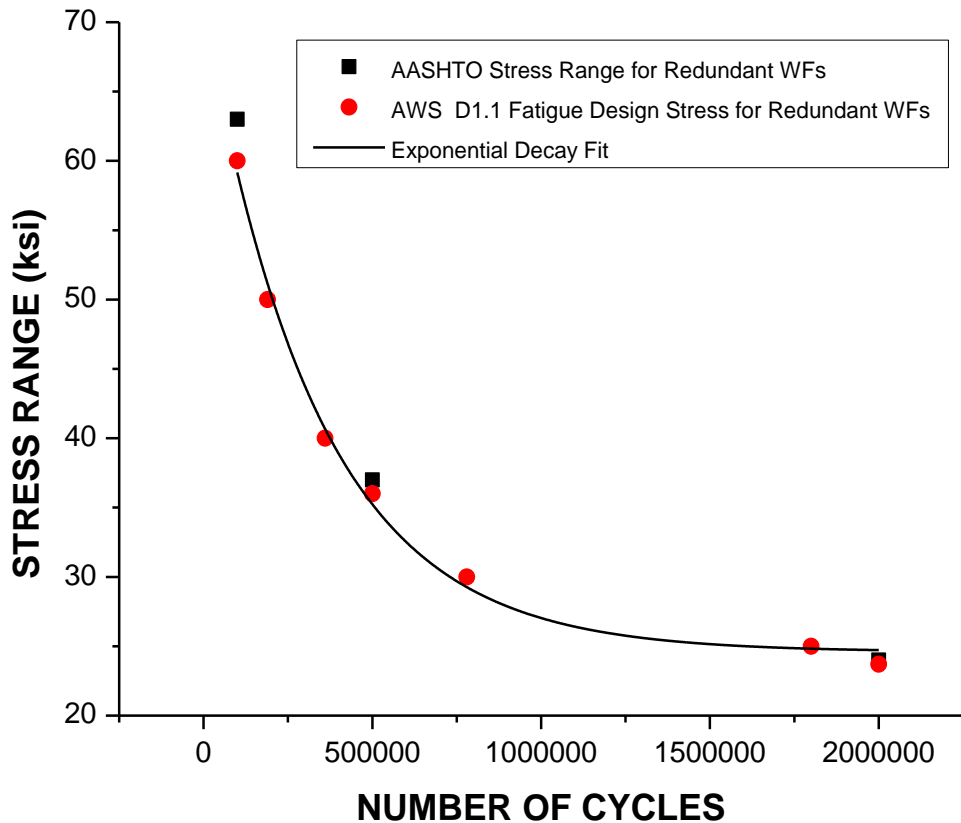


Figure 31. Hot rolled wide flanges in bending are considered as a “Category A” structural fatigue detail by both AASHTO and AWS. The fatigue curve for permissible stress ranges (S_{range}) for AASHTO / AWS Category A details is an exponential decay function. Data points were taken from Ref. 18.

SAE 1020 is a widely-used commercial steel that has very similar composition and properties compared to ASTM A36. Unnotched smooth 2.0 in diameter SAE 1020 bars had fatigue strengths of 28 ksi at 10^7 cycles. When notched with a stress concentration factor of $K_t = 2.0$, fatigue strength decreased to 16 ksi at 10^7 cycles (Ref. 24).

The stress range S_{range} vs. number of life cycles N for an unnotched steel Category A HP pile is an exponential decay function, $S_{range} = 24.6 + 46.4 e^{(-N / 339,639)}$, as shown in Figure 31. The life of integral abutment bridges is required to be 75 years of service. Since 365 temperature changes will be sustained in one year, the absolute minimum fatigue life would be $75 \times 365 = 27,375$ cycles. Taking unforeseen conditions into account, a fatigue strength at 200,000 cycles

was calculated from the Category A exponential decay fatigue equation. The stress range for 200,000 cycles in air is $S_{\text{range}} = 24.6 + 46.4 e^{(-200,000 / 339,639)} = 50.4$ ksi. Based on strain gage readouts from HP piles in this study, peak stresses routinely exceeded the minimum yield strength of 36 ksi required for HP piles made of A36 steel. Inserting the value of 36 ksi for S_{range} , the equation to determine HP life cycle becomes $36 = 24.6 + 46.4 e^{-N / 339,639}$. Subtracting 24.6 from 36.0, the \log_e form of the equation then becomes $\ln(11.4) = \ln(46.4) - (N \div 339639)$. Further subtraction of the quantity $[\ln(46.4) = 3.837]$ from $[\ln 11.4 = 2.434]$, then $-N \div 339639 = -1.403$, whereby $N = 476,515$ cycles. However, there is some uncertainty as to what actual stresses were sustained by piles in the plastic range because strain gages are not linear after their elastic ranges are exceeded and disbonding may also have occurred.

The value of 50.4 ksi is only for fatigue life of HP piles cyclically stressed in air. However, the effect of driving of steel piles into soils with low resistivity will significantly reduce the AASHTO fatigue strength obtained in air, depending on soil resistivity, which may vary as a function of soil depth. Soil characteristics and their effects on the fatigue characteristics of steel are addressed in the next sections of this report.

Using the AASHTO / AWS design stress ranges, the fatigue strength in dry air at a conservative life of 200,000 cycles was to take unforeseen conditions into account. The fatigue strength in air at 200,000 cycles was calculated to be $S_{\text{range}} = 24.6 + 46.4 e^{(-200,000 / 339,639)} = 50.4$ ksi. A value of 50.4 ksi is later used in this report for fatigue strength to determine factors of safety in the Goodman fatigue failure equation for piles located in low resistivity soils (Ref. 14).

C. Daily Temperature Changes Inducing Pile Strains. Depending on locations where the strain gages were placed and the behavior of the pile when driven into variable soil conditions, stresses could be direct functions of temperature or be inversely related to temperature. The pile strains at the top of the Pike and Scott County bridges were inverse functions of air temperature throughout the several days of measurement. However, on the Scott County Bridge, the strains exhibited opposite behavior and were direct functions of air temperature below the top of the piles. For the piles of the Pike County Bridge down to only 2 ft depth, strains were inverse functions of air temperature, but below 2 ft, pile strains were directly related to temperature. The variability of strain with ambient surface temperatures for these bridges is summarized in *Table 6*. It is noted in *Table 6* that strains are not entirely predictable in terms of whether they are directly or inversely related to temperature. Moreover, in several cases, they

do not reflect the normal behavior of a cantilever pile subject to end forces and deflections, but were subject to changes in soil characteristics as a function of pile depth.

A normal pile deflection, assuming uniform soil characteristics as a function of pile depth, would be expressed as a polynomial function (Ref. 25), as a function of depth along the pile and the length of the pile, as determined from its point of fixity:

$$y = [W (2L^3 - 3L^2a + a^3)] \div (6 E I)$$

where

y = deflection, inches

a = depth from surface end of the pile, inches

L = surface end of pile to its point of fixity, inches

E = modulus of elasticity of steel, 29×10^6 psi

I = moment of inertia of pile, inches⁴

For the HP piles in this study, the moment of inertia was taken from the strong axis. In some cases, there appeared to be abnormal responses to small temperature changes way beyond typical values of 1.0 to 3.0 μ strain / °F as shown in *Table 6*.

Table 6. VARIABILITY OF PILE STRAIN WITH DAILY TEMPERATURE CHANGES

County	Abutment	Pile Number	Depth, ft	Average μ strain/°F *
Scott	North	6	Top	-2.2708 \pm 0.290
Scott	North	6	2	+1.799 \pm 0.917
Scott	North	6	4	+1.317 \pm 0.282
Scott	North	6	6	+1.975 \pm 0.664
Scott	North	6	8	GNR
Scott	North	6	10	+1.573 \pm 0.146
Madison	North	6	Top	+3.004 \pm 0.585
Madison	North	6	2	GNR
Madison	North	6	4	GNR
Madison	North	6	6	-1.277 \pm 0.590
Madison	North	6	8	-16.430**
Madison	North	6	10	-10.900
Pike	North	5	Top	-0.955
Pike	North	5	2	-12.95
Pike	North	5	4	+1.066 \pm 0.342
Pike	North	5	6	+1.458 \pm 0.664
Pike	North	5	8	+1.568 \pm 0.394
Pike	North	5	10	GNR

*When listed as negative, the strain function is inversely related to temperature; when positive, it is directly related to temperature.

**Gage indicated both direct and inverse behavior; treated as largely inverse.

GNR = gage not responsive due to malfunction.

D. Consideration of Pile Fatigue from Daily Thermal Cycles. Piles that are sustaining daily changes in strain and stress are subject to fatigue. The magnitude of the changes in strain or stress and their frequency determine the extent of fatigue damage. For an HP pile with an ASTM minimum yield strength of 36 ksi, the required tensile strength range is 58 to 80 ksi. The typical ultimate tensile strength for these piles averages about 65,000 psi. The AASHTO and AWS fatigue strength for a fatigue life greater than 2×10^6 cycles is 24,000 psi. According to AASHTO requirements, an integral abutment bridge requires at least 75 years of service. Since the bridge life only requires $75 \text{ years} \times 365 \text{ days/year} = 2.7 \times 10^4$ cycles, use of the AASHTO fatigue strength of 24 ksi at 2×10^6 cycles would be very conservative. A life cycle requirement of 2×10^5 cycles at a fatigue strength of 50.4 ksi was considered to be more realistic.

For the Scott County Bridge, $-2.708 \mu \text{ strain} / ^\circ\text{F}$ at the top of the pile was the largest amount of strain per day. The average change in daily temperature is $20.2 ^\circ\text{F}$, resulting in 1,334 psi of alternating stress. For the Madison County Bridge, $3.004 \mu \text{ strain} / ^\circ\text{F} / \text{day}$ also was at the top of the pile. Average daily temperature change was $15.5 ^\circ\text{F}$, resulting in 1,350 psi of alternating stress. For the Pike County Bridge, the largest changes occurred at 8 ft at $1.568 \mu \text{ strain}/^\circ\text{F}$ per day. Average daily temperature change was $15.3 ^\circ\text{F}$, resulting in 696 psi of alternating stress.

All these alternating stresses are very low, but since these nominal stresses are locally magnified due to surface corrosion and pitting, they were multiplied by an average stress concentration factor of 2.5. Fatigue strengths were taken from the AASHTO and AWS stress ranges for Category A hot rolled wide flanges at 200,000 cycles. These concentrated daily stresses were then combined with mean stresses to evaluate a factor of safety using the widely accepted Goodman fatigue failure equation. The Goodman fatigue failure relationship with specific quantities for its variables is as follows:

$$(\sigma_a / \sigma_f) + (\sigma_m / \sigma_u) = 1$$

Where σ_a = alternating stress, $(\sigma_{\max} - \sigma_{\min}) / 2$
 σ_f = fatigue strength at required life of 200,000 cycles = 50.4 ksi
 σ_m = mean stress, $(\sigma_{\max} + \sigma_{\min}) / 2$
 σ_u = ultimate tensile strength, taken as 58 ksi for A36 steel

Table 7 summarizes the average temperatures, mean stresses, and alternating stress due to daily thermal changes at the various locations on specific piles for three bridges. Fatigue safety factors for the Pike, Macon, Madison and Scott County bridges were calculated based on the

widely used Goodman fatigue failure relationship (Ref. 14). These calculations of safety factor would be applicable examples if the soil resistivities were greater than 5,000 ohm-cm. It should be noted that soil resistivities were not determined prior to construction of these bridges.

Table 7. SUMMARY OF DAILY STRESS CHANGES

County	Pile Number & Depth	Average Daily Temperature Change, °F	Alternating Stress, psi	Concentrated Alternating Stress, psi*	Average Mean Stress, psi	Factor of Safety**
Scott	6; top	20.2	1,375	3,437	31,804	1.63
Madison	6; top	15.5	1,395	3,487	25,072	1.99
Pike	5; 8 ft	15.3	720	1,800	30,247	1.80

*Stresses in localized surface pits have stress concentration factors that range between 2-3 times their nominal stress. An average stress concentration factor K_t of 2.5 was applied to the alternating stress.

** The Goodman failure equation was used to calculate factors of safety.

E. *Determination of fatigue factor of safety for piles.* The factors of safety for the four bridges, based on annual changes of stress, are summarized in Table 8.

Table 8. FATIGUE SAFETY FACTORS
BASED ON MAXIMUM ANNUAL STRESS CHANGES*

County	Alternating Stress, psi	Mean Stress, psi	Factor of Safety**
Pike	34,800	-3,625	1.59
Macon	20,387	31,349	1.06
Madison	15,892	14,036	1.80
Scott	4,292	31,755	1.58

*Failure life in this table considers mean stress, but does not address any adverse soil conditions. The safety factors are based on the AASHTO fatigue strength of 50.4 ksi at 200,000 cycles for A36 piles in air.

**Factor of safety, including mean stress, was determined using the Goodman failure equation.

F. *Corrosion Fatigue and Crack Propagation.* Corrosion fatigue affects the fatigue strength of steel under cyclic loading by decreasing the number of fatigue cycles to failure in moist conditions when compared to the number of fatigue cycles to failure in dry air. Corrosion fatigue is typically presented by plotting the cyclic stress vs. number of cycles (S-N curve) to failure in air or dry nitrogen alongside the same specimen S-N curve, except that the fatigue test conditions are completed in a conductive aqueous media or water spray. Saline or sea waters are also used to simulate the conductivity of moist soil, although most of those tests were

conducted at much higher frequencies compared to the very low frequency of loading in integral abutment piles.

In *Figure 32a*, corrosion fatigue of 50 ksi yield steel specimens in a 3% salt solution without cathodic protection is plotted against the same specimens fatigue-tested in air. The “endurance limit” of 42.7 ksi in air disappears when steel is fatigue-tested in water and is further reduced to 14.2 ksi [10 kg/mm^2] in salt water at 3×10^6 cycles.

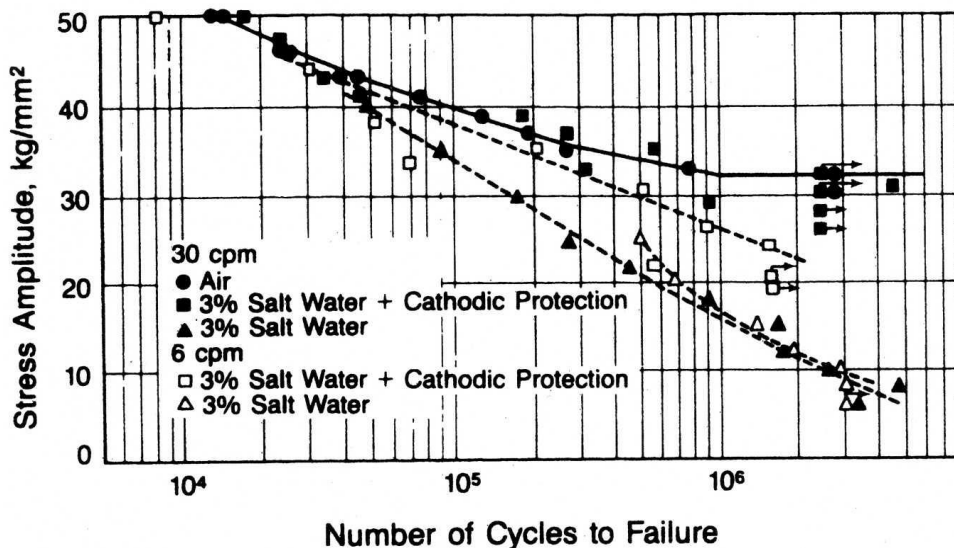


Figure 32a. Exposing cyclically stressed steel to moist and conductive media at 30 cycles per minute causes a substantial loss of fatigue strength when compared to the same cyclic stress levels in dry air. To convert from 1 kg/mm^2 to psi, multiply by 1419. From Ref. 19.

The steel in *Figure 32a* was a 50 ksi yield steel of 0.17% carbon and 1.35% manganese, similar to compositions of ASTM A36 and A572 structural steels. At 2×10^6 cycles, fatigue strength in air is relatively constant at 43 ksi, but sharply decreases to a range of 8-13 ksi when fatigued in salt water. Similar studies have shown that the fatigue strength of lower carbon steels at 1×10^7 cycles decreases from 24 ksi to 15 ksi in fresh water and from 24 ksi in air to 5 ksi in salt water (Ref. 27). However, the rate of stress application is 30 cycles per minute, in contrast to stress cycling in an integral abutment bridge which occurs over 12 hours. See *Figure 33* to see the effects of rate of stress cycling on the severity of corrosion fatigue.

The cracking of the web detail in *Figure 32b* is a good example of conjoint action of corrosion fatigue and the effects of low winter temperatures, which resulted in significant expansion and

contraction of bridge girder lines. Most steels have lesser impact toughness at sub-zero temperatures which were sustained in early 2019 in the Chicago area. The load transfer across this expansion joint originates from truck axle loadings, resulting in continual cyclic stresses, thereby causing crack propagation which originated from a sharp corner crack.



Figure 32b. In this photograph, an expansion joint shelf consisting of equal leg angles bolted to a girder web sustained a crack at a sharp corner due to cantilever action from the adjacent girder, causing crack advancement under repeated cyclic stress due to heavy truck traffic. The failure of the girder web and bending of the lower flange caused a shutdown of the expressway. Temporary supports are shown to keep traffic moving. Crack was discovered on Lake Shore Drive Bridge at Randolph St. in Chicago by electrical crews working on traffic signals. *Chicago Tribune* photo, dated February 13, 2019.

Corrosion fatigue occurred because the angles that are bolted to the girder web form a shelf, trapping moisture which included saline deicing fluids. The crack initiated at a sharp corner because it is a point of stress concentration and the web crack is further constrained by the horizontal bolted angles. After the crack path travels at or slightly beyond the shelf angles, it propagates directly downward through the web due to direct tension induced by cantilever bending forces. The flow lines of the entrapped water and visible drainage from the web angles are evident from the corrosion products that surround the crack pathway.

G. *Factors Affecting Corrosion Fatigue in Soil Environments.* The corrosion fatigue of steel in soils environments is affected by the following variables: (a) corrosion fatigue increases with decreasing soil resistivity; (b) increases when more dissolved oxygen or aeration is present in the soil; (c) increases as temperatures increase; (c) increases as the frequency of applied stresses decreases; (d) increases if more chlorides and sulfides are present in the soil; (e) decreases if coatings are present or if cathodic protection is applied.

Compared to most laboratory tests, the strain rates applied due to expansion and contraction of decks are slow in integral abutment piles, permitting greater time for the opening of pits and crack formation and propagation. When the frequency of cyclic loading is decreased, the effects of corrosion fatigue are further accentuated. As shown in *Figure 33*, corrosion fatigue increased because the cyclic strain rate decreased from 17 cycles / min to 1.1 cycles / hr.

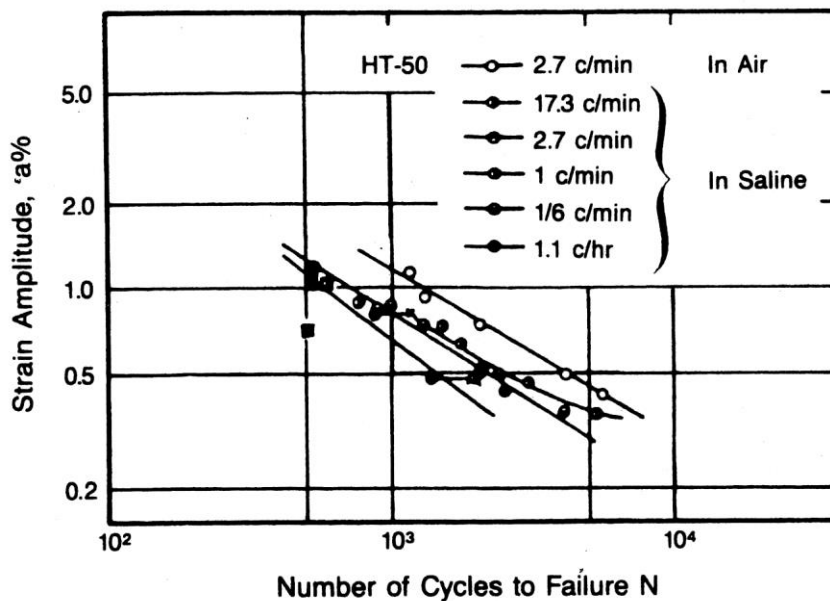


Figure 33. In the above graph, the % of decrease of strain amplitude of fatigue in air is shown as a function of cyclic frequency. Lower cyclic frequencies resulted in greater fatigue damage compared to higher cyclic frequencies. At the lowest frequency of 1.1 cycles / hr, the tolerable strain amplitude was only 40% of the number of cycles to failure in air. The SAE steel in this study had a 50 ksi yield strength with properties similar to ASTM A588 and A572 steels (Ref. 28).

This has definite implications for piles which are being stressed at very slow rates of 1 cycle per day, permitting corrosion pits to form. Pits can eventually form cracks if stresses are at or above yield, permitting cracks to propagate into the pile due to applied stress ranges and crack

lengths. Corrosion fatigue is problematic in conductive soils when resistivity is 2,000 ohm-cm or less. Since piles are driven to depths of 20 ft or more and their points of fixity vary between 10 to 16 ft, they are not as sensitive to temperature changes, except for pile sections near the surface. If the piles are in locations where deicing salts are in prevalent use, or the soils contain sulfide and chloride ions, these ions are particularly damaging since they tend to cause the formation of pits and acidification of the corroded areas.

Fortunately, not all soils will have high salt concentrations and the backfill used to support the approaches should have high resistivity. In addition, there are provisions for adequate drainage in integral abutment designs. However, where deicing salts are frequently used, the buildup of chlorides could be appreciable. Barrier materials, after a long period of service, are subject to diffusion of the saline media due to expansion and contraction and subsidence of the backfill. This effect has been identified by the State of Iowa (Ref. 29).

However, the effect of soil resistivity on the corrosion rates of carbon steels is dramatic, as shown in *Figure 34*. The exponential decay rate equation to predict the corrosion rate of A36 and other lower carbon steels, based on the data contained in *Figure 34*, is:

$$C_{rate} = 0.5 + 2.2 e^{(-R / 1846)}$$

Where

C_{rate} = corrosion rate in mils / yr (mpy)

R = resistivity, ohm-cm.

Pitting rates can range from 2-5 times the overall corrosion rate. The pitting depth rate at 100 ohm-cm was estimated to range from 5.2 to 7.8 mils/yr.

Another problem of concern is driving the piles into foundation soils which contain waste materials such as cinders or slag, which create substantial galvanic differences vs. steel. Cinders and slag are coarse particles that can generate pits and are good cathodes that provide sites for the oxygen reduction reaction which affects corrosion rates in most neutral solutions.

When cinders are dispersed in clay or peaty or loam soils which do not drain well, they can also increase the corrosion rate of steel. When R = 1,000 ohm-cm, the corrosion rate is 1.78 mpy; at 100 ohm-cm, the rate is 2.58 mpy.

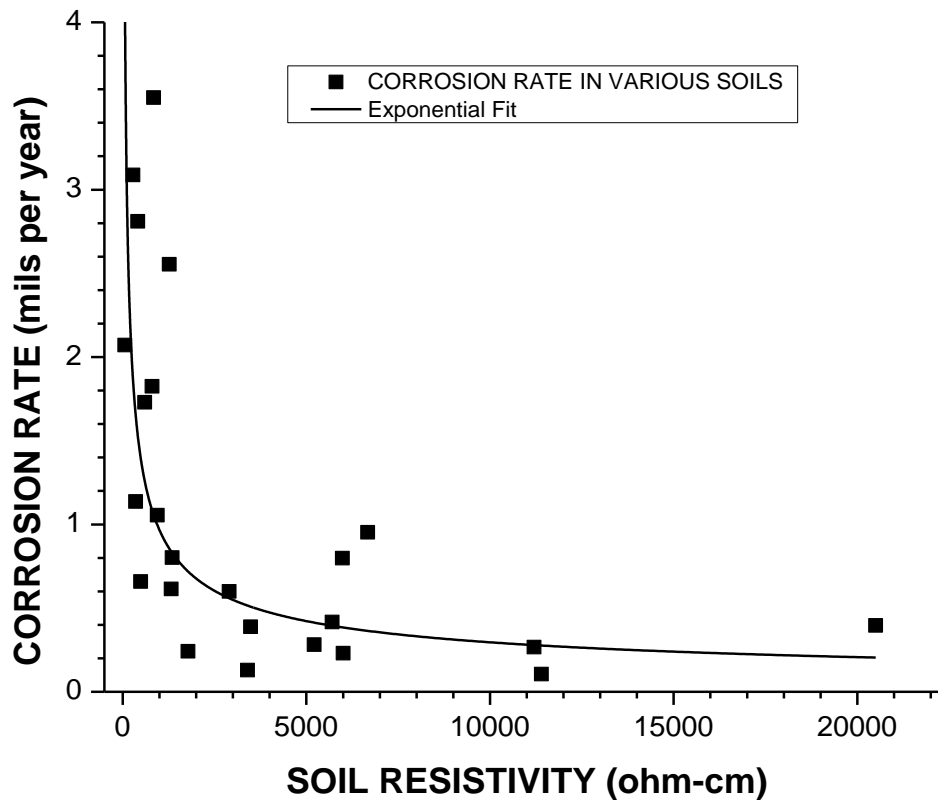


Figure 34. The change in corrosion rate of carbon steels as a function of resistivity is very substantial as the soil resistivity decreases to 2000 ohm-cm or less. Unfortunately, pit depths can be up to 2-5 times the overall corrosion rate, resulting in many pitting sites for crack initiation. Pitting rates are dependent on the soil resistivity. Data is derived from Ref. 20.

H. *Effects of Temperature on Corrosion Rates.* In general, most chemical reaction rates in water solutions or moist soils typically increase as a function of temperature. However, if the temperatures exceed 180°F or more, the dissolved oxygen in water solutions will be either reduced or driven out, causing corrosion rates to substantially decrease. The effect of temperature on corrosion rates of steel in lower resistivity media is shown in Figure 35.

The relative change in corrosion rates, as in many other chemical reactions, generally increases as a function of increasing temperature. The effect of temperature on corrosion rates of steel is represented by several rate changes obtained from a variety of water solutions and is presented here in Figure 35 as a relative temperature function.

The data of *Figure 35* represents relative changes in general corrosion rates for several different salt solutions when temperatures were progressively increased. The plot of relative corrosion rates for steels in *Figure 35* is an exponential growth function of temperature, $C_{rate(rel)} = 0.386 + 0.108 e^{T/(55.6)}$, where T is the solution temperature.

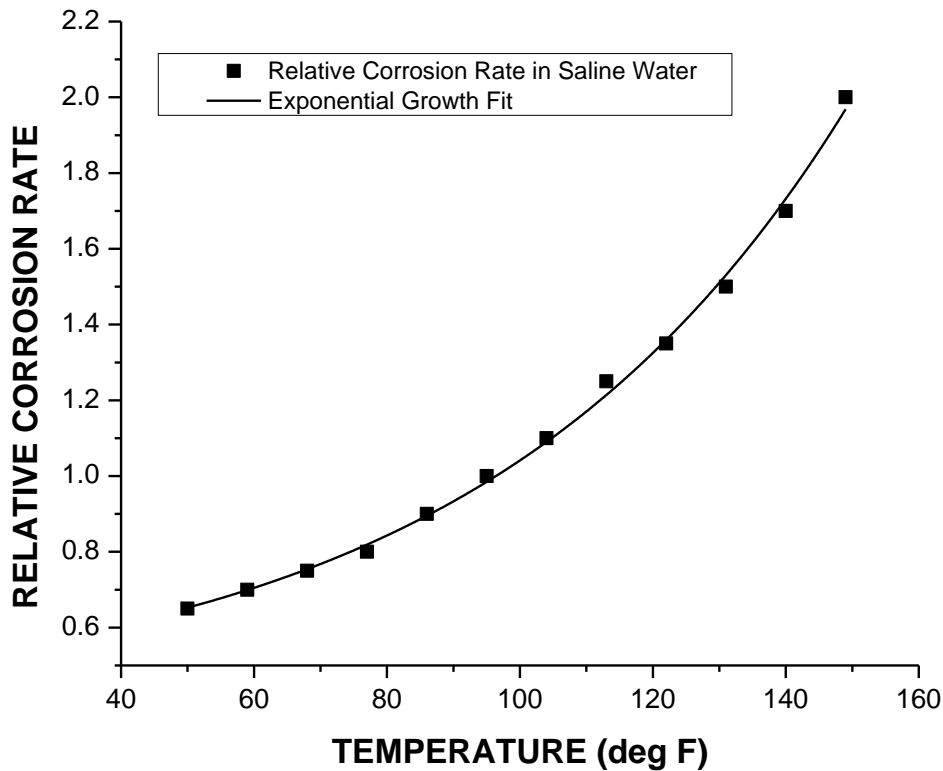


Figure 35. This graph provides the relative effect of temperature increases on the corrosion rate for steels in low resistivity soils. Data represents relative increases in corrosion rate as a function of increasing temperature for a variety of aqueous media. Data source Ref. 19.

The term “relative corrosion rate” of *Figure 35* is a useful generalization to account for the effect of temperature on corrosion rates in different media. For example, if the corrosion rate at 70°F is 1.5 mpy, the relative corrosion rate at 100 °F would increase from 0.767 to 1.038. This is a rate increase of $1.038 \div 0.767 = 1.353$, meaning that 1.5 mpy corrosion rate of steel at 70°F would increase to 2.03 mpy at 100°F.

In general, temperatures along the length of the pile can vary from 40-120°F. At depths of 10 to 20 ft, temperatures will be largely insensitive to surface temperature change. From the point of fixity to the surface, an increasing temperature gradient will be established. Elevations near the surface of the pile will experience higher corrosion rates. Piles set in rigid containment (such as in the Madison County Bridge; see *Figure 13*), would be subject to higher corrosion rates since their points of fixity will be closer to the surface.

I. Effects of Specific Ions on Resistivity. Section 10.7.5 of the AASHTO *LRFD Bridge Design Specifications* requires that corrosion be considered when selecting piles. Soils that have resistivities of less than 2,000 ohm-cm, or those containing higher concentrations of sulfates and chlorides, or low pH (< 5.5), are specifically cited.

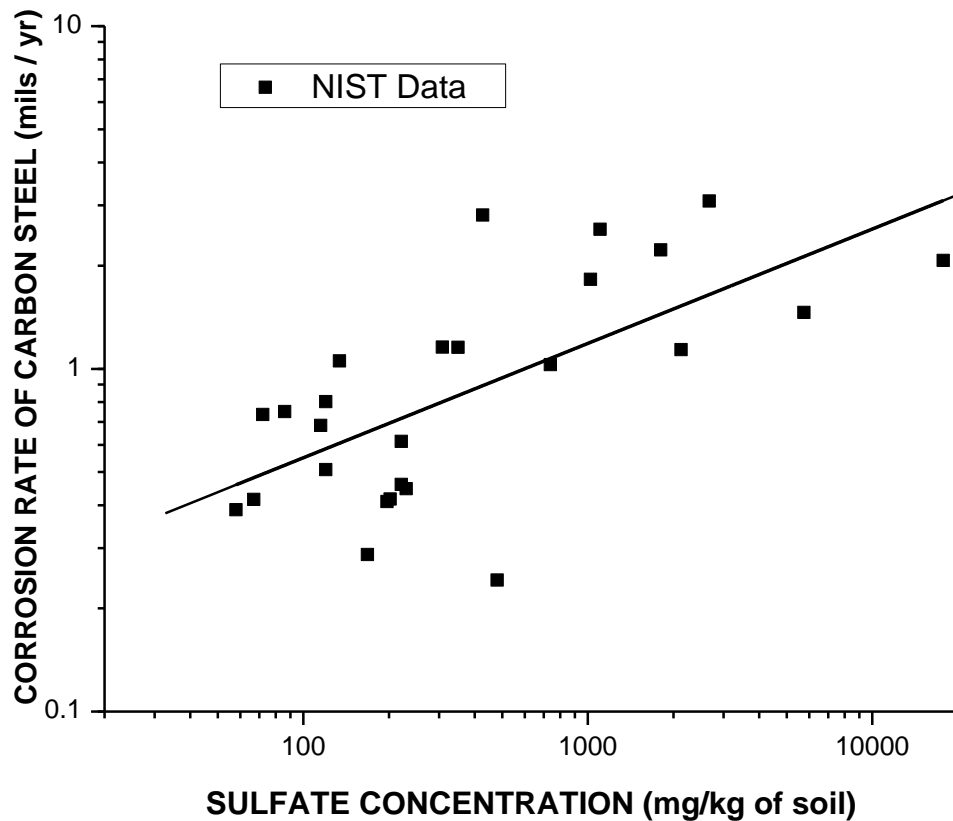


Figure 36. The effect of sulfate concentration on the corrosion rate of steel in various soils can be roughly predicted (± 1.6 mpy) by $C_{rateSO4} = 0.118 \times [SO_4]^{0.334}$. Data from Ref. 20.

Soils with sulfate concentrations greater than 1,000 mg/kg (ppm) are typically found in peaty or marshy areas and in clay or clay loam soils where soil resistivities are low. Corrosion rates

of steel are also directly related to the sulfate content in soils, although the correlation between corrosion rate and sulfate concentration as shown in *Figure 36* has considerable scatter.

Elevated chloride levels in soils also stimulate the rate of formation of deep pits in corroded steels. Chlorides, whether naturally present in the soils, or from infiltration and accumulation into the soil due to repetitive use of deicing salts, also contribute to decreased soil resistivity. Chlorides tend to cause acceleration of the depth of pitting in steel due to localized acidification of pits. *Figure 37* shows the effect of chloride concentration in soils which directly increases the formation of deeper corrosion pits in steel.

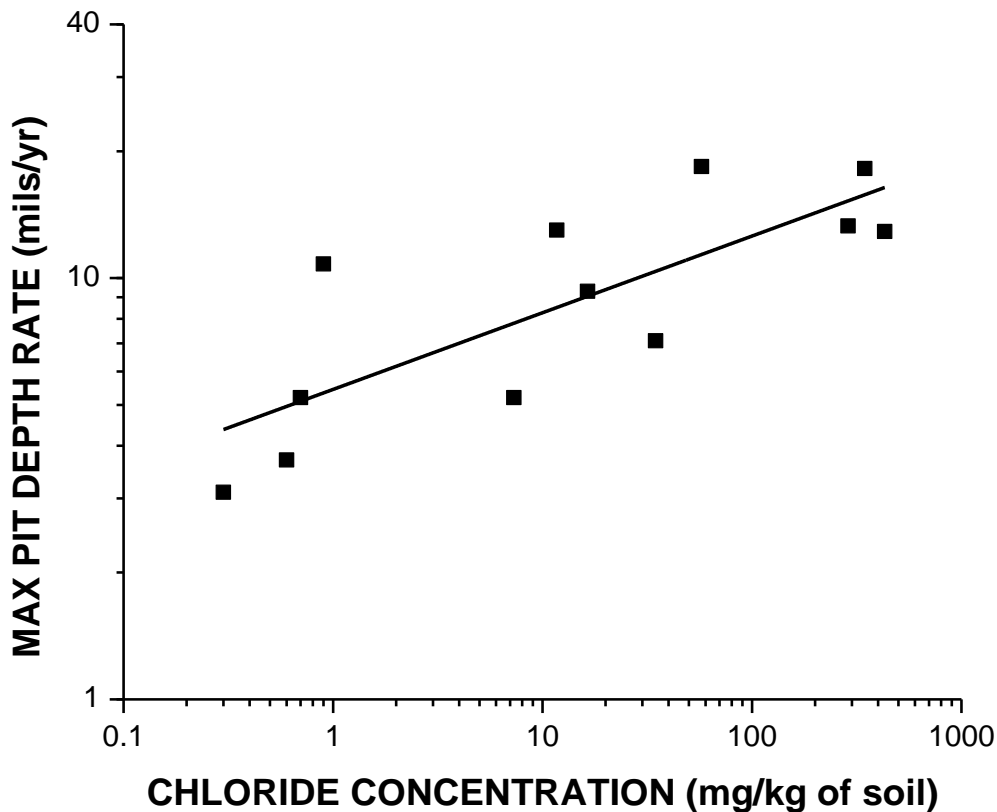


Figure 37. This plot shows the maximum pit depth rate of steel as a function of chloride concentration in mg/kg (ppm), $C_{\text{pit rate}} = 5.44 [\text{Cl}]^{0.182}$, after longer-term exposure ranging from 6 to 18 years in various soils. Data from Ref. 20.

J. Examples of Bridges Unexpectedly Affected by Corrosion. Many bridges located in the United States have experienced severe failures due to corrosion losses that were unobservable during routine inspections or unforeseen during construction. Two notable examples are now described:

1. In the Pittsburgh area, a tied arch bridge built in 1976, suffered an over-rotation of rocker bearings in 2008, indicative of buckling of piles, causing an 8 in overnight drop of the span and cracking of the piers. Subsequent soil borings indicated that the first 8 ft consisted of a clayey sand filled with slag, wood, cinders, rock fragments and coal. Below that strata was sandy gravel fill filled with blast furnace slag. The retrofit consisted of providing an additional pier support with an extensive array of micropiles (Ref. 30).

2. In Green Bay WI, the I-43 truss bridge that crosses over the Fox River and carried 40,000 vehicles per day sustained a collapse of pier pilings (40 total) which supported Pier 22 of the bridge, resulting in a significant sag of the span, as shown in *Figure 38*. Built in 1980, the collapse of Pier 22 occurred in October 2013. The previous inspection of 2012 considered the bridge to be in “excellent condition”. Additional investigations showed that Piers 22, 23 and 25 also had cinder-laden fill surrounding those pilings, causing substantial corrosion damage, leading to buckling and deformation due to section loss (Ref. 31).

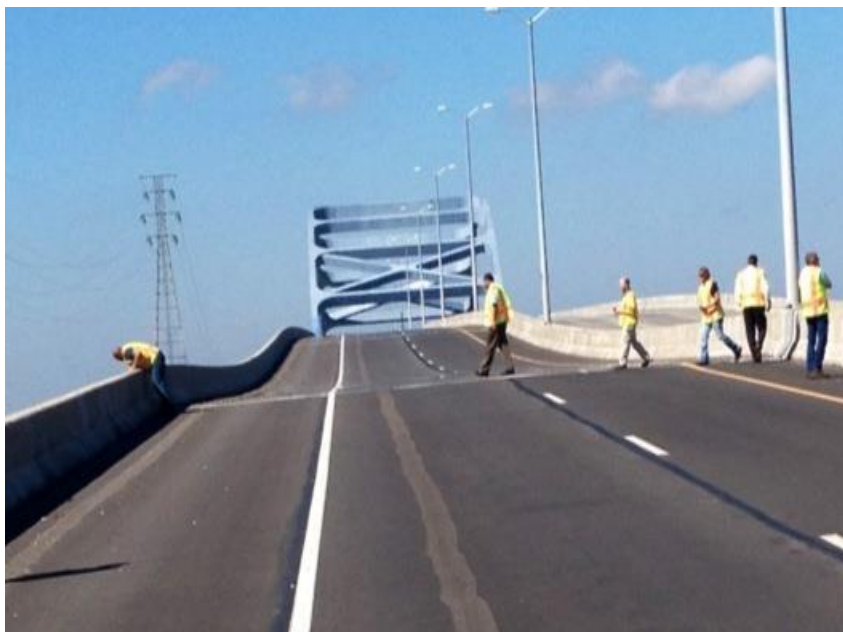


Figure 38. The obvious pavement sag sustained by the collapse of Pier 22 in October 2013 after 30 years of service of the I-43 tied-arch truss bridge over the Fox River in Green Bay, WI, necessitated an \$8 million emergency repair. Photo source: Wisconsin DOT.

A pile driven into soil containing any sharp rocks, or scored during shipment and handling, could also sustain notches. Soils with very low resistivity (50 ohm-cm or less) caused by deicing salt intrusion, can have corrosion rates of 3-5 mpy, resulting in pits that are 9-12 mils deep and about twice as wide. To reach a pit depth of 0.125 in at 9 mpy, it would take about 14 years. The pile strains measured each day for this study ranged from 24 to 47 micro-strain per day, which is equivalent to a stress range of 720 to 1,410 psi. Since a pit or crack can magnify the nominal stress by factor of 2.5 to 3 or more, a nominal stress of 1,410 psi can locally rise to 4,230 psi. However, these minor stress changes occur within a mean stress of 32-34 ksi, where the stress intensity changes as pits or cracks deepen due to corrosion of steel piles driven into low resistivity soils.

K. Importance of Fracture Toughness. Fracture toughness is a measure of resistance of steels to rupture under the influence of applied stress and the presence of cracks of varying depth in structural sections. The fracture toughness of ASTM A36, A572 and A588 steels varies widely from 15 to 80 ft-lbs, depending on carbon, sulfur, phosphorus, alloying elements and grain size. Table 8 of ASTM A709 *Standard Specification for Structural Steel for Bridges*, requires that ASTM A36, A572 and A588 steels for redundant members have a minimum impact toughness of 15 ft-lbs at various temperatures, depending on its Zone location. The State of Illinois is located in Zone 2.

Numerous investigators have derived empirical correlations between Charpy V-notch impact toughness with fracture toughness. Two reliable correlations where loadings are applied at slow-strain rates are the Roberts - Newton (Ref. 15) and Barsom - Rolfe equations (Ref. 32) for the transition region of impact toughness vs. temperature curve, and are stated as follows:

$$\text{Roberts - Newton: } K_{Ic} = 9.35 [\text{CVN}]^{0.63}$$

$$\text{Barsom - Rolfe: } K_{Ic}^2 = 0.03 [\text{CVN}] \times \sigma_{ys} + 2739$$

Steels with an impact toughness of 15 ft-lbs using both these equations provide a fracture toughness range of 51.5 to 52.5 ksi [in]^{0.5} for A36 and A572 steels. For ASTM A36 Grade 36 and A572 Grade 50 pile steels cited in this report, a K_{Ic} value of 52 ksi [in]^{0.5} was used as a fracture toughness equivalent to a Charpy V-notch impact toughness of 15 ft-lbs at slow strain rates.

At the nominal yield strength of 36 ksi for ASTM A36 steel, the stress intensity for a 0.549 in deep notch crack is $K_{Ic} = 1.1 (36) [\pi (0.549)]^{1/2} = 52 \text{ ksi [in]}^{1/2}$ (Ref. 16). For an A572 steel with a notch toughness of 15 ft-lbs and stressed at or near its minimum yield strength of 50 ksi, the critical crack depth is reduced to 0.285 in.

The nominal yield strengths for steel piles are 36 ksi for A36 and 50 ksi for A572. Since these are minimum yield strength requirements, actual yield strengths may be slightly higher. For A36 and A572 HP steel piles with an impact toughness of 15 ft-lbs and the HP pile stressed at or near yield, the stress intensity is very near a critical level when the crack depth for an A36 pile is 0.549 in deep and 0.285 in deep for A572 piles. This is because the stress intensity meets or exceeds the fracture toughness of $52 \text{ ksi [in]}^{1/2}$, which is dependent on ambient or localized stress and crack depth. If piles are driven into conductive soils or become saline because of frequent winter deicing over a 20 to 50-year period and are annually subjected to stress levels at or above their nominal yield strengths of 36 or 50 ksi, crack advancement or partial rupture of the HP piles can take place.

L. Pile Axis Orientation and Corrosion. The loading axis orientation of HP piles influence their susceptibility to corrosion and the formation of cracks. Atmospheric thermal changes result in expansion or contraction of the span which is integrally connected to each HP or pipe pile. A “strong” axis HP pile has a neutral X-X axis which passes perpendicular through the web midpoint. A “weak” axis pile has its neutral axis perpendicular through the vertical axis of the web. For AISC HP piles from HP 14 to HP 8 (Ref. 33), the ratio of the moment of inertia of the X-X axis to the Y-Y axis ranges from 2.75 to 3.05. Although the “weaker” Y-Y axis permits more deflection, it reaches yield strength by a factor of 0.333 x the moment force than a “stronger” X-X axis pile orientation. The relationship between end loadings, deflection and surface stresses for an AISC 12 x 84 HP pile in both the X-X and Y-Y orientations are shown in *Table 9*.

For abutment spans with rigidity and exerting greater forces on the piles, “strong” axis X-X piles are indicated. For spans with lesser rigidity and greater length, “weak” Y-Y axis orientations are preferable.

The flange edge exposure of a “weak” Y-Y pile orientation has far less surface area than the flange face for an X-X “strong” pile orientation. Edge surfaces, which range from 0.420 in to

0.805 in thick for AISC HP piles, generally sustain slightly higher corrosion rates than larger and smoother surface areas of flanges, which range in width from 8.155 in to 14.885 in.

Once corrosion pits form on a weak axis flange edge and the pile is at yield, cracks can form and propagate through the flange. For X-X axis piles in comparison, although “thumbnail” cracks can form at pitting sites in the flange face, they cannot propagate as quickly because they are surrounded by a larger volume of sound metal which helps to blunt crack formation and propagation.

*Table 9. DEFLECTION AND SURFACE STRESSES FOR A 12 X 84 HP PILE**

<i>Pile Loading Axis</i>	<i>End Loading, lbs</i>	<i>Surface Stress, psi</i>	<i>Deflection, inches</i>
Y-Y (“weak”)	1,000	6,930	0.746
	2,000	13,859	1.492
	3,000	20,788	2.238
	4,000	27,718	2.984
	5,195	36,000	3.879
X-X (“strong”)	1,000	2,267	0.244
	2,000	4,534	0.489
	3,000	6,801	0.733
	4,000	9,068	0.978
	5,195	11,788	1.271
	6,250	14,169	1.528
	10,000	22,671	2.445
	12,500	28,338	3.056
	15,879	36,000	3.882

*The HP pile in this table has a point of fixity at 20 ft after being driven into the soil foundation. Deflection is derived from the equation $y = WL^3 \div (3EI)$, where moment $M = WL$ and surface stress $\sigma = (M \times c) \div I$. For the Y-Y axis, the distance from neutral axis $c = 6.15$ in and $I_{Y-Y} = 213$ in⁴; for the X-X axis, $c = 6.14$ in and $I_{X-X} = 650$ in⁴ (Refs. 33 and 25).

M. Integral Abutment Piles in Low Resistivity Soils. Piles driven into soils with low resistivity can experience corrosion rates of 2 to 3 mils/yr (mpy) with pitting depth rates of 5.0 to 7.5 mpy. As previously described, corrosion rates increase when cyclic frequencies are very low. The effects of cyclic frequency and crack propagation in air and conductive media are shown in *Figure 33* and *Figure 39*. Crack propagation rate is related to the stress intensity changes experienced by the pile, which is a function of crack pit depth or length and applied stress. Considering that the mean stresses encountered in the piles were of the order of 32-36 ksi, this can cause the stress intensity to increase as pit depths increase and form cracks that advance into the pile sections.

The stress intensity of an edge crack of an HP pile in bending is $K = 1.1 \sigma [\pi a]^{0.5}$ (Ref. 16). For a pile with an impact toughness of 15 ft-lbs, this is approximately equivalent to a fracture toughness of $K_{Ic} \approx 52 \text{ ksi [in]}^{0.5}$ according to the Roberts-Newton or Barsom-Rolfe correlations. The threshold stress intensity for crack growth starts at about $6 \text{ ksi [in]}^{0.5}$ in conductive soils.

If an ASTM A36 HP pile is yielding at 36 ksi, the critical crack depth for an edge crack is determined by the following relationship:

$$K_{Ic} = 1.1 \sigma [\pi a]^{0.5}$$

Where

$$\sigma = 36 \text{ ksi (yield strength)}$$

$$K_{Ic} = 52 \text{ ksi [in]}^{0.5}$$

$$a = \text{critical crack depth}$$

Solving for $\pi a = [52 \div (1.1 \times 36)]^2$, the critical crack length a for an A36 pile yielding at 36 ksi with an impact toughness of 15 ft-lbs is 0.549 in.

N. Pitting and Crack Formation in Piles Reaching Critical Crack Depth. Examples of the determination of time-to-failure for piles in lower resistivity soil environments are now described.

1. Pitting and crack formation. The change in daily concentrated stresses in piles was estimated to be about 4 ksi. The change in threshold cyclic stress intensity ΔK for crack propagation to begin is about $6 \text{ ksi [in]}^{0.5}$ in low resistivity soils, as shown in *Figure 39* and about 9-10 $\text{ksi [in]}^{0.5}$ for steel in air (Ref. 28). Daily stress changes in this pile study would not result in significant crack advancement by daily changes in ΔK because they were below the threshold to sustain cracking by mechanical means alone. However, the failure of bare piles in low resistivity soils would be primarily caused by the formation of multiple pits that accompany the general corrosion of steel in soils and are aided by the presence of mean stresses which increase stress intensity.

Corrosion fatigue is a combination of surface roughening, corrosive penetration and pitting that provides for the formation of shallow cracks, even at low cyclic stresses. As corrosion occurs and the pits grow to greater depth as a function of their contact with low resistivity soils, the stress intensity increases to a point where it becomes critical. Since piles were either yielding or sustaining high mean stresses near yield strength in this study, a pit can easily become a crack. Pits that form in HP piles situated in soils containing chlorides, sulfates or sulfides can become acidified when the hydrogen reduction reaction dominates over oxygen reduction, which are the

principal chemical reactions associated with the corrosion of steel. Acidification may cause localized embrittlement, even in lower carbon steels, resulting in crack formation from the high bending stresses applied to the piles. The corrosion pits become permeated with monatomic hydrogen, decreasing toughness of the steel and causing localized brittle fracture and crack initiation (Ref. 34). Since the threshold for crack propagation is only 6 ksi [in]^{0.5} and the pile is yielding at either 36 or 50 ksi, the crack depth is substantially reduced to 0.007 in to start cracking. Corrosion fatigue is most prevalent where pitting attack occurs (Ref. 26).

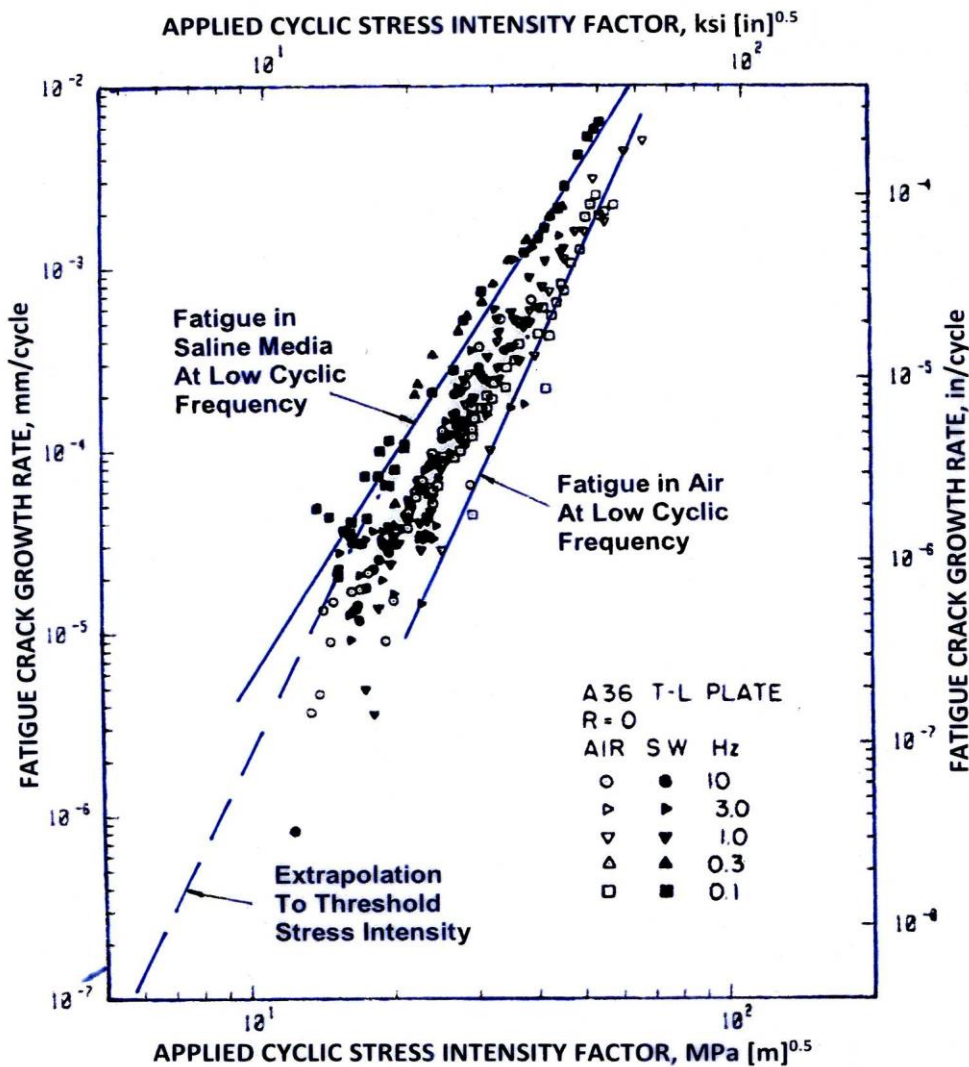


Figure 39. Crack growth rates in saline water have a lower threshold of advancing under a stress intensity of 6 ksi [in]^{0.5} compared to 10 ksi [in]^{0.5} in air. For an A36 steel at 36 ksi yield, the depth for a crack to begin advancement in a saline environment is about 0.0073 inches. For corrosion pits penetrating at a rate of 6 mpy, a pit depth of 7.3 mils will be reached in 1.2 years. Source of graph, Ref. 19.

A. *Resistivities in Common Corrosive Media.* Resistivity is the reciprocal of conductivity. The lower the resistivity, the greater the conductivity of the soil to carry electrical current by the mobility of ions that transfer electrons. Without a conductive media, section loss is very minimal because without rapid electron transfer, corrosion reaction rates are very slow. Examples of low conductivity media are very dry sandy soils or low permeability concrete that contains no chlorides or sulfates. *Table 10* lists the resistivities of common water environments that will corrode carbon steels.

Table 10. RESISTIVITIES OF COMMON WATER ENVIRONMENTS

<i>Description of the Water Environment</i>	<i>Resistivity, ohm-cm</i>
Fresh water saturated sand	8,000-10,000
Saltwater water saturated sand	200-2,000
Power plant boiler water	1,000,000
Chemically pure water	18,000,000
Distilled water	2,000,000
Rainwater	20,000
Tap water	1,000-2,000
Waste water	100-1,000
Brackish river water	200
Seawater	20
3.5% NaCl water solution at 20°C (saline water)	17

Source: "Conductivity of Various Aqueous Solutions at 25 °C", *Education Series Conductivity Guide*, Van London-Phoenix Co., Houston, TX, www.vl-pc.com web site.

B. *Temperature Compensation.* To account for temperature changes in the colder months, the pitting rate was reduced proportionally according to the relative temperature equation of *Figure 35*. The relationship between relative corrosion rate and temperature equation is expressed as $C_{\text{rate(temp)}} = 0.386 + 0.108 e^{T/55.6}$. The average temperature during the warmer months was estimated at 70°F and 40°F during the colder months. The relative rate at 70°F is 0.766 and at 40°F it is 0.608, which is a reduction factor of 0.79. The pitting penetration rate during the colder months was proportionally reduced by 0.79 x (pitting rate).

C. *Overall Corrosion Pitting and Stress Intensity.* In the following calculations, it is assumed that the pitting penetration rate and any accompanying crack growth due to yielding would primarily advance during the warmer months of the year, and then be attenuated during the three colder months. The pitting and corrosion rates in the warmer months and pitting rates

in the colder months were treated as linear functions. Most corrosion rates in water solutions show higher corrosion rates during the first year of exposure, but afterwards generally continue to corrode at linear rates. Although stresses continue to rise as the HP piles corrode and lose section, pit depth is very influential because the pits are subjected to yielding stresses that were first recorded when the piles were newly installed. The following calculations do not take into account section losses due to general corrosion. Even though section losses continue as years in service continue, yield stresses would remain as prevailing overall stress even though some work hardening of the piles may be occurring.

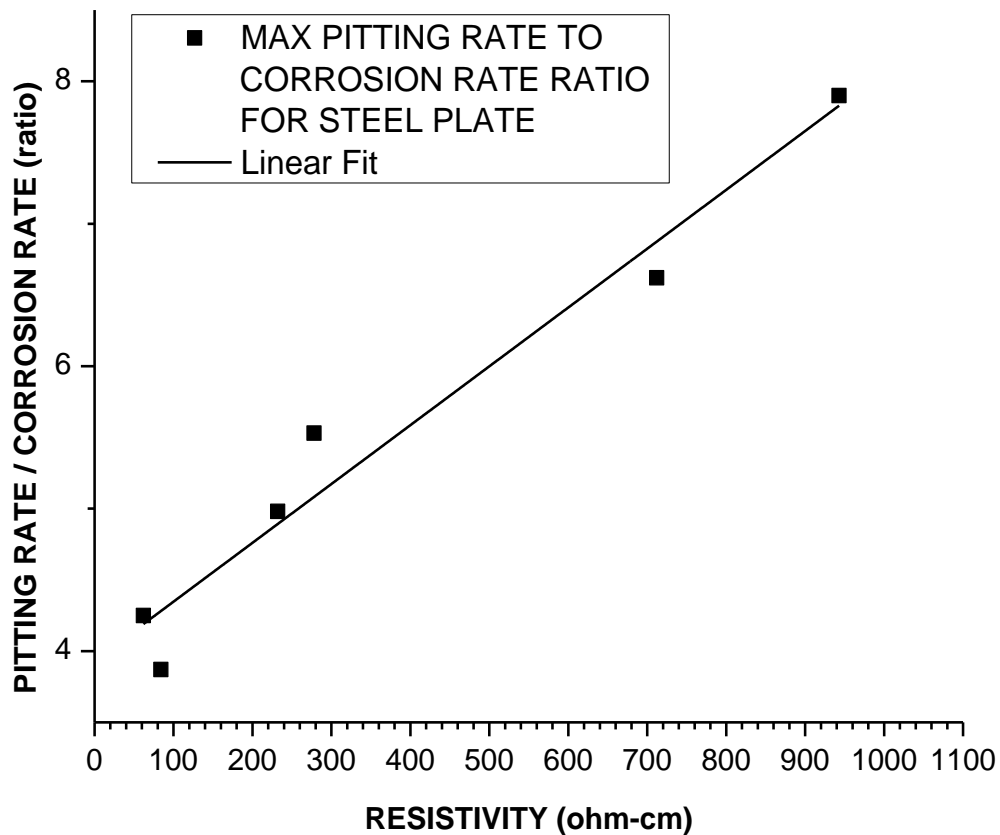


Figure 40. Between 10 to 1000 ohm-cm, the maximum pitting rate for steel plates is a function of soil resistivity. The pitting rate for a very conductive soil (10 ohm-cm or less) is 3.9 mpy and gradually increases by a factor of $0.00413 \times$ soil resistivity. As resistivity increases, pitting rates becomes more aggressive due to the fact that corrosion is less uniform in soils with decreasing conductivity. Each data point in the above plot represents the average pitting penetration rate of seven different carbon and low-alloy steels. In the range of 60 to 250 ohm-cm resistivity, the average max pitting to corrosion rate is 5.05 mpy. Since these are maximum penetration rates, an average multiplier of 2.5 x corrosion rate was used to determine pitting rate. From Ref. 20.

D. *HP Piles Driven into 100 Ohm-Cm Soils.* Piles in 100 ohm-cm soils have an average corrosion rate of 2.58 mpy. When the general rate is multiplied by 2.5, the average pitting rate is 6.5 mpy. Over 10 years, pit depths at 6.5 mpy would be penetrating for 75% of each year ($0.0065 \times 0.75 \times 10 = 0.049$ in) and at 5.2 mpy over 25% of the year ($0.0052 \times 0.25 \times 10 = 0.013$ in). The stress intensity for an HP pile made of ASTM A36 steel at its yield strength of 36 ksi is $K = 1.1 (36) [\pi (0.062)]^{0.5} = 17.5$ ksi [in]^{0.5}. The fracture toughness of an A36 or A572 pile was determined to be 52 ksi [in]^{0.5} which in turn determines the critical stress intensity. Stress intensity for a pile with a side crack in bending is $K = 1.1 \sigma [\pi a]^{0.5}$, (Ref.16) where σ is the applied stress and a is the crack length or depth. If $K_{Ic} = 52$ ksi [in]^{0.5}, then the critical crack depth for an A36 HP pile at yield (36 ksi) is 0.549 in.

Table 11. PIT DEPTH AND STRESS INTENSITY FOR A36 PILES IN SOILS WITH A RESISTIVITY OF 100 OHM-CM *

Years	Pit Depth in Warmer Months, inches	Pit Depth in Colder Months, inches	Pit Depth Total, Warm + Cold, inches	Stress Intensity at Pit Root**, ksi [in] ^{0.5}
10	$0.065 \times \frac{3}{4} = 0.049$	$0.052 \times \frac{1}{4} = 0.013$	0.062	$36(1.1)[\pi(0.062)]^{0.5} = 17.5$
20	0.098	0.026	0.124	$36(1.1)[\pi(0.124)]^{0.5} = 24.7$
30	0.147	0.039	0.186	$36(1.1)[\pi(0.186)]^{0.5} = 30.2$
40	0.196	0.052	0.248	$36(1.1)[\pi(0.248)]^{0.5} = 34.9$
50	0.245	0.065	0.310	$36(1.1)[\pi(0.310)]^{0.5} = 39.1$
60	0.294	0.078	0.372	$36(1.1)[\pi(0.353)]^{0.5} = 42.8$
70	0.343	0.091	0.434	$36(1.1)[\pi(0.434)]^{0.5} = 46.2$
75	0.368	0.098	0.466	$36(1.1)[\pi(0.466)]^{0.5} = 47.9$
80	0.392	0.104	0.496	$36(1.1)[\pi(0.496)]^{0.5} = 51.0$
88	0.431	0.114	0.545	$36(1.1)[\pi(0.545)]^{0.5} = 51.8$

*Pit depths are based on linear approximations of corrosion rates over the predicted time to failure. The corrosion rate at 100 ohm-cm was estimated 2.6 mpy and a pitting rate of 6.5 mpy.

**The critical stress intensity for an A36 pile with 15 ft-lbs CVN impact toughness at yield was estimated at 52 ksi [in]^{0.5}.

For A36 HP piles with a fracture toughness of 52 ksi [in]^{0.5} after 75 years of soil embedment, an estimated crack depth of 0.466 in results in a nearly critical stress intensity of 48 ksi [in]^{0.5}. Since corrosion rates in soil environments can substantially vary due to changes in field conditions where resistivities could decrease to < 100 ohm-cm, critical pit depths may be reached earlier than the planned 75-year design life or the predicted life of 88 years.

When A572 steel piles are subject to expansion or contraction at 50 ksi or more, higher stress intensities are created. The critical fracture toughness of 52 ksi [in]^{0.5} is reached earlier than for A36 piles. Time-to-criticality for A572 piles at 50 ksi is summarized in *Table 12*.

*Table 12. PIT DEPTH AND STRESS INTENSITY FOR A572 PILES IN SOILS WITH A RESISTIVITY OF 100 OHM-CM **

Years	<i>Pit Depth in Warmer Months, inches</i>	<i>Pit Depth in Colder Months, inches</i>	<i>Pit Depth Total, Warm + Cold, inches</i>	<i>Stress Intensity at Pit Root**, ksi [in]^{0.5}</i>
10	0.065 x ¾ = 0.049	0.052 x ¼ = 0.013	0.062	50(1.1)[π(0.062)] ^{0.5} = 24.1
20	0.098	0.026	0.124	50(1.1)[π(0.124)] ^{0.5} = 34.3
30	0.147	0.039	0.186	50(1.1)[π(0.186)] ^{0.5} = 41.9
40	0.196	0.052	0.248	50(1.1)[π(0.248)] ^{0.5} = 48.5
46	0.225	0.060	0.285	50(1.1)[π(0.285)] ^{0.5} = 52.0

*Pit depths are based on linear approximations of corrosion rates over the predicted time to failure.

**The critical stress intensity for an A572 pile with 15 ft-lbs CVN impact toughness at yield was estimated at 52 ksi [in]^{0.5}.

Fortunately, most A572 steels generally have improved impact toughness values compared to A36 steels, depending on the carbon, sulfur, phosphorus and manganese present in the A572 steel. The value of 52 ksi [in]^{0.5} was considered a conservative estimate of fracture toughness for A572 steel.

E. Piles in Soils Infiltrated by Deicing Salts or Poorly Aerated. According to the predictive exponential decay equation developed in *Figure 34*, $C_{rate} = 0.5 + 2.2 e^{-(R / 1846)}$, soils with a resistivity of 17 ohm-cm would have a calculated corrosion rate of 2.68 mpy. Since pitting rates in very low resistivity soils are about 2.5 times the general corrosion rate, the pitting penetration rate was calculated to be 6.7 mpy.

To account for temperature changes in the colder months, the pitting rate was reduced proportionally according to the relative temperature equation of *Figure 35*. The relative corrosion rate vs. temperature equation is $C_{rate(rel)} = 0.386 + 0.108 e^{T / (55.6)}$. The average temperature during the warmer months was estimated at 70 °F and 40 °F during the colder months. Per the previous reduction for 100 ohm-cm soils, the pit penetration rate during the colder months was proportionally reduced by 0.79 x 6.7 mpy = 5.3 mpy. As in previous

calculations, it is assumed that pitting penetration rate and accompanying crack growth due to yielding will primarily advance during the warmer months of the year and be attenuated during the three colder months. The pitting rates of 6.7 mpy in the warmer months and 5.3 mpy in the colder months were treated as linear functions.

Over 10 years, pit depths at 6.7 mpy would be penetrating for 75% of each year and at 5.3 mpy over 25% of the year. The stress intensity for a pile with a side crack in bending remains the same at $K = 1.1 (36) [\pi (a)]^{0.5}$ when the A36 pile is yielding at 36 ksi and a is the crack or pit depth. The critical fracture toughness of a pile still remains as $K_{Ic} = 52 \text{ ksi [in]}^{0.5}$ when CVN impact toughness = 15 ft-lbs and $E = 29 \times 10^6 \text{ psi}$ and critical crack depth remains at 0.549 in. The estimated life for A36 steel integral abutment piles in soils with a resistivity of 17 ohm-cm stressed to its minimum yield strength is summarized in *Table 13*.

*Table 13. PIT DEPTH AND STRESS INTENSITY FOR A36 PILES IN SOILS WITH A RESISTIVITY OF 17 OHM-CM **

Years	<i>Pit Depth from Warmer Months, inches</i>	<i>Pit Depth from, Colder Months, inches</i>	<i>Pit Depth, Warm + Cold, inches</i>	<i>Stress Intensity at Pit Root**, ksi [in]^{0.5}</i>
10	$0.067 \times \frac{3}{4} = 0.050$	$0.053 \times \frac{1}{4} = 0.013$	0.063	$36(1.1)[\pi(0.063)]^{0.5} = 17.6$
20	0.100	0.026	0.126	$36(1.1)[\pi(0.126)]^{0.5} = 24.9$
30	0.150	0.039	0.189	$36(1.1)[\pi(0.189)]^{0.5} = 30.5$
40	0.200	0.052	0.252	$36(1.1)[\pi(0.252)]^{0.5} = 35.2$
50	0.250	0.065	0.315	$36(1.1)[\pi(0.315)]^{0.5} = 39.4$
60	0.300	0.078	0.378	$36(1.1)[\pi(0.378)]^{0.5} = 43.2$
70	0.350	0.091	0.441	$36(1.1)[\pi(0.441)]^{0.5} = 46.6$
75	0.375	0.098	0.473	$36(1.1)[\pi(0.473)]^{0.5} = 48.3$
80	0.400	0.104	0.504	$36(1.1)[\pi(0.504)]^{0.5} = 49.8$
86	0.430	0.112	0.542	$36(1.1)[\pi(0.542)]^{0.5} = 51.7$

*Pit depths are based on linear approximations of corrosion rates over the predicted time to failure.

**The critical stress intensity for an A36 pile with 15 ft-lbs impact toughness at yield is $52 \text{ ksi [in]}^{0.5}$.

To obtain a minimum 75 years of life for a bare A36 HP pile, the overall pitting rate should be less than 7.3 mpy. This was determined by estimating that the pitting rate is constant, whereby $0.549 \div (75 \text{ years}) = \text{pitting rate} = 0.0073 \text{ in/yr} = 7.3 \text{ mpy}$. Since pitting rates are estimated at about 2.5 times the uniform corrosion rate, this corresponds to a corrosion rate of 2.9 mpy or less.

Although the preceding table indicates that the A36 HP piles have more than a 75-year life span, the user of this report must be cautioned that corrosion rates significantly vary and that corrosion can also become localized. The determination of “general corrosion rate” assumes that the weight loss is uniform over the entire surface, when in reality it is often non-uniform. Also, HP piles do not always have a required minimum of 15 ft-lbs impact toughness or more, unless ASTM A709, which includes structural shapes, is specified in either special provisions or purchase orders. For piles placed in the “weak” Y-Y axis direction, they sustain yield strengths at lower end loadings since they have lesser moments of inertia than “strong” X-X axis piles. For an A572 HP pile with an impact toughness of 15 ft-lbs, the critical crack depth is reduced to 0.285 in if the pile is yielding at 50 ksi or more each year.

For an A572 HP pile in a 17 ohm-cm soil, the estimated general corrosion rate is 2.7 mpy. Since pitting rates in very low resistivity soils are about 2.5 times the overall corrosion rate, this results in a pitting rate of $2.7 \times 2.5 = 6.8 \approx 7$ mpy. The estimated life span for an ASTM A572 HP pile stressed to its yield strength of 50 ksi in a soil with a resistivity of 17 ohm-cm is calculated in *Table 13*.

*Table 14. PIT DEPTH AND STRESS INTENSITY FOR A572 PILES IN SOILS WITH A RESISTIVITY OF 17 OHM-CM **

Years	Pit Depth from Warmer Months, in	Pit Depth from, Colder Months, in	Pit Depth Total, Warm + Cold, in	Stress Intensity at Pit Root**, ksi [in] ^{0.5}
10	$0.070 \times \frac{3}{4} = 0.053$	$0.055 \times \frac{1}{4} = 0.014$	0.067	$50(1.1)[\pi(0.067)]^{0.5} = 25.2$
20	0.106	0.028	0.134	$50(1.1)[\pi(0.134)]^{0.5} = 35.7$
30	0.159	0.042	0.201	$50(1.1)[\pi(0.201)]^{0.5} = 43.7$
40	0.212	0.056	0.268	$50(1.1)[\pi(0.268)]^{0.5} = 50.5$
42	0.223	0.059	0.282	$50(1.1)[\pi(0.282)]^{0.5} = 51.8$

*Pit depths are based on linear approximations of corrosion rates over the predicted time to failure.

**The critical stress intensity for an A572 pile with 15 ft-lbs impact toughness at yield is 52 ksi [in]^{0.5}.

The required pitting rate for 75 years of life to reach the critical crack depth of $0.285 / 75 = 0.0038$ in / yr or 3.8 mpy. Since the average pitting rate is 2.5 times the corrosion rate for steel in most soils, this is a general rate of 1.5 mpy, which corresponds to about 1455 ohm-cm. This is based on the soil corrosion rate equation $C_{rate} = 0.5 + 2.2e^{-R/1846}$, a function of resistivity R.

The AASHTO LRFD restriction that soil resistivity should be 2000 ohm-cm or more is rationally conservative, based on known variability of corrosion rates of steel in various soils. Uncoated piles in soils with resistivities of 2000 ohm-cm or greater should provide at least 75 years of life.

CalTrans (Ref. 36) has a more restrictive classification, considering soils to be corrosive when any of the following conditions are present: (a) soil chloride concentrations are 550 ppm or more; (b) sulfate concentrations are 1500 ppm or greater; (c) soil is acidic if pH is 5.5 or less; and (d) soil resistivity is 1,100 ohm-cm or less.

F. Effects on Moment of Inertia with Respect to Pile Axis. Although the previous tables emphasized the effects of pitting corrosion on piles, section losses during 75 years of life can markedly affect the elastic properties of piles. Assuming a uniform corrosion rate of 3.0 mpy, the penetration on one side of a pile in 75 years would be $75 \text{ yrs} \times 0.003 \text{ in / yr} = 0.225 \text{ in}$. Since corrosion would penetrate on both sides, the section loss would be 0.450 in.

Using a 12 x 84 HP shape as an example, the X-X axis depth would decrease from 12.280 in to 11.830 in, which is about equivalent to a 12 x 53 HP shape. The AISC moment of inertia would decrease from 650 in⁴ to 393 in⁴. Also, the flange width would decrease from 12.295 in to 11.845 in which is less than 12.045 in for a 12 x 53 HP shape. The Y-Y moment of inertia would be reduced from 213 in⁴ to slightly less than 127 in⁴. When bent around the “strong” X-X axis, the web section would be reduced from 0.625 in to 0.175 in, resulting in web buckling. In the “weaker” Y-Y axis, non-uniform penetration of the webs and flanges may be enough to also result in buckling.

Results of this investigation indicated that HP piles had yielded. For a new 12 x 84 HP pile loaded in the “weak” Y-Y axis with a point of fixity at 20 ft, yielding would occur with an end load of 5,195 lbs. After 75 years of uniform corrosion rate at 3 mpy, the decrease in flange and web dimensions would accordingly reduce the moment of inertia to 127 in⁴, requiring only 3,215 lbs to induce yielding. The progressive losses of section simply permit yielding to occur more frequently with pile end loadings derived from lesser thermal expansion and contraction of the bridge decking. This does not even include any uplift tensile forces on the pile ends induced by heavy trucks and the number of lanes inherent in the design of integral abutments.

In the preceding calculations, corrosion & pitting rates were considered to be constant, as well as soil conditions over a 75-year life span. The user of this report is cautioned that conditions can vary in locations due to nearby construction or industrial activity which disturbs area soil conditions or results in chemical changes, or climatic changes which either increase prevailing temperatures, or require application of more deicing salts.

PIPE PILES

Pipe piles were also instrumented in this study. Pipe piles have an advantage to some degree because their moments of inertia are not axis-dependent like H piles and epoxy coated if ASTM A972 is invoked. However, they are also subject to corrosion penetration problems similar to HP piles.

In general, pipe piles have thinner wall thicknesses than HP pile webs, although wall thickness can be specified up to 0.500 in thick for 8.625-in, 10.75-in, 12.75-in and 14-in diameters, as per Table 3 of ASTM A252. Thin-wall pipe piles are more vulnerable to pitting and section loss, leading to cracking or buckling if subjected to yield stresses. Minimum yield stresses for A252 piles are as follows: Grade 1, 30 ksi; Grade 2, 35 ksi; Grade 3, 45 ksi.

Another factor to consider is that wall thickness is permitted in A252 to vary up to 12.5% of the “nominal” wall thickness. For a specified wall thickness of 0.500 in, actual wall thickness could be only 0.438 in thick and still be within acceptable tolerances. “Surface imperfections” is a term used in A252 to characterize localized pits or surface defects in the pipe piles, which can be up to 25% of specified wall thickness. Defects deeper than 25% of wall thickness can be repaired by the manufacturer by welding if less than 33% of nominal thickness. This exception largely applies to pipe piles, whereas other pipe and tubing standards restrict variations in wall thickness not to exceed 12.5%.

These exceptions can limit the life of pipe piles, so any order of pipe should place restrictions in special provisions regarding surface finish, wall thickness tolerances and acceptable repair methods. Pipe piles must also have a required CVN impact toughness of 15 ft-lbs since they are redundant load-carrying members.

“General” corrosion rates increase in lower resistivity soils in piping and tubing, but the tendency to form deeper pits is decreased as soil resistivity decreases, as shown in *Figure 42*. Similar behavior is found in steel plates and shapes.

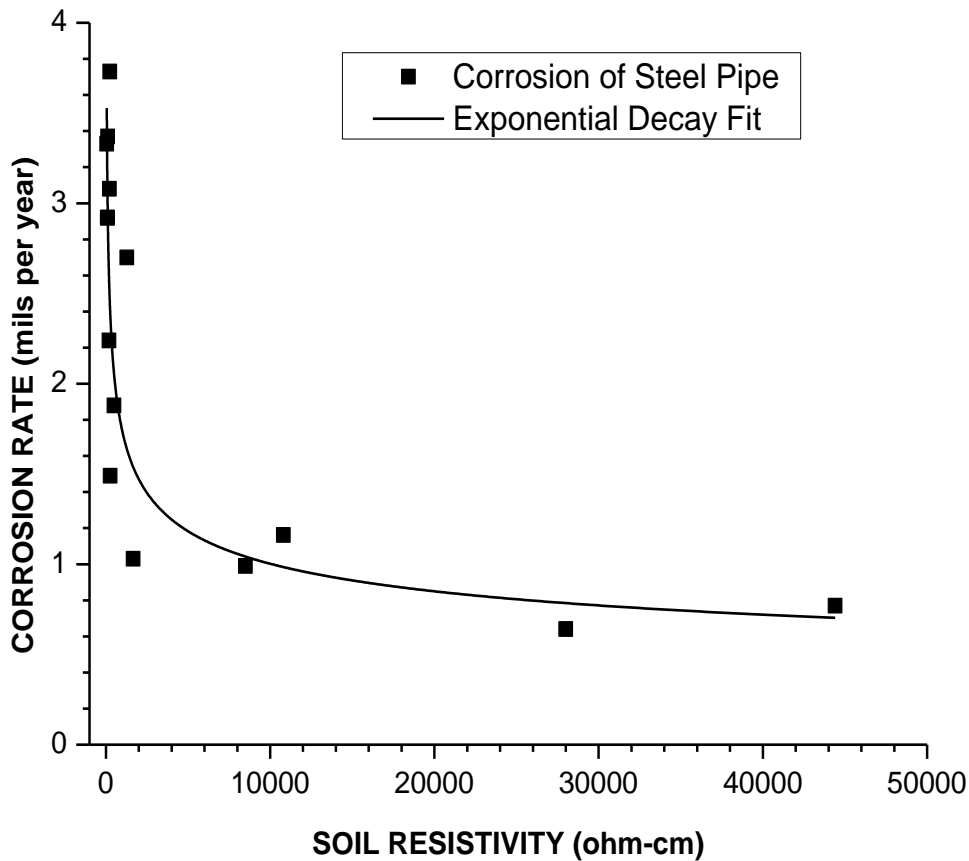


Figure 41. Pipe piles have corrosion rates similar to HP piles. The corrosion rate of steel pipe is an exponential decay function of soil resistivity, whereby $C_{rate(pipe)} = 0.9 + 2.2 e^{-R/1280}$. Soil corrosion rates in pipe are slightly higher than H piles due to their lesser surface area and symmetrical shape.

Long-term exposure of steel plates and pipes in various soils with low resistivity indicated that although the corrosion rates in many cases accelerated, the description of these “general corrosion” rates, whereby weight losses are uniformly distributed over the entire surface area of the specimens, were not actually uniform. Corrosion penetration tended to be concentrated around the pitted areas, often causing deep depressions or nearly complete penetration of plate and pipe specimens. Although the calculations of the previous tables are somewhat idealized, they give a general indication of when corrosion pits in piles could become cracks and approach criticality as a function of time in corrosive soil environments.

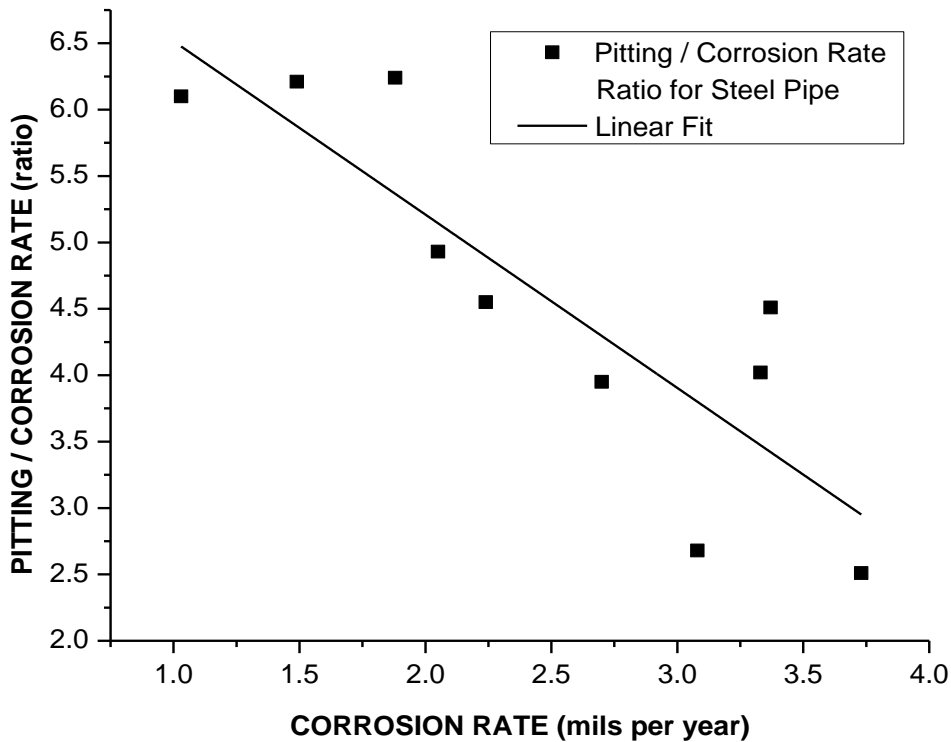


Figure 42. The pitting rate / corrosion rate ratio decreases as corrosion rates increase when uncoated steel piping is buried in soils. A more aggressive corrosion rate tends to lessen the fixation of pits and distributes penetration more evenly than when corrosion rates are 1.5 mpy or less. From Ref. 20.

Another factor not considered in the previous tables is that soil horizons have a heterogeneous nature where permeability and oxygenation may substantially vary from one horizon to another. In such situations, corrosion of the steel piles may be affected by differential aeration. This form of corrosion occurs when one area of the long pile, which is poorly oxygenated, is the principal corrosion site and the more oxygenated areas are where oxygen is reduced by the reaction $2\text{H}_2\text{O} + 4\text{O}_2 + 4\text{e}^- \rightarrow 4\text{OH}^-$ to form hydroxyl ions. This reaction has a driving voltage of -0.4 V and the hydroxyl ions help to stabilize oxygenated areas. This permits more corrosion of the areas that are receiving less oxygen.

For the above reasons, piles require additional protection to counteract any unanticipated conditions or changes in soils or atmospheric conditions where the piles are located.

METHODS TO EXTEND THE LIFE OF THE PILES UNDER ADVERSE CONDITIONS

There are several important methods to protect piles subjected to adverse conditions. These include: (a) brackish water or industrial chemical intrusion; (b) conductive backfill which may be partially comprised of water absorptive soils like clays or waste products like cinders or blast furnace slag; (c) highways and bridges subject to frequent application of deicing salts which percolate down into the soils surrounding the H-piles; and (d) flooding which disturbs the foundation soils surrounding the piles. Life extension methods include zinc or aluminum coatings or sacrificial anodes that provide additional corrosion resistance, in conjunction with abrasion resistant organic coatings like epoxy. The substantial difference in fatigue life, with or without the benefit of protective coatings and sacrificial anodes, is shown in *Figure 42*.

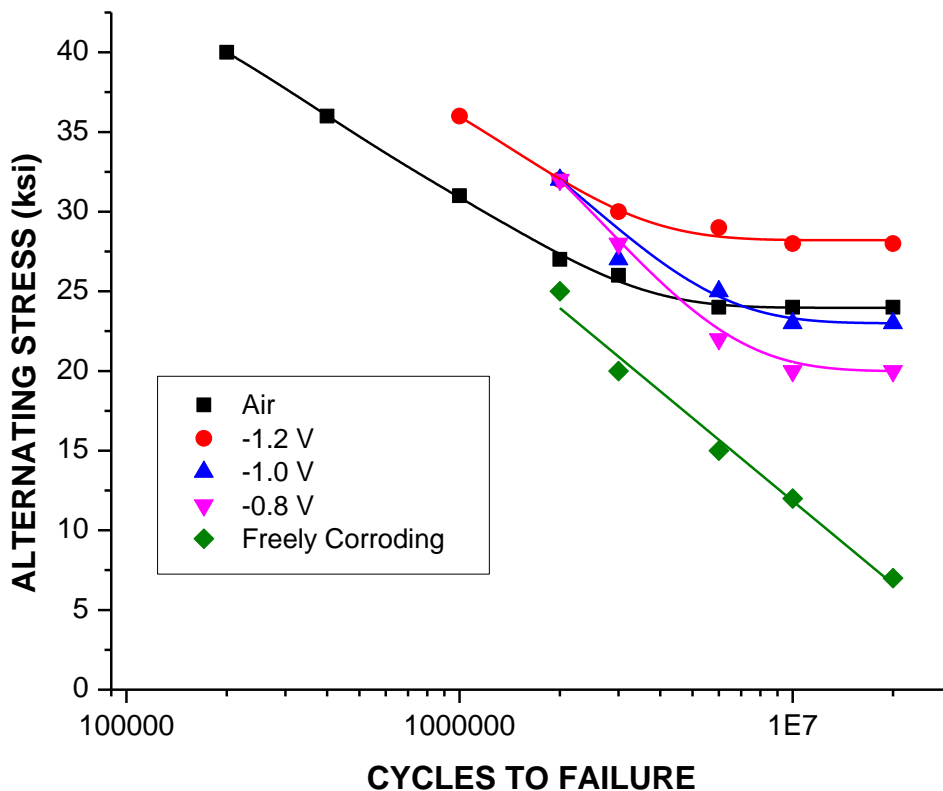


Figure 43. Sacrificial anodes and coatings improve the fatigue life of steel when placed in saline waters, even when compared to their fatigue life in air if sufficient potential is applied. The slight improvement compared to fatigue in air is because even air contains moisture as a function of relative humidity. The voltages shown approximate those of -1.2 V for magnesium anodes, -1.0 V for aluminized coatings, and -0.8 V for galvanized zinc. The above data is for structural steel in saline water with a resistivity of 20 ohm-cm (Ref. 19).

A. *Thermal Spray of Aluminum Coatings.* Aluminum coatings can substantially extend the life of steel buried in soil environments. The aluminum coating can be thermally sprayed onto the HP pile surface after shot-blasting which removes mill scale and is then cleaned of any loose debris. Coatings can vary in thickness up to 2-6 mils. Corrosion rates of aluminized steels in various soil environments are shown in *Figure 43*.

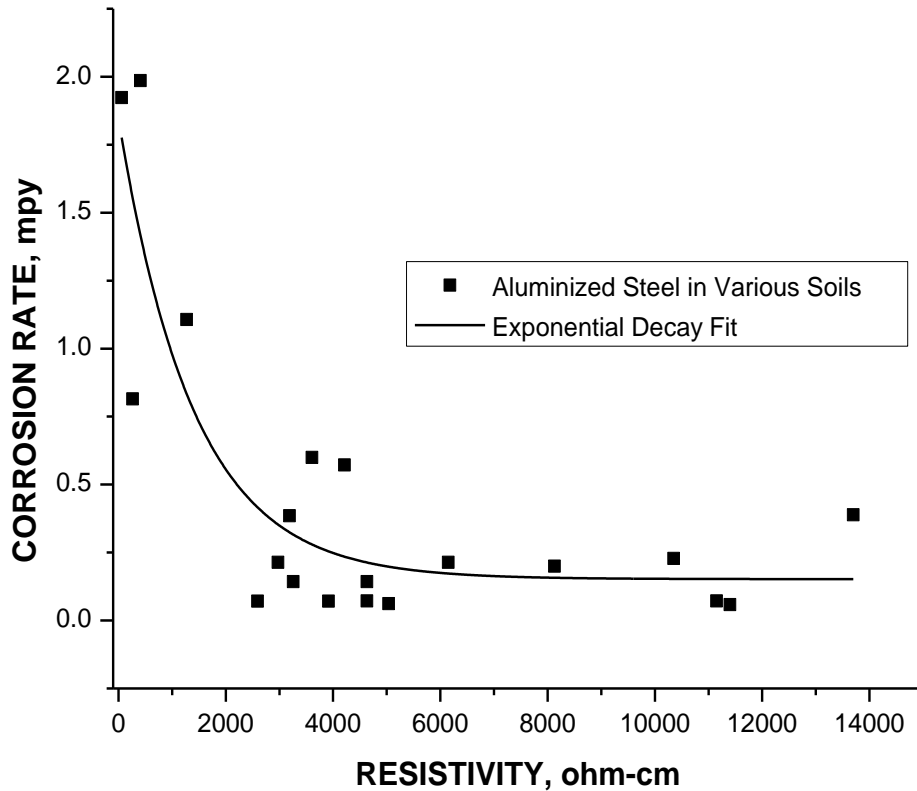


Figure 44. The corrosion rate of aluminized steels shows a reduction in corrosion rate versus the corrosion rate of uncoated steel. An empirical predictive relationship between soil resistivity and the corrosion rate for aluminized steel is: $C_{Almzdstl} = 0.15 + 1.7 e^{-R/1394}$. A 6-mil coating in a soil with a resistivity of 2000 ohm-cm has a corrosion rate of 0.55 mpy, which provides an additional 11 years of protection before the steel sustains section loss. Data from Ref. 20.

B. *Thermal Spray of Zinc and Hot-Dip Zinc Galvanizing.* Zinc and zinc-aluminum coatings can also be thermally sprayed onto pre-driven piles. To hot-dip galvanize a steel HP pile, mill scale is first removed by immersion in an acid bath. After removing mill scale from the HP pile, it is then dipped in molten zinc. Depending on its length and the size of the zinc bath, it can be single-dipped if short enough, or double-dipped if longer than the zinc bath. Although AASHTO M111 requires a zinc thickness of 3.9 mils for structural shapes, thicker coatings up to 10 mils

are possible, depending on the time of immersion in the zinc bath. The corrosion rates of zinc coated steels in soils environments vs. increasing soil resistivities are shown in *Figure 44*.

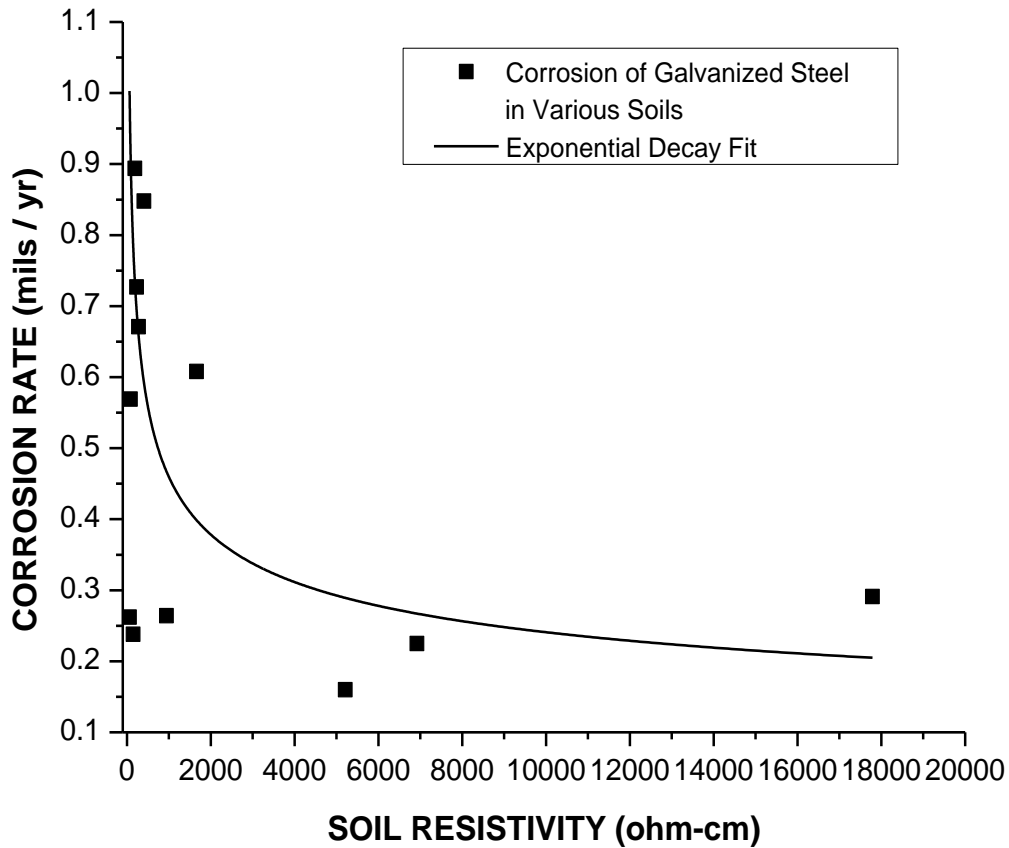


Figure 45. The corrosion rate of galvanized zinc coatings on steel in various soils as a function of increasing soil resistivity. Corrosion rate of zinc-coated steel is reduced compared to the rate of uncoated steel. The corrosion rate equation for uncoated steel is $C_{rate} = 0.5 + 2.2e^{-R/1846}$. At 1000 ohm-cm, the soil corrosion rate of steel is 1.78 mpy. For hot-dip galvanized zinc coatings, the corrosion rate in mpy is estimated by the relationship $C_{galZn} = 3.2 R^{-0.281}$, where R = soil resistivity. A 6-mil thick zinc coating at 1,000 ohm-cm resistivity has an average corrosion rate of 0.46 mpy, which provides about 13 years of added protection before the steel sustains section losses. From Ref. 20.

C. *Welding coated piles.* HP piles are typically stocked at service centers in lengths of 20, 40 and 60 ft. If the pile is to be spliced, the ends to be spliced should be masked off by at least 1 inch to permit welding. Coatings of aluminum and zinc can contaminate the weld metal and inhibit proper fusion. Although the points of fixity in this study ranged from 10-16 ft, the entire pile should be coated to protect all locations that could sustain additional damaging stresses

and moments. Welded areas that were masked off to prevent weld metal contamination can be subsequently thermally sprayed with zinc or 98% zinc cold galvanizing compounds to protect those areas if conductive soil horizons extend deeper than 16 ft below the surface.

D. Sacrificial Anodes for Uncoated and Coated HP piles. Fusion-bonded epoxy coatings last about 20-30 years, depending on soil location characteristics and its ability to drain run-off water or moisture. Fusion-bonding of epoxy results in coatings with fewer voids and lesser moisture permeability. Coating voids and permeability are the principal causes of debonding of coatings. Epoxy coatings are also more resistant to abrasion under pile driving conditions than conventionally applied polyurethane or acrylic coatings.

As shown previously in *Figure 42*, cathodic protection virtually eliminated corrosion fatigue. However, use of impressed current systems is not recommended because they require an exterior power source. Impressed current systems can also result in stray currents that could damage nearby electrical conduits or underground pipelines carrying natural gas. The corrosion of the electrical conductors at distribution panels and electrical connections of impressed current systems can also impede their efficiency.

Instead, sacrificial magnesium or zinc anodes are electrically connected to each epoxy-coated steel pile and will provide long-term protection in locations where piles are driven into conductive soils or where brackish water intrusion or deicing salts or industrial waste are present. Sacrificial anodes do not cause stray current problems since they are relatively isolated, and their driving voltages are less than 1.6 volts.

ASTM A950 provides requirements for fusion-bonded epoxy coating of structural HP piles and for sheet piling. The use of magnesium or zinc anodes can extend HP pile life for an additional 15-20 years for uncoated piles, or 40-50 years of protection (Ref. 38) if enough anode weight is provided for coated HP piles.

Depending on field conditions, holes for anodes may be vertically or horizontally drilled. Surface terminals to permit the monitoring of voltage and current output of anodes must be incorporated into each design. Provisions should also be made for the withdrawal of spent anodes and for the insertion of replacement anodes during the expected lifetime of the bridge. *Table 15* summarizes the types and characteristics of commercially available sacrificial anodes.

Table 15. TYPES OF SACRIFICIAL ANODES

Type of Anode	Range of Sizes Available	Voltage vs. Cu-CuSO ₄ Reference Electrode	Output Efficiency, ampere-hrs/lb	Consumption Rate, lbs / ampere-year
Standard Magnesium	3-60 lbs; 2-5 in diameter; 5-60 in length	-1.55 V	1000	8.8
Standard Zinc	5-60 lbs; 1.4-2 in diameter; 9-60 in length	-1.10 V	372	23.5
Aluminum Type I	30-240 lbs	-1.10 Type I	1280	6.8
Aluminum Type II	3-10 in width	-1.09 Type II	770	11.4
Aluminum Type III	3-10 in height 12-60 in length	-1.15 Type III	1150	7.6

Source: Galvanic Anode Material, Selection, Design Considerations (Ref. 38).

Life extension of uncoated and coated steel HP piles is a function of soil resistivity and the ampere-year capacity of sacrificial anodes. Uncoated HP piles require substantially more anode protective current than epoxy coated HP piles. Magnesium is the most commonly specified sacrificial anode, since it can be used in higher resistivity soils and has higher potential than aluminum or zinc anodes. Aluminum and zinc anodes are typically specified when soil resistivities are very low (20 to 500 ohm-cm).

E. *Determining anode life and weight.* All the following example calculations in this report are for 12 x 84 HP piles of 40-ft length and use magnesium anodes for life extensions of 15 to 30 years.

1. Uncoated HP pile. The average soil resistivity chosen for this design example was 200 ohm-cm. The surface area of a 40 ft 12 x 84 HP pile is 885 in² / ft, which is about 6 ft² / ft. A 40-ft HP pile therefore has a surface area of 240 ft². There are ten HP piles of 40-ft length on one side of the bridge, making the total surface area 2400 ft². The requirement for current coverage by magnesium anodes is 2 mA/ft². Since the surface is 2400 ft², the amperage required is 4800 mA or 4.8 A.

For other piles of different lengths and sizes, the surface areas must be calculated because adequate cathodic protection is determined by distribution of current on a mA per ft² basis.

The weight of magnesium anodes required for 15 years of life is determined by the following equation:

$$W = (Y \times S \times I) \div E$$

Where

W = total weight of the anodes to meet design life

Y = design life in years (15 in this example)

S = anode consumption rate, lbs per ampere-year

I = current required for protection

E = efficiency of the anode

The efficiency of a standard magnesium anode is 0.65, but 0.50 is commonly used for design purposes. Inserting the following values for magnesium, $W = (15) (8.8) (4.8) / 0.5 = 1267$ lbs. If 60 lb anodes are used, 21 anodes will be required per side of the integral abutment bridge.

2. Epoxy coated HP pile. An epoxy coated HP pile meeting the requirements of ASTM A950 has significantly less uncoated steel surface area for the anodes to protect. ASTM A950 requires that the surface not have more than 2 small “holidays” per ft² and not be discernible to the unaided human eye. This uncoated surface area was estimated to be about 0.25 in² per ft. However, as the pile may suffer some distress during driving and the efficiency of the coating will decrease due to undercutting of the holidays, it is estimated that 5% of the pile surface is not coated by the fused epoxy or is damaged during driving. Since each pile has an area of 240 ft², the total area of 10 piles per side of the bridge to be protected by the magnesium anodes is:

$$A = (2400 \text{ ft}^2) \times (0.05) = 120 \text{ ft}^2.$$

Since only a total of 120 total ft² is to be protected, this is a substantial reduction in the amount of amperage required: $120 \text{ ft}^2 \times 2 \text{ mA/ft}^2 = 240 \text{ mA} = 0.24 \text{ A}$. Because of the substantial reduction in surface area, the design life was increased to 30 years. The weight of magnesium anodes required is therefore $W = (30) (8.8) (0.24) / 0.5 = 127$ lbs. Since each side of the bridge requires 127 lbs, a total of 254 lbs of magnesium anodes is needed. These anodes would have dimensions of 4 in x 4 in x 17 in and each weighs 17 lbs. A series of eight 17 lb anodes per side of the bridge would then be vertically set and connected to the 10 piles.

3. Anode resistance as a function of soil resistivity. The current a magnesium anode can produce is related to its dimensions and soil resistivity. The magnesium anode selected for the ten piles on one side of the bridge has dimensions of 4 in x 4 in x 17 in.

The initial resistance of each anode is calculated by the following expression:

$$\Omega = (K R) \times [\ln (4L/r) - 1] \div L$$

Where

Ω = anode resistance, ohms

K = a constant = 0.0627

R = soil resistivity, ohm-cm

r = anode radius, inches

L = length of anode, inches

For the 4 in x 4 in x 17 in anode, $\Omega = (0.0627) (200) \times [\ln (4 \times 17 / 2) - 1] \div 17 = 2.6$ ohms.

Actual output in amperes of this anode in 200 ohm-cm soil is determined by the voltage difference between steel and magnesium:

$$I_o = (V_{Fe} - V_{Mg}) / \Omega$$

Where

I_o = current output, amperes

$V_{Fe} = -0.5$ V

$V_{Mg} = -1.1$

Ω = anode resistance, ohms

For a magnesium anode of 4 x 4 x 17 inches in 200 ohm-cm soil, the current output of the anode is $I = 0.6 / 2.6 = 0.231$ A = 231 mA. However, when the soil resistivity is increased to 1000 ohm-cm, the resistance substantially increases to 12.9 ohms, causing current output per anode to drop to 0.047 A = 47 mA. The only compensation available to increase amperage for anodes placed in higher resistivity soils is to increase anode length. In very low resistivity soils (< 200 ohm-cm) subjected to salt infiltration due to repetitive use of deicing salts, aluminum or zinc anodes may be more economical than using magnesium anodes. Only 0.23 A is required to protect the 10 epoxy-coated HP piles in this example. The current output of a single anode is 0.231 A.

Based on a calculated current output of 0.231 amperes per anode, its life is determined by the following expression:

$$L = (W \times S) \div (I_o \times 8766 \text{ hr/yr})$$

Where

L = life, years

W = weight of anode, 17 lb

S = anode current capacity, ampere-hrs/yr (1000 for magnesium)

I_o = current output, amperes (0.231 A for this example)

The life calculated for a single anode is therefore $L = (17) (1000) \div (0.231 \times 8766) = 8.4$ years. To extend the life of the H-piles to 30 years, the number of anodes must be increased. During 30-year life of the HP piles, there may be some deterioration of the epoxy coating, increasing the amount of steel surfaces to be protected. Assuming that the amount of “holiday” surface area to be protected increases to 10%, the current requirements would also increase to 0.48 A.

If required life $L = 30$ years and current requirements for protection is proportionally increased to 0.48 A, the above expression then becomes $30 = (W \times 1000) \div (0.48 \times 8766)$. Solving for W , total anode weight required is then 126 lbs. Since anodes weigh 17 lbs each, $7.4 \approx 8$ anodes are required for 30 years of life extension.

DECK AND APPROACH SLAB PROBLEMS

The approach slab in integral abutment bridges has presented problems when it is rigidly attached to the abutment, typically causing deck cracking or opening the interface joint to debris or separation of the filler due to contraction of the bridge. To prevent deck damage but prevent entry of road debris, a new connection was developed which employs the use of special polyurethane polymers that have elongations of 1,000%. Because of the expense of these polymers to completely fill a large hole for expansion as shown in *Figure 43*, the hole is filled with tire chips and then the polymer fills in the remainder of the void spaces. As a result, the required polymer volume is only about 10%, with the remainder as tire chips.

The effects of deformation on the polyurethane-tire chip composites showed no adverse effects after three severe compressions. The tire chips maintained their bond with the polyurethane and no delaminations were noted even after several progressively increasing compressions. These preliminary tests indicate that these polyurethanes can be good sealants and are promising materials for use in expansion joints. Compression testing results are summarized in *Figure 46* and *Figure 47*. Additional ultraviolet light exposure tests on the polyurethane – tire chip composites need to be conducted before field use is recommended.

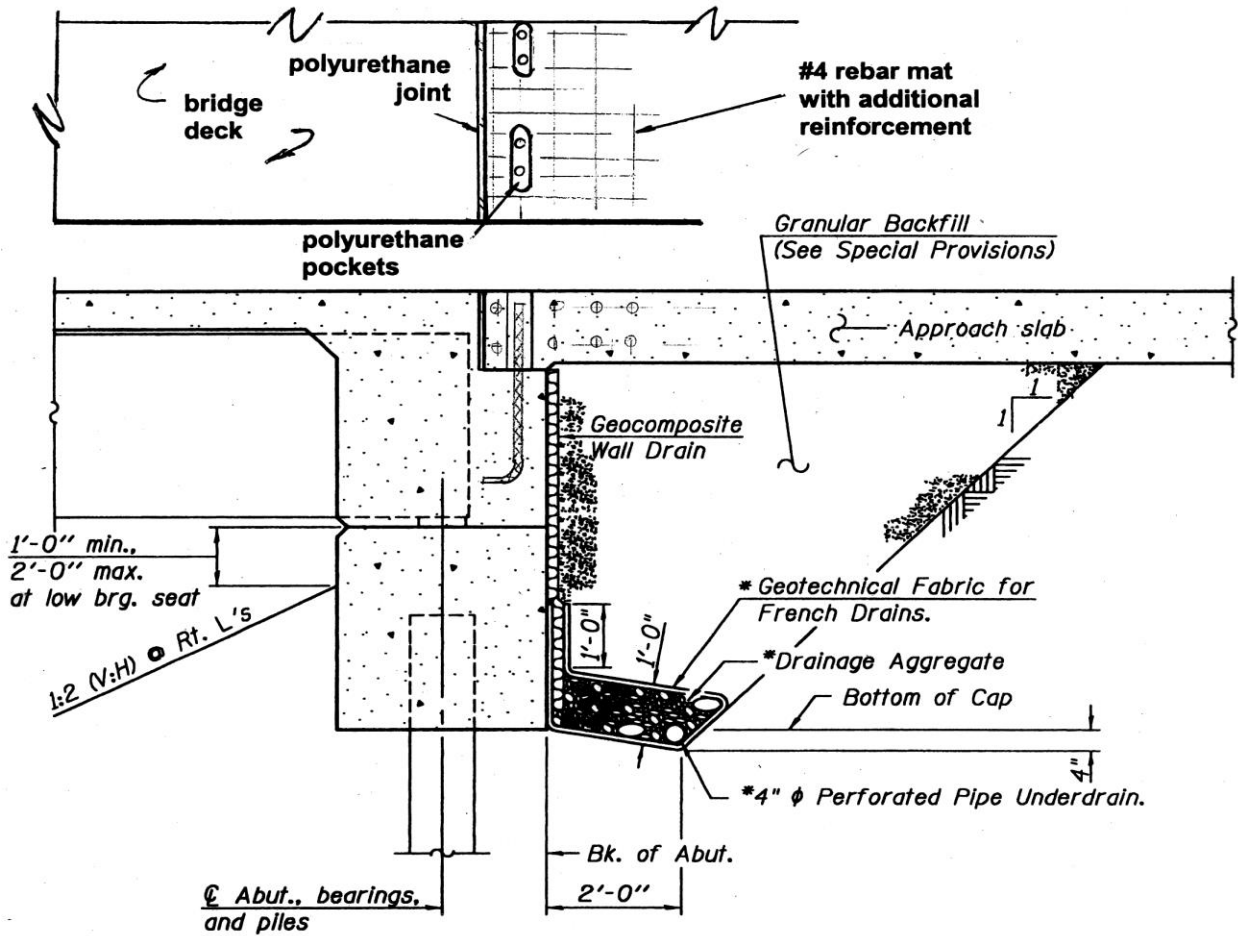


Figure 46. The polyurethane pockets connect the abutment to the approach slab by a #4 reinforcing bar, permitting deflection of the bar and absorption of that force by the polyurethane-tire chip composite. The rebar is anchored into the concrete, and the thin joint between the deck and the approach slab is filled with the specialty polyurethane-tire chip composite material.

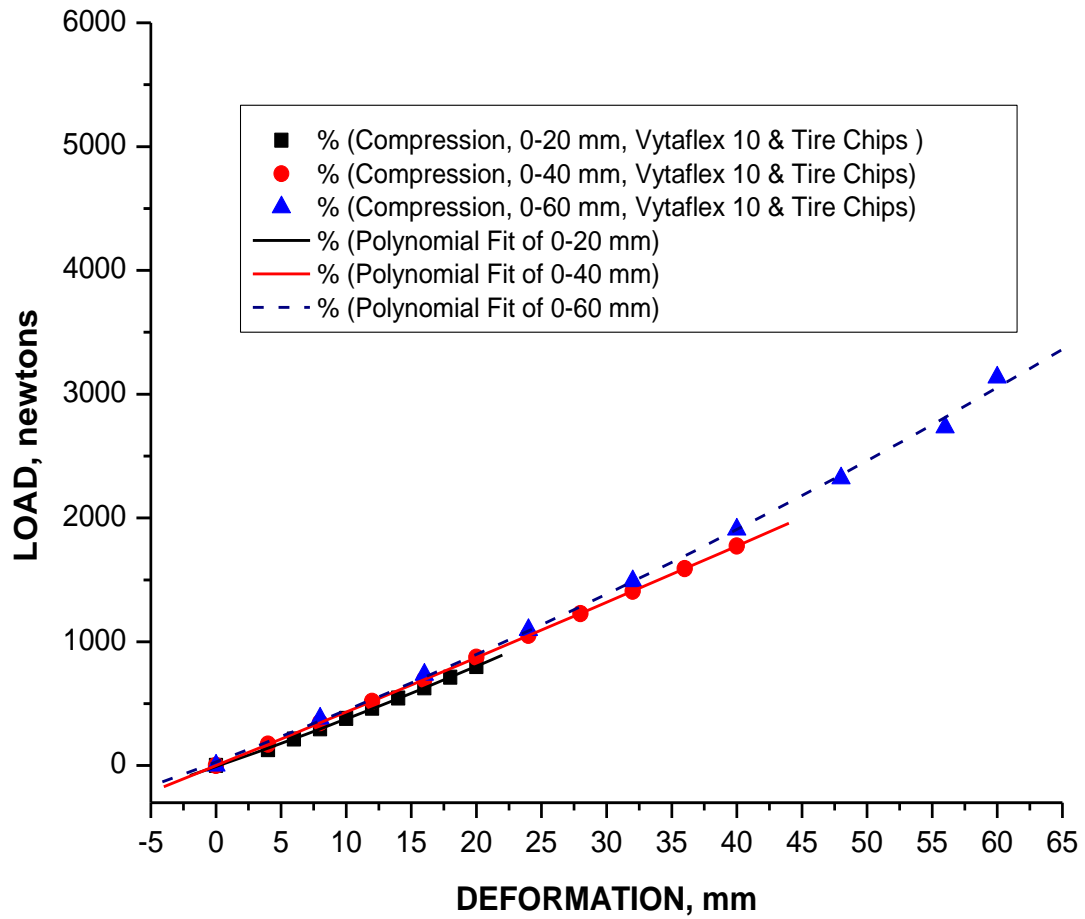


Figure 47. The deformation characteristics of 4 in x 8 in cylinders of Vytaflex 10 polyurethane resin with tire chips in compression. The polyurethane binds well with the tire chips, and there was no delamination noted during any of the compression testing. For conversion purposes, 1 N = 0.225 lbs force; 3000 N = 675 lbf; 25.4 mm = 1 inch.

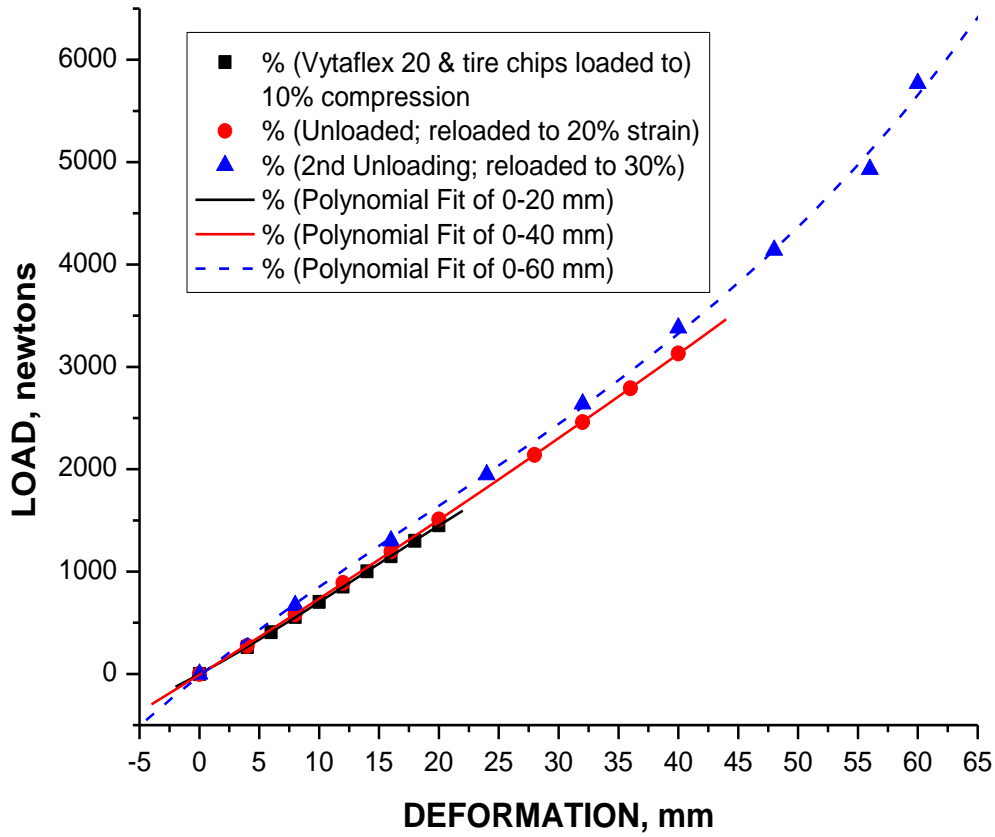


Figure 48. The deformation characteristics of 4 in x 8 in cylinders of Vytaflex 20, a polyurethane resin with even greater elongation characteristics than the Vytaflex 10 resin of Figure 42. Both resins cured well and bonded to tire chips, as well as concrete. For conversion purposes, 1 N = 0.225 lbs force; 3000 N = 675 lbf; 25.4 mm = 1 inch.

REDUCING PILE DEFORMATION STRESSES IN INTEGRAL ABUTMENTS

Based on the collected data which monitored pile stresses and integral abutment reinforcing bar stresses, it was evident that present integral abutment designs do not lend themselves to completely relieving pile stresses. Switching the pile orientation from the strong axis to the weak axis permits an increase in deflection in an HP 12 x 84 pile by a factor of 3.05, providing for greater expansion and contraction before yielding of the pile.

However, this may make the pile more susceptible to flange pitting and potential cracking if the pile is not protected by various coatings (zinc, aluminum or epoxy) or sacrificial anodes. Inserting the pile where bridge expansion and contraction is opposed by a predictable fill material like sand or polyurethane foam will substantially improve the pile response so that it better conforms to the shape of a cantilever in bending. This permits improved estimation of stress levels at each depth of the pile until fixity is reached.

Iowa State University investigators (Ref. 29) found that 70% of compacted granular backfill materials contained particles which were smaller than the openings in the perforated holes around the subdrain piping, leading to moisture storage and sometimes collapse afterwards. Moisture eventually penetrates the so-called waterproofing membrane that separates the piles and cap, leading to pitting of the uncoated piles. Tire chips were recommended to increase moisture outflow.

Numerous ideas and concepts were considered in this project to completely relieve the stresses induced in piles but keep the joint connections at the abutments integral. These concepts included use of integral keyway joints set within the abutments and use of large diameter shafting within bronze bearings in the abutment.

A. Dovetail Keyways in the Pile Cap. By modifying steel girders by welding plates at 45° angles from the flanges to webs, the girders can act as keys which slide backwards and forwards in nylon-lined keyways in the abutments, in response to thermal changes causing expansion and contraction of the deck.

B. Shafting in Slotted Bearings. In this alternate design, large diameter shafts with elliptical ends are anchored within the ends of the decking and slide back & forth on slotted bronze bearings, permitting translation of the deck during contraction and expansion. The shafting is

made of Nitronic 60, an anti-galling stainless steel and the bronze bearings are greased with high pressure lubricants or bronze alloys that are impregnated with lead or graphite. The expanding or contracting deck would slide between and on graphite-impregnated nylon sheets anchored to the pile cap and sides of the deck.

Each of these concepts must be carefully evaluated for durability since they are required to perform effectively for at least 50 years or more. The previously described concepts have not been constructed yet to evaluate them in actual construction to determine their effectiveness. Because they are design concepts at this stage, they were not included in this report, which solely focused on actual bridge performance of existing designs in field conditions.

Promising design concepts would permit complete linear translation of the bridge superstructure due to expansion and contraction, yet have deck end fixity which would limit deck uplift due to truck loadings. The pile caps would still be integral by connection to HP or pipe piles, but their geometry would permit deck translation. Other variations of this concept have been proposed by other states, but all were semi-integral and had insufficiently rigid bridge deck end fixity.

SUMMARY AND CONCLUSIONS

General

Integral abutment bridges have definite advantages. They have less deck deflection than simply supported members due to span end fixity, and their construction is simplified to some degree. The maintenance of the deck to approach joints is appreciably decreased because of the lesser accumulation of debris which tends to limit runoff water saturated with deicing salts into expansion joints. However, the magnitude of strains induced by thermal expansion and contraction in driven HP piles that the decks connect to and support the abutment were of concern, particularly with respect to yielding of piles and their fracture toughness. Due to requirements for 75-year design life, uncoated HP piles are subject to corrosion fatigue and pitting damage when driven into soils with low resistivity (less than 2000 ohm-cm). Piles loaded with respect to the strong X-X axis can sustain pits which can form surface cracks, whereas HP piles loaded against the weaker Y-Y axis can form cracks from corrosion pits on flange edges.

Stress Determination, Deformations and Points of Fixity

Piles in four different integral abutment bridges of single and multiple spans were instrumented with strain gages attached to piles and reinforcing bars at the interface between the pile cap and the abutment. Strain data collected from strain gages attached to piles and reinforcing bars during warm and colder months were then translated into stresses. Results indicated that piles oriented in the strong axis had variable stresses as function of depth from the top of the pile to its point of fixity. The distribution of stresses and strains in several piles did not conform to the deformed shape of a pile subjected to cantilever end loading as predicted by theoretical mechanics, but was related to uneven force distribution and differences in soil compressive strengths at different pile depths.

Depending on the type of pile encasement and its depth, and if the pile point of fixity is well below the frost line, the impact test temperature of 40°F is probably sufficient. For northern Illinois, the typical lowest ambient air temperature is -20°F; for central Illinois, -15°F; and for southern Illinois, -10°F. The frost line history of the area should determine pile temperatures as a function of driven depth.

Safety Factors

Mean and alternating stresses were determined from strain data for fatigue safety factor calculations using the Goodman failure equation. In many cases, contraction of the superstructure during colder weather or its expansion in warm weather, resulted in strains that

indicated stresses at or exceeding the minimum yield strength of piles made of A36 steel. Mean stresses in several piles were substantial and generated some concern as to their factors of safety with respect to fatigue life.

In two bridges, the Goodman fatigue failure equation indicated marginal-to-insufficient factors of safety for reinforcing bars connecting the pile cap to the diaphragm. Strain gage data at cold and warm ambient temperatures indicated that reinforcing bars were particularly vulnerable due to mean and alternating stresses. Several bars had clearly sustained stress levels significantly beyond the high cycle fatigue limit of 23 ksi for reinforcing bars which has been established by the *AASHTO LRFD Bridge Design Specifications*.

Soil Resistivity and Corrosion Fatigue

Concerns regarding corrosion fatigue of the piles indicated a potential for cracking or partial failure if the backfill beneath the approach slab has poor drainage characteristics and low resistivity. Backfills and soils with resistivity of 200 ohm-cm or less, or those with limited drainage permeability, can result in the absorption of runoff water containing deicing salts. Backfills incorporating waste products like cinders or blast furnace slag also contribute to corrosion and deep pitting of steel as demonstrated by previous bridge failures and burial of steel specimens by other investigations. Such conditions can result in marked pitting of the piles, decreasing their life span. When higher yield strength piles of 50 ksi or more are used, and their impact toughness is 15 ft-lbs or less, they are subject to life span reduction due to pile yielding and corrosion fatigue. This is particularly the case if integral abutments bridge designs must accommodate longer span lengths.

Sites where integral abutment bridges will be located must have their soil resistivities determined prior to construction. This includes measurements taken from soil borings and volume resistivity measurements of the general area where the abutments will be located.

Load Carrying Capacity, Redundancy and Requirements for Toughness

HP piles are redundant members and are subject to impact toughness requirements that are in accordance with the *AASHTO LRFD Bridge Design Specifications* and Table 8 of *ASTM A709 Structural Steel for Bridges*. This study confirmed that HP piles are stressed in tension by bending moments induced from expansion and contraction of the decking. For HP piles with either 36 or 50 ksi yield strengths, 15 ft-lbs at 40°F is the minimum Charpy V-notch impact test requirements for Illinois bridges, which is in Zone 2.

Because HP piles typically have no specified minimum requirements on impact or fracture toughness, including ASTM standards A252 and A972 (pipe piles), A690 (H piles), and A328 and A857 (sheet piles). Controls on steel composition regarding reduced carbon and sulfur levels are very beneficial, since lower carbon and sulfur contents in steels increase their impact and fracture toughness. As a minimum, HP steels should be specified to conform to ASTM A709 since they are structural shapes which requires controls on impact toughness and composition. Additionally, carbon contents should be less than 0.20% and 0.02% max sulfur or less than provide some assurance of adequate fracture toughness at sub-freezing temperatures. The manganese - carbon (Mn/C) ratio should be 3.0 or more; reductions of carbon for every 0.01% permit an increase of 0.06% manganese, up to 1.60% manganese max. Acceptable HP pile steels include ASTM A36 at 0.20% C max; A572 Grade 50, A588 Grade C and A992 Grade 50. Impact toughness requirements should preferably be 15 ft-lbs for the lowest anticipated service temperature (LAST), even though the minimum requirement for Grade 50 steel for Zone 2 is only 15 ft-lbs at 40°F. CVN test specimens should be obtained from HP pile flanges according to the test requirements of ASTM A673 and A370.

Protection of Piles Under Adverse Conditions

Prior to driving the steel piles, they should be sufficiently protected by one or more of the following options: (a) thermally sprayed with aluminum or zinc or zinc-aluminum coatings; (b) be hot-dip galvanized; or (c) coated with abrasion-resistant fusion-bonded epoxy in accordance with ASTM A950, and (d) further protected by sacrificial anodes. These measures will lessen the effects of corrosion fatigue and the formation of stress concentrations in surface corrosion pits formed during the 75-year requirement of embedment for H piles into low resistivity soils.

Although not always an option, piles should be preferably driven into soils with higher resistivity (2000 ohm-cm or more) as indicated by resistivity measurements obtained from soil borings or overall volume measurements of resistivity in the intended abutment locations. After pile installation, sacrificial magnesium, aluminum or zinc anodes should be selected, depending on the predominant soil resistivity. For higher resistivity soils, magnesium anodes are more desirable. For lower resistivity soils, aluminum or zinc anodes are often specified. Anodes should be electrically connected by fusion brazing to the HP piles. Sacrificial anodes can increase the service life of epoxy-coated piles by at least 15 to 40 years when epoxy coatings are used. Spent anodes should be retrievable and provisions must be made for monitoring of applied voltage and anode currents to determine electrical continuity and remaining anode life.

Joint Sealants

A very flexible polyurethane with 1,000% elongation, when combined with tire chips, was developed and was tested in this project under severe repeated compression. Polyurethane-tire chip composites can be used for expansion joints due to their ability to absorb strains sustained by the approach slab and attenuate deck stresses caused by contraction. Tire chips are inexpensive recycled material additions compared to the polyurethane resins, decreasing cost by at least 80%, since the tire chips occupy almost 90% of volume, compared to the more expensive polyurethane binder.

REFERENCES

1. A. Paraschos and A. Amde, "Survey on the Status of Use, Problems and Costs Associated with Integral Abutment Bridges", *Better Roads*, Nov 2011.
2. E. Wasserman, "Integral Abutment Design Practices in the United States", *Federal Highway Conference on Integral Abutment Bridges*, Baltimore, MD, 16-18 Mar 2005.
3. V. Mistry, "Integral Abutment and Jointless Bridges", *Federal Highway Conference on Integral Abutment Bridges*, Baltimore, MD, 16-18 Mar 2005.
4. J. Horvath, "Integral Abutment Bridges: Geotechnical Problems and Solutions Using Geosynthetics and Ground Improvement", *Federal Highway Conference on Integral Abutment Bridges*, Baltimore, MD, 16-18 Mar 2005.
5. J. Huang, C. Shield and C. French, "Time Dependent Behavior of a Concrete Integral Abutment Bridge", *Journal of the Transportation Research Board*, Washington, DC, 2005, pp 299-309.
6. A. Blake, *Practical Stress Analysis in Engineering Design*, Marcel Dekker, New York, 1990, pp 236; 245.
7. "Integral Abutment Bridges", Section 15, *New Jersey Design Manual for Bridges and Structures*, pp 1.15-1 to 1.15-12.
8. D. Liu, R. Magliola, and K. Dunker, "Integral Abutment Bridges—Iowa and Colorado Experience", *Federal Highway Conference on Integral Abutment Bridges*, Baltimore, MD, 16-18 Mar 2005.
9. S. Olson, K. Holloway, J. Buenker, J. Long and J. LaFave, *Thermal Behavior of Illinois DOT Integral Abutment Bridges and Proposed Design Modifications*, Illinois Center for Transportation Report ICT-R27-55, Champaign, IL, May 2013.
10. D. Puzey, "2012 Integral Abutment Policies and Details", Illinois Dept. of Transportation Design Memorandum, July 2012, pp 1-33.
11. "Thermal Coefficient of Portland Cement Concrete", *Portland Cement Concrete Pavements Research*, Federal Highway Administration Internet Site, fhwa.dot.gov.
12. "Physical Properties of Carbon and Low-Alloy Steels", *Metals Handbook, Volume 1 Properties and Selection: Irons, Steels and High-Performance Alloys*, ASM International, Materials Park, OH, 1990, p 195.
13. *LRFD Bridge Design Specifications*, 6th Edition, AASHTO, Washington, DC, 2012.
14. H. Fuchs and R. Stephens, *Metal Fatigue in Engineering*, Wiley, New York, 1980, p 72.
15. J. Barsom and S. Rolfe, *Fracture and Fatigue Control in Structures*, Prentice-Hall, Englewood Cliffs, NJ, 1987, p 173.

16. J. Collins, *Failure of Materials in Mechanical Design*, Wiley-Interscience, New York, 1981, p 65.
17. *Standard Specifications for Highway Bridges*, 15th Edition, Washington, DC, 1992, pp 187-193.
18. *Structural Welding Code—Steel*, AWS D1.1, American Welding Society, Miami, FL, 2000, pp 13-17.
19. F. Stonesifer and J. Krafft, *Fatigue Crack Growth in A36 and A283 Plate in Air and Seawater Environments*, Naval Research Laboratory Report 4467, Washington, DC, March 1981, p 58.
20. M. Romanoff, *Underground Corrosion*, National Bureau of Standards, Dept. of Commerce, Washington, DC, April 1957, pp 40-42.
21. *Corrosion Fatigue of Metals in Marine Environments*, Defense Metals & Ceramics Center Report MCIC-81-42, Columbus OH, July 1981, pp 50-59.
22. B. Boardman, "Fatigue Resistance of Steels", *Metals Handbook, Volume 1 Properties and Selection, Irons and Steels*, 9th Edition, American Society for Metals, Metals Park, OH, 1978, pp 665-682.
23. R. Juvinall, *Fundamentals of Machine Component Design*, Wiley, New York, 1983, pp. 203-215.
24. H. Grover, S. Gordon and L. Jackson, *Fatigue of Metals and Structures*, NAVWEPS Report 00-25-534, Dept. of the Navy, Washington, DC, June 1960, p 283.
25. R. Roark and W. Young, *Formulas for Stress and Strain, 5th Edition*, McGraw-Hill, New York, 1975, p.96.
26. H. Uhlig, *Corrosion and Corrosion Control*, Wiley, New York, 1971, p 161.
27. SAE Fatigue Design and Evaluation Technical Committee, *Fatigue Design Handbook AE-10*, Warrendale, PA, 2nd Edition, 1988, pp 43-44; 53.
28. O. Burnside, S. Hudak, E. Oelkers, K. Chan and R. Dexter, *Long Term Corrosion Fatigue of Welded Marine Structures*, US Coast Guard, Washington, DC, 1984.
29. D. White, "Best Practices for Bridge Approaches", *Iowa Dept. of Transportation Tech Transfer Summary (TR-481)*, Ames, IA, Jan 2005, pp 1-4.
30. T. Holman and S. Stonecheck, "Emergency Micropile Repair of the Penn DOT Birmingham Bridge", MORETRENCH Report, Monroeville, PA, 2008.
31. L. Mulvany and K. Crowe, "Corrosion Suspected in I-43 Green Bay Bridge Sag", *Milwaukee Journal-Sentinel*, October 3, 2013.

32. S. Tauscher, *Correlation of Fracture Toughness with Charpy Impact Test Data*, US Army Armament Research and Development Command Report ARLCB-TR-81012, p 13, March 1981.
33. *Manual of Steel Construction*, 8th Edition, AISC, Chicago, 1980, pp. 1-34 to 1-35.
34. M. Djukic, G. Bakic, V. Zeravcic, A. Sedmak and B. Rajicic, "Hydrogen Embrittlement of Industrial Components: Prediction, Prevention and Control", *Corrosion*, Vol. 72, No. 7., 2016.
35. M. Fontana, *Corrosion Engineering*, McGraw-Hill, New York, 1986, p141.
36. Materials Engineering & Testing Services, *Corrosion Guidelines, Version 3.0*, California Department of Transportation, March 2018.
37. R. Morales, *Designing for Durability*, Gerdau Ameristeel / LB Foster Piling internet web site, p 13.
38. *Galvanic (Sacrificial) Anode Material Selection, Design Considerations*, TSEWG Report TP-17, US Army Corps of Engineers / Naval Facilities Engineering Command, May 2017.

USER NOTES